Metallic glasses for biological applications and opportunities opened by laser surface texturing: A review

N. Lebrun, F. Dupla, H. Bruhier, M. Prudent, A. Borroto, C. Der Loughian, F. Bourquard, Jean-marc Pelletier, M. Rousseau, J. -P. Colombier, et al.

Applied Surface Science 670 (2024) 160617

Contents lists available at ScienceDirect

Applied Surface Science

journal homepage: www.elsevier.com/locate/apsusc

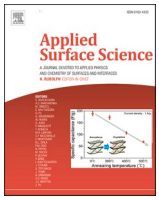

Metallic glasses for biological applications and opportunities opened by laser surface texturing: A review

N. Lebrun [a], F. Dupla [a], H. Bruhier [a], M. Prudent [b], A. Borroto [c], C. Der Loughian [a], F. Bourquard [b], J-M. Pelletier [a], M. Rousseau [d], J.-P. Colombier [b], J.-F. Pierson [c], F. Garrelie [b], P. Steyer [a,*]

[a] UCBL, CNRS, MATEIS, Université de Lyon, INSA Lyon, Villeurbanne, France
[b] Université Jean Monnet, CNRS, Institut d'Optique Graduate School, Laboratoire Hubert Curien, Saint-Etienne, France
[c] Université de Lorraine, CNRS, Institut Jean Lamour, Nancy, France
[d] INSERM, Mines Saint-Etienne, Université Jean Monnet, SAINBIOSE, Saint-Etienne, France

ARTICLE INFO

Keywords:
Bulk metallic glasses
Thin film metallic glasses
Antibacterial
Biocompatible
Bioinert
Biodegradable
Laser Surface Texturing
Femtosecond laser
Laser-induced periodic surface structures

ABSTRACT

Implants and surgical tools are commonly used in the medical field. However, issues including poor osseointegration, rejection, or bacterial contamination may still occasionally occur, causing serious complications susceptible to lead even to the patient death. It is therefore necessary to move toward new alternative advanced surfaces, that may possess both antibacterial properties and improved biocompatibility compared with existing solutions. Metallic glasses may constitute this kind of promising materials, gathering a high physico-chemical resistance combined with outstanding mechanical properties. The first part of this review explores the interest of metallic glasses for biomedical applications, and focuses on their biological properties. Metallic glasses are considered under their two forms: bulk, as well as thin films. The behaviour of these metallic glasses towards micro-organisms (bacteria, cells in particular) is then described. Besides, surface texturing by pulsed laser represents a further degree of freedom to deeply functionalize the metallic glasses' surface. The induced modifications may not only concern the morphology of the surface, but also its chemistry at a small scale. In this sense, the review demonstrates the importance of such a surface modification on the biological properties, and on the dynamic of cells on these advanced surfaces in particular. Finally, the last part is dedicated to the latest developments of ultrashort laser irradiation of metallic glasses. It is shown how these nano-engineered surfaces can influence the biological behaviour of metallic glasses. Explanations rely on the patterning design on the one hand, on chemistry of the irradiated material on the other hand.

1. Introduction

Metallic glasses, discovered in 1960, are still widely studied. Scientists are increasingly interested in these materials because of their unique combination of properties, which emerge from their amorphous structure mainly composed of metallic elements. Metallic glasses are metallic materials which possess interesting properties like their low elastic modulus but higher strength and corrosion resistance thanks to the amorphous and disordered structure allowing the absence of lattice defects, grains and grain boundaries [1]. Metallic glasses are studied in particular for biological applications, such as implants or surgical tools [2]. These medical objects need to be as antibacterial as possible to avoid infections as well as biocompatible for ease of integration in the biological environment. Recently, the use of lasers to texture surfaces has been shown to have a significant effect on biological properties [3]. The combination of metallic glasses and laser surface texturing is therefore very promising for the implants and surgical tools of tomorrow as a means of limiting the risks associated with surgery or stays in hospital. This review focuses on the interaction between three different fields: metallic glasses, biological properties (*i.e.* antibacterial as well as biocompatible characteristics), and laser surface texturing. As this review addresses different scientific fields representing different scientific communities, a pedagogic approach has been favored. First, the origin, synthesis, and properties of metallic glasses will be presented. Then, the microorganisms, their importance, and their behavior will be explained. After that, a literature review of recently studied metallic glasses for

* Corresponding author at: UCBL, CNRS, MATEIS, Université de Lyon, INSA Lyon, Villeurbanne, France.
E-mail address: philippe.steyer@insa-lyon.fr (P. Steyer).

https://doi.org/10.1016/j.apsusc.2024.160617
Received 4 April 2024; Received in revised form 15 June 2024; Accepted 26 June 2024
Available online 27 June 2024

antibacterial and biocompatibility applications will be covered. The techniques of laser surface texturing will then be presented, including results of irradiation of surfaces. Finally, the interest of laser surface texturing for biological applications as well as its use on metallic glasses will be discussed. This review aims to demonstrate that any researcher can learn enough about these three fields to have the necessary keys to understand the interest of combining them, regardless of their original scientific skills.

2. Metallic glasses

The first metallic glass, of composition $Au_{75}Si_{25}$, was synthesized in 1960 by splat quenching [4]. This technique induces the quenching of the liquid alloy at a rate of approximately 10^5–10^6 K.s^{-1}[5]. Subsequently, many metallic glass systems, such as Pd–Si, Pd–Au–Si, Pd–Ag–Si, and Pd–Cu–Si, were synthesized by rapid cooling, which limited their shape to ribbons, foils, or wires[6]. The invention of the melt spinning method accelerated the study of metallic glasses. Thicker ribbons became obtainable (10–50 μm), and ternary or quaternary alloys were easily synthesized [7,8]. For a long time, only alloys containing noble metals such as Pd and Pt led to large thicknesses (10 mm); however, their cost was prohibitive. In the early 1990 s, there was a new boom in interest in metallic glasses with the discovery of systems enabling the formation of glass at very slow cooling rates lower than 10 K.s^{-1} [9]. These slow rates are caused by the small temperature range for the occurrence of nucleation and crystallization (due to the high glass transition temperature) and the different atomic radii (of usually 4 or 5 elements). The metallic glasses could then be synthesized by conventional mold casting, creating the first bulk metallic glasses (BMGs) of several centimeters thickness.

2.1. Bulk metallic glasses

It was therefore discovered that some compositions that easily formed metallic glasses were composed of transition metals, greatly decreasing their cost compared with that of Au, Pd, or Pt-based compositions. Vitreloy® 1 ($Zr_{41.2}Ti_{13.8}Cu_{12.5}Ni_{10.0}Be_{22.5}$) was developed in 1993 [9] and became the first commercially used BMG in 2003, under the name LiquidMetal®. To date, this composition remains among those with the best glass-forming ability (GFA). Due to the high toxicity of beryllium, it was later replaced with aluminum. Over the past 30 years, full expansion of BMGs has occurred with the synthesis of numerous Fe-, Ni-, Ti-, and Cu-based systems [2]. Given their larger dimensions than the first synthesized metallic glasses, measurement of their properties became easier. Fig. 1 compiles some photographs of large BMG pieces of different quaternary alloys, and highlights progress made in the characteristic size of final parts in 15 years, with a maximum diameter of 80 mm achieved in 2012 for the Pd-Cu-Ni-P system (Fig. 1B) [10]. A recent critical review [11] indicates that this maximum diameter is still relevant today. Furthermore, it is worth mentioning that new opportunities are now opened to fabricate big parts of complicated shapes through innovating processes linked to additive manufacturing. In this sense, promising results on BMGs can be found in the recent review of W. Wu et al. [12].

The GFA of a metallic glass alloy corresponds to its ability to form a glass when cooled and thus to avoid its ordered crystallization. For a high GFA, it is easy to obtain an amorphous phase even at low cooling rates. The quantification of GFA is under discussion, as the best way to calculate it would be to know the critical cooling rate (below which the alloy crystallizes) and the maximum diameter or thickness that can be obtained while remaining amorphous. Many criteria for estimating a GFA value have been developed, usually based either on transition temperatures or thermodynamic properties. A critical evaluation of all these different criteria is presented by Chattopadhyay *et al.*[15].

Most multicomponent BMGs have been synthesized through numerous trials on many compositions, which makes the synthesis of new metallic glasses very time consuming. From a qualitative perspective, Inoue *et al.* proposed several empirical rules to properly synthesize amorphous BMG alloys: many components (confusion principle), strong differences in atomic size ratio of metallic elements (at least 12 %), and a negative enthalpy of mixing [16]. A high GFA is also usually achieved for compositions close to eutectic compositions [17]. Even if the vast majority of BMGs with a strong GFA follow these rules, there are some exceptions, which indicates that the proposed mechanisms of BMG formation are not yet completely understood. It is worth mentioning that innovative approaches involving machine learning are under development. For instance, possible glass-forming compositions in the Co–V–Zr ternary system were rapidly predicted (compared with the time required for empirical research) using machine learning [18]. The same approach has also been applied for a selection of biocompatible alloys in the Ti-Zr-Cu-Pd system [19]. Such a strategy can offer considerable time saving if the algorithm is supplied with a sufficient amount of reliable data.

As a consequence of their amorphous structure, metallic glasses are devoid from conventional metallurgical defects causing chemical segregations, such as grain boundaries, precipitates… Therefore, another key-characteristic inherent to all metallic glasses whatever their geometry (rod, ribbon, film…), is their chemical homogeneity. The correlation is so high that, most often, authors prove the metallic glass character of their materials by indirect global technics (differential scanning calorimetry (DSC) or X-ray diffraction (XRD)), without deeply characterizing the chemical composition. Some works present for

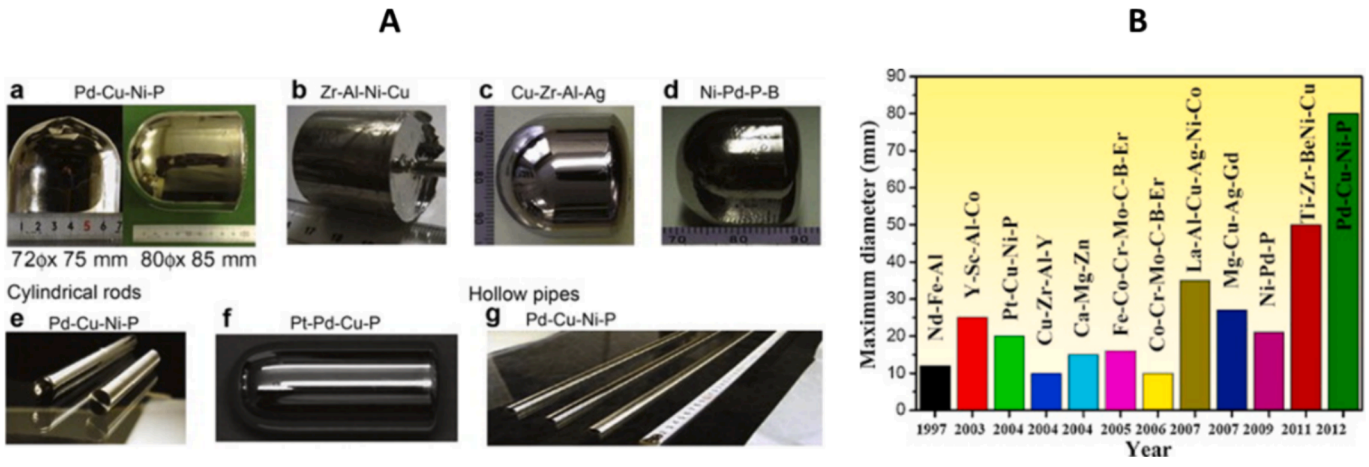

Fig. 1. A: Pd-, Zr-, Cu-, Ni-, and Pt-based large centimeter-sized BMGs[13]; B: time- diameter evolution for different systems of BGM [14].

instance the distribution of metallic elements through TEM-scale spectroscopic (Energy dispersive Spectroscopy (EDS)) X-ray images (Fig. 2A) on Zr-based thin films. More quantitatively, the same homogeneity is also shown by X-ray photoemission spectroscopy (XPS) on a Ti-based BMG developed for the dental implantology (Fig. 2B). The depth profile indicates that, except on the top-surface where a 15-nm thick passive oxide layer is formed, the respective ratios of all elements are maintained in the inner part of the alloy.

Today, different processes can be used to form a BMG, such as high- and low-pressure die casting (HPDC and LPDC, respectively) [22,23], centrifugal casting [24], and the conventional copper mold casting. In addition, there are also many different processes used to shape the metallic glass for a specific product: thermoplastic forming (TPF) [25], cold rolling [26], joining [27], electro-discharge [28], and micro-forming [29]. Additive manufacturing using different techniques such as selective laser melting (SLM), laser engineered net shaping (LENS), thermal spray 3D printing (TS3DP), laser foil 3D printing (LFP), and fused filament fabrication (FFF), has also been reported in recent years [30–33]. More details on the processing of BMGs can be found in the review of Halim *et al.* [11].

BMGs tend to possess great mechanical strength and high resistance to corrosion or degradation. As illustrated in Fig. 3, many BMG compositions exhibit a strength higher than that of conventional biomaterials, combined with a good elastic modulus.

Even though many BMG compositions with good properties have been synthesized, one of the limitations is that only a narrow range of multi-element chemical compositions can lead to the disordered amorphous state. Slight changes in the composition often result to a lowered GFA. Also, as mentioned before, the dimensions of the BGM are limited

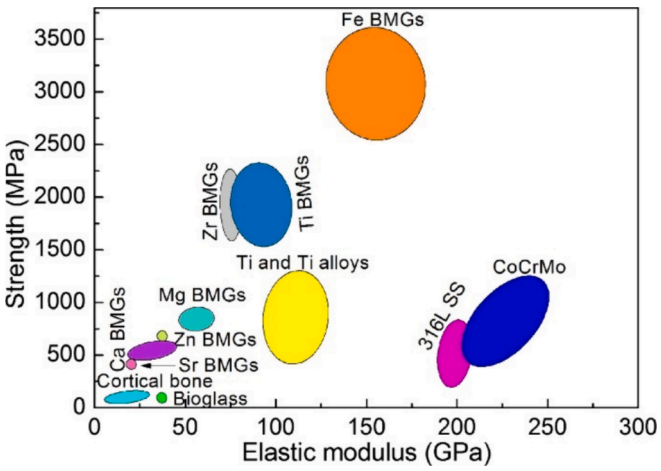

Fig. 3. Mechanical properties of conventional biomaterials compared with those of BMGs [34].

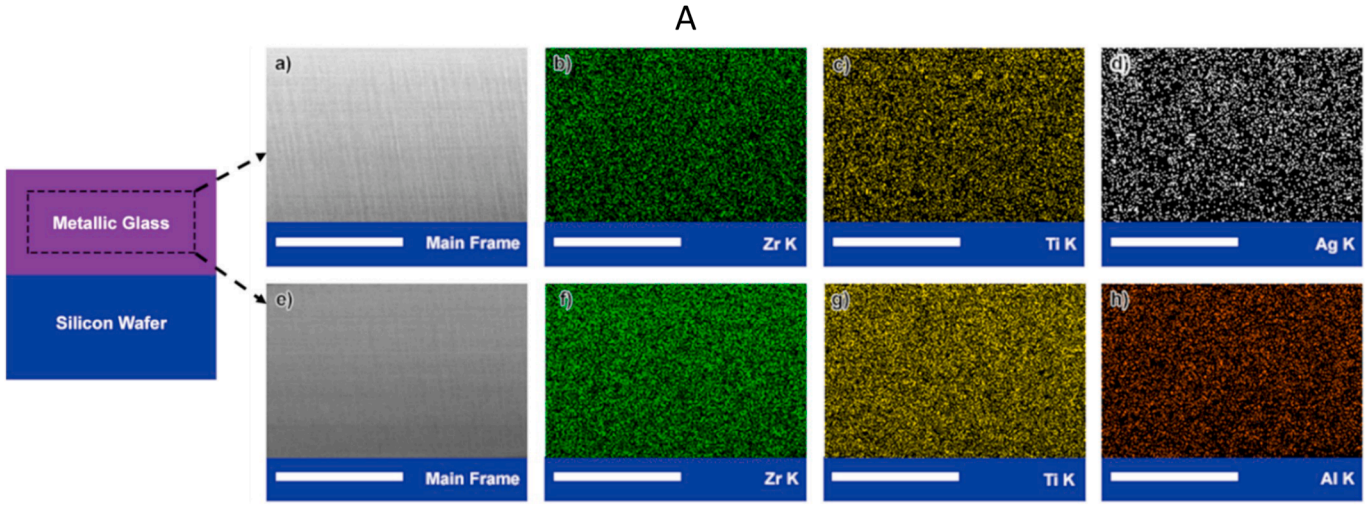

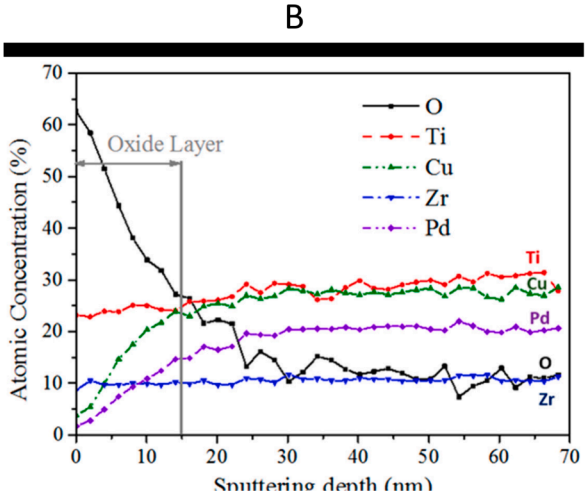

Fig. 2. Fine-scale chemical analysis of A: $Zr_{46}Ti_{40}Ag_{14}$ and $Zr_{46}Ti_{43}Al_{11}$ thin films (a,e: ADF images, b, f: Zr X-ray images, c, g: Ti X-ray images, d: Ag X-ray image, h: Al X-ray image) [20] and B: XPS atomic concentration profile of $Ti_{40}Zr_{10}Cu_{36}Pd_{14}$ BMG [21].

by the ability to maintain the disordered structure inside the volume of the piece, making bigger volume difficult to realize. These were some of the motivating factors for the development of thin film metallic glasses (TFMGs).

2.2. Thin film metallic glasses

Thin film metallic glasses (TFMGs) are produced by physical vapor deposition (PVD) sputtering, a process that consists of using a plasma to extract atoms from a target and eject them toward the substrate to be coated, like magnetron sputtering [35,36] or pulsed laser deposition (PLD) [37]. This process induces the deposition of a solid film, generating a very high cooling rate (up to 10^{12} $K.s^{-1}$ [38]). This very fast cooling induced by the PVD process allows a wider range of fully amorphous systems and compositions than those of BMGs [39]. TFMGs can be synthesized in two different ways using the PVD sputtering technique: (1) by using a single BMG-based target to realize a thin film of perfectly known composition [38,40] and (2) by using multiple targets (Fig. 4). A combinatorial approach is then possible by placing multiple samples at different places of the sputtering chamber, thus inducing different film compositions depending on their distance from each target [41–43]. Many samples of different compositions but belonging to the same system can thus be sputtered at once. Another multi-target sputtering technique consists of applying different currents to each target, permitting a controlled co-deposition on a single sample [44].

Recently, pulsed laser deposition (PLD) was also used to create TFMGs [45,46]. This technique uses a high-power pulsed laser to vaporize the material to be deposited from a target placed in a vacuum chamber. A plasma is then created, and the particles are deposited on the substrate, forming a thin film. However, this deposition method implies the presence of a heat affected zone, which can lead to possible structural modifications because of the rise of temperature in some areas of the material.

The first TFMGs synthesized in the 1980 s were binary alloys, such as Cu–Zr [47], Cu–Ta [48], Cu–W [49], or Bi–Fe [50] systems. Subsequently, the development of BMGs and the combinatorial approach favored TFMGs in more complex systems containing at least three elements. As a result, the film's amorphous structure has to be demonstrated at different scales: from a global viewpoint by DSC and XRD, as well as by TEM at the atomic-scale (Fig. 5) [51]. Besides, at a mesoscale, the metallic glass character of a film can also be shown through a simple SEM cross-section examination. In that case, films are deposited onto a brittle substrate (Si wafer in general); when fractured, some specific vein-like features appear, characteristic of the metallic glass nature (Fig. 5 c). Their presence was most often related to the dynamic of shear-bands, while, more recently, a new theory considering the melting temperature was proposed [52].

Owing to their disordered structure, TFMGs have various very interesting properties. Compared with the properties of other conventional sputtered thin films, their roughness and coefficient of friction are very low and their microstructure is very fine (so-called glassy-like), as presented in Fig. 6. From a functional viewpoint, they possess relatively high plasticity and ductility, good corrosion resistance, and are interesting for biological applications thanks to their wide composition range and low roughness [53,54]. Many studies on TFMGs have focused on their biological properties, including their antibacterial activity and biocompatibility. Adding their low synthesis cost to their interesting properties, TFMGs show great potential for use as implants or surgical consumables, *i.e.* needles, blades, guidewires, or catheters [55].

In order to assess a potential "small scale effect", it could be interesting to compare properties of the two types of metallic glasses under their bulk and film forms. However, such a comparison is made difficult considering composition aspects on the one hand, and characterization aspects on the other hand. Indeed, TFMGs have in general simple chemical compositions (2 or 3 elements *versus* 4 or 5 for BMGs), and characterization techniques are also often different (e.g. "conventional" mechanical tests for BMGs in comparison to nano-indentation-based tests for TFMGs). In this sense, the recent paper from M. Jain et *al.* deserves to be considered [57]. It indeed presents an interesting multiscale direct comparison of mechanical and thermal behaviors of a similar Zr-Cu-Ag alloy, synthesized either by PVD or by arc-melting processes. Authors conclude on better performance of the film, explained on the basis of oxygen contents and homogeneous deformation considerations.

3. Microbiological aspects

Before discussing the specific biological properties of TFMGs, it is necessary to properly define the type of microorganisms of interest for antibacterial and biocompatible surfaces. This chapter aims to describe the prokaryotic organisms, of which bacteria belong to, and the eukaryotic organisms, often used to estimate the biocompatibility of a surface.

3.1. Prokaryotic bacterial cells

Prokaryotic cells are omnipresent and are unicellular microorganisms that do not have a nucleus. Their genome consists of DNA concentrated in an area called the nucleoid region, floating in the cytoplasm (liquid filling the bacteria) together with ribosomes. They are encased in a cell membrane and sometimes in additional external

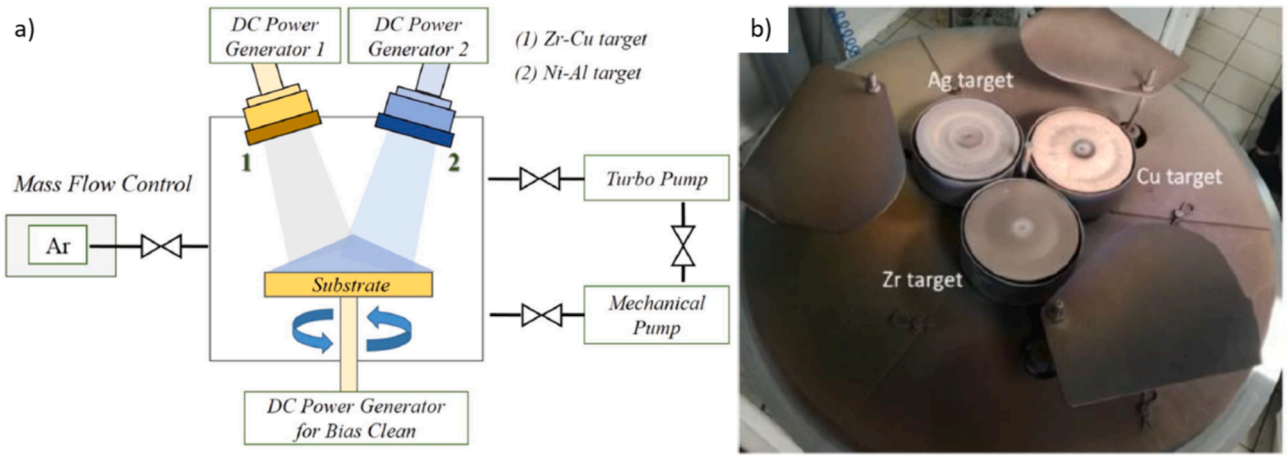

Fig. 4. PVD magnetron co-sputtering system: a) schematic diagram of a two-target system (ZrCu–NiAl) [39] and b) example of three-target sputtering apparatus (Zr–Cu–Ag) [43].

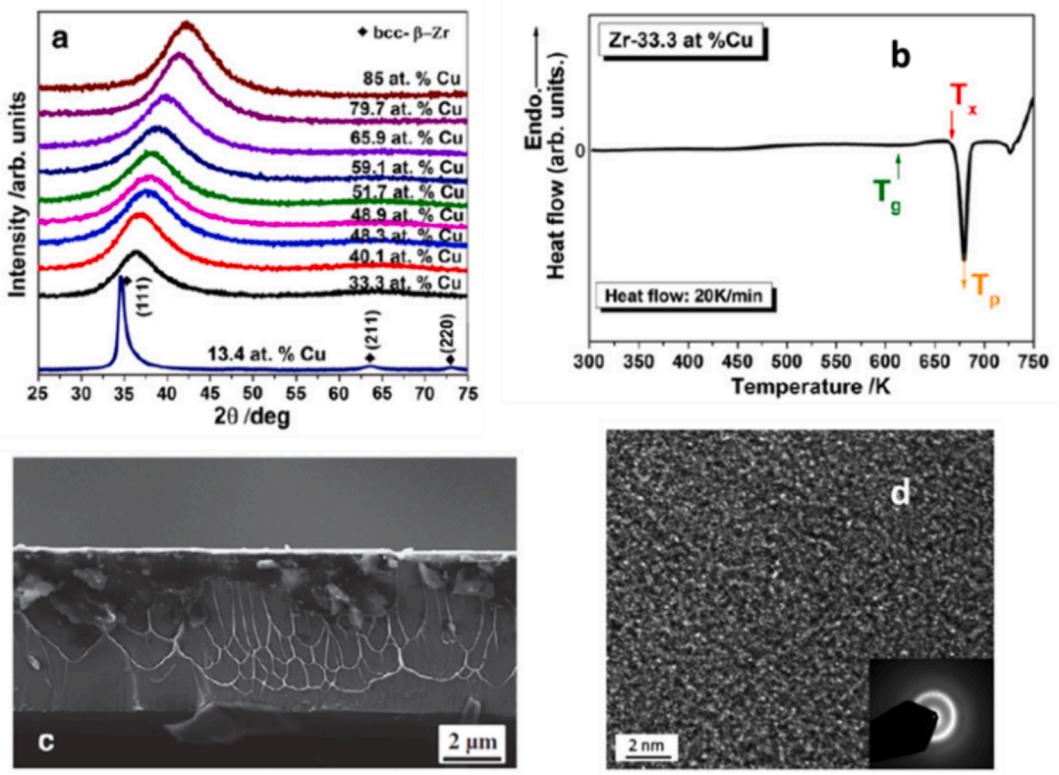

Fig. 5. Multiscale characterization of a Zr-Cu TFMG: global characterization by (a) XRD and (b) DSC and more local analysis (c) by SEM (vein-like features) and (d) TEM [51].

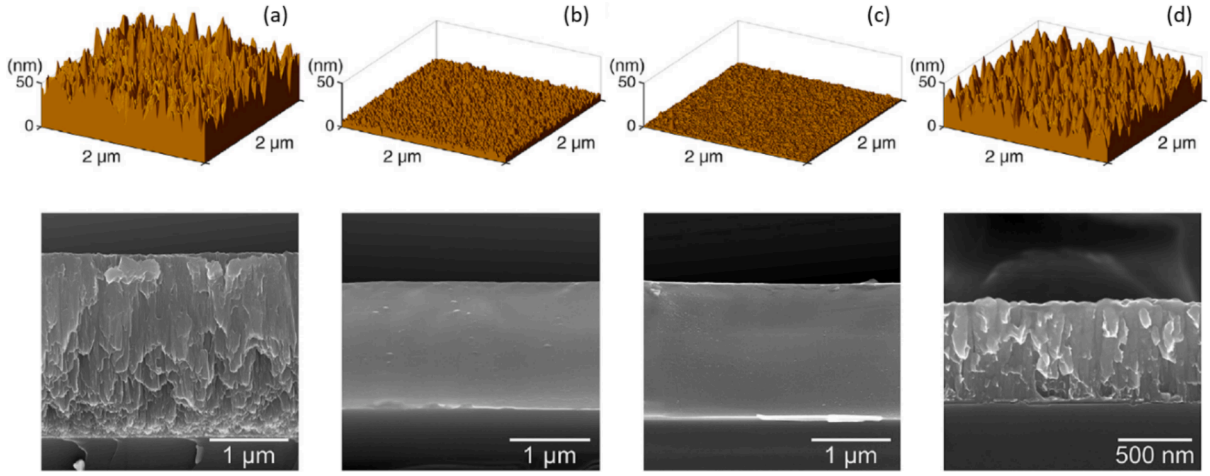

Fig. 6. Atomic force microscopy (AFM) images and cross-sectional SEM images: a) pure Zr film, b) 49 at.% Cu–51 at.% Zr TFMG, c) 69 at.% Cu–31 at.% Zr TFMG, d) pure Cu film [56].

structures like cell walls, capsules, pili, or flagella [58]. Prokaryotic cells are divided into two groups: the archaea and bacteria. The former do not exhibit any pathogenicity, contrary to the latter; thus, only bacterial cells are described here. Some bacteria can be pathogenic [59]. In humans, the symptoms of a bacterial infection are similar to those of a viral infection (skin rash, cough, runny nose, watery eyes, fatigue, nausea, fever, and muscle aches). Sometimes, they can even be fatal for fragile or untreated patients. Certain bacteria regularly cause hospital-acquired infections (HAI), *i.e.* infections contracted during a stay in a healthcare institution. The most frequently identified bacteria involved in a nosocomial infection are *Escherichia coli* (*E. coli*), *Staphylococcus aureus (S. aureus)*, and *Pseudomonas aeruginosa*.

According to a 2011 World Health Organization (WHO) report, HAIs are directly responsible for 37,000 deaths in Europe and contribute to an additional 110,000 indirect deaths as they weaken the body [60]. This represents 16 million additional days in the hospital and result in an estimated annual cost of €7 billion. The numbers are similar in the United States. Considering that many low- and middle-income countries (developing countries) do not have any HAI surveillance system, the number of deaths caused by HAIs is unknown. However, given the difficulties in accessing high-level healthcare, the HAI-induced death may be high. Overall, hundreds of millions of patients are estimated to be affected worldwide, resulting in very high human and economic losses.

Bacteria vary greatly in size and shape. Typical bacterial cells are

between 0.5 and 5 μm in length. They are usually divided into two groups called gram-positive and gram-negative, which are easy to differentiate using a simple Gram stain technique. The categorization by Gram stain is related to the composition, thickness, and resistance of the membrane of the bacteria [61]. Gram-negative bacteria have a thin peptidoglycan cell wall surrounded by an outer membrane. Gram-positive bacteria do not have any outer membrane; rather, they possess multiple layers of peptidoglycan, providing thicker and more resistant protection [62]. Most bacterial species do not live individually but in complex communities, adhering to surfaces within a mucous gel called a biofilm [63].

In the literature focusing on the interactions between bacteria and surfaces, *E. coli* and *S. aureus* are the most studied prokaryotes, especially because they are common and can be responsible for HAI.

E. coli is a gram-negative bacterium in the shape of a 1.0–2.0 μm long cylinder, with a radius of approximately 0.5 μm (see Fig. 7a). It multiplies at temperatures between 7 °C and 50 °C, the optimum temperature being 37 °C. Some strains grow in acidic foods, up to a pH of 4.4, as well as in foods with a water activity of at least 0.95. Cooking destroys Shiga toxin-producing E. coli if the food is cooked through, the temperature reaching at least 70 °C all over [52]. E. coli is a dominant bacterium in the intestinal microbiota of humans and homeothermic animals from the first hours of life. Most strains are harmless or even beneficial to humans because they produce vitamin K or can prevent colonization of the intestine by pathogenic bacteria [2]. However, some serotypes can be pathogenic, as the Shigatoxin-producing E. coli. This strain can cause serious foodborne illnesses, such as cholecystitis, bacteremia, cholangitis, urinary tract infection (UTI), traveler's diarrhea, neonatal meningitis, and pneumonia [64]. The spread in the community of this kind of bacterium is unlikely; there is usually effective prophylaxis or treatment [50] and [51].

S. aureus is gram-positive, spherical shaped with a smooth surface, and has a diameter ranging from 0.5 to 1.5 μm (see Fig. 7b) [65]. They are rounded gram-positive cocci about 1 μm in diameter, immobile, devoid of spores and they have a polysaccharide capsule. They appear in clusters called "bunch of grapes", they can also be isolated, in pairs or in very short chains. Colonies formed aerobically are golden yellow pigmented and opaque and about 4 mm in diameter. *S. aureus* is a preferential facultative anaerobic bacterium, and grows well on minimum media (basal media). It is a mesophilic (optimal growth 37 °C), neutrophilic (optimal pH 7) and halophilic (grows at high concentrations of NaCl) bacteria. It is also relatively resistant to bacterial inhibitors such as crystal violet and potassium tellurite. This is a bacterium that can usually be found on the skin or in the nostrils of people. Generally harmless in healthy people, *S. aureus* can sometimes cause infections. These are then treated with an antibiotic. Health care facilities, especially hospitals, are places prone to infections caused by *S. aureus*. Indeed, the installation of venous catheters or urinary catheters or surgeries are interventions favoring the entry of the bacteria into the blood and wounds. This bacterium usually causes skin infections, bacteremia, endocarditis, pneumonia, and food poisoning. *S. aureus* has the ability to develop strong resistance to antibiotics (especially methicillin) which vary depending on the strain [54], making it difficult to treat with drugs [66]. These bacteria are called methicillin-resistant *Staphylococcus aureus*, also called MRSA. The risk of being exposed to MRSA is greater in healthcare settings. However, strains of MRSA are present in the community and can be transmitted in groups of individuals who have close contact with each other, for example athletes practicing contact sports or injection drug users. MRSA is mainly transmitted by direct contact with the contaminated hands of a carrier or infected person or those of healthcare personnel or with contaminated surfaces and objects. A person can remain a carrier of MRSA for several months and sometimes even for a few years [56].

3.2. Eukaryotic cells

Eukaryotic cells are more complex than bacteria (prokaryotic cells) because they have a nucleus containing the DNA and some other organelles, which are basically the organs of the cell. Among these organelles and in addition to the nucleus, the endoplasmic reticulum, Golgi apparatus, mitochondria, and flagella can be mentioned, although there are several other components whose existence depends on the role and complexity of the cell [59]. The term "eukaryote" also includes multicellular and very complex organisms such as animals, plants, and fungi, which is why the simple term "cell" is generally used to refer to the eukaryotic organisms in microbiology. These cells tend to be larger than the usual bacteria, with a size generally between 10 and 100 μm.

There are more than 10,000 different species of cells, each with a specific role in various living organisms. However, when biomaterials are discussed, it is necessary to focus on a few types of cells that can be easily cultured, stored, and observed. In the literature, the following microorganisms are the ones that are mainly used for *in vitro* surface studies [69]. These cells are listed according to their order of prevalence in the literature cited throughout our review.

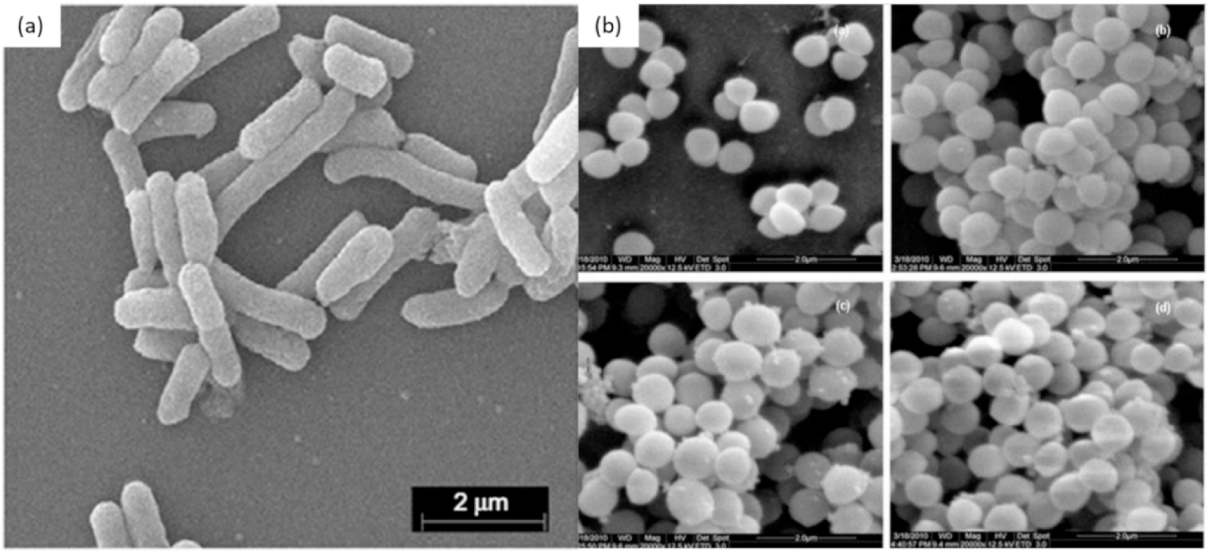

Fig. 7. SEM images of: a) E. coli[67] and b) S. aureus at different biofilm growth stages[68].

- Pre-osteoblastic cell line MC3T3-E1, coming from mouse calvaria (upper part of the skull). These cells have the ability to differentiate into osteoblasts (which synthesize, mineralize, and renew the bone matrix), and they form calcified bone tissue *in vitro*. MC3T3-E1 is often used to observe the cell/material interactions [70,71].
- Human osteosarcoma cell line MG63 (usually called osteoblast-like cells), coming from an osteosarcoma (cancerous bone tumor) of a 14-year-old male. These cells are derived from cancerous tumors but do not have the potential to create tumors on their own. The advantage of using MG63 is that they proliferate relatively rapidly [72].
- Fibroblasts L929, coming from the subcutaneous areolar adipose tissue of a mouse. This is the oldest continuous cell line (1948 by Earle). They have the advantage of being easily cultured and are often used for cytotoxicity testing [73].
- Human mesenchymal stem cells (hMSCs), coming from fetal tissues or some adult tissues (especially from the bone marrow). Human MSCs can differentiate into several different cell types (multipotent behavior) and are therefore ideal for monitoring the integration of implants into the biological environment [74,75].
- Primary human osteoblasts (hOBs), coming from femoral trabecular bone tissue (knee or hip joint). They can produce a collagen rich extracellular matrix during *in vivo* testing [76].
- Human umbilical vein endothelial cells (HUVECs), coming from the endothelium of veins from the umbilical cord. They are fairly low cost and can easily be isolated and cultured in a laboratory [77].
- Saos-2 is a human osteosarcoma cell line that presents osteoblast-like properties (differentiation & mineralization). They can be cultured shortly in large amounts, are well-characterized, and are often used to monitor the events related to the late osteoblastic differentiation stage [78].
- NIH 3 T3 mouse embryonic fibroblast cells, which are easy to grow and often used to observe adhesion, proliferation, and migration on surfaces [79].
- Primary mesenchymal stromal cells (BMSCs), HOS, U2, human adipose-derived stromal cells (hADSCs), human gingival fibroblasts (HGFs)…

Considering the influence of the cells size with respect to the surface topography on their adhesion and concomitant development (see Chapter 6), it is important to have in mind the approximative dimensions of the different types of cell, reminded here: MC3T3-E1, MG63 and hOBs: 20–50 μm; L929: 5–10 μm; HUVECs: about 15 μm; hMSCs:15–30 μm and NIH 3 T3: about 20 μm in diameter.

Studies on biomaterials aim to prove that a living organism can integrate and tolerate them, for example by adhesion of cells such as those mentioned above. In the biomaterial field, some specific terms need to be clearly defined. For instance, biocompatibility is achieved when the biomaterial fulfills its function without causing any harmful effect to the living tissues. Biocompatibility is defined as the absence of several components: cytotoxicity (direct damage of the cell), genotoxicity (damage of genetic material), mutagenicity (induction of permanent changes in the genetic material, causing DNA or RNA mutations), carcinogenicity (cancer formation), and immunogenicity (provocation of an immune response) [80]. It is worth mentioning that, in some biomaterial studies, the term “biocompatibility” is sometimes used to refer to cytocompatibility. Most studies on biomaterials consist of observing their cytotoxicity (or cytocompatibility), *i.e.* the survival rate of cells on their surface. Good cytocompatibility means that the cell can continue to perform its intended functions. Following the ISO 10993–5 standard, a reduction of cell viability by more than 30 % corresponds to a cytotoxic effect [81]. When an eukaryotic cell adheres to a surface, it tends to flatten in order to maximize the contact area with the substrate, as observed in Fig. 8. This behavior is visible as a simple evidence of the good cytocompatibility of the surface. After adhesion, the cell may migrate. It uses filopodia (thin projected filaments), which are used as antennae to probe the surrounding environment. The stimulus of filopodia through satisfactory signals (mechanical, chemical, electrical…) leads to the displacement of the cell. The proliferation of cells is induced by mitosis. A single cell has the ability to replicate itself into two new identical cells. This process allows the replacement of dead cells and induces an increase of the cell population.

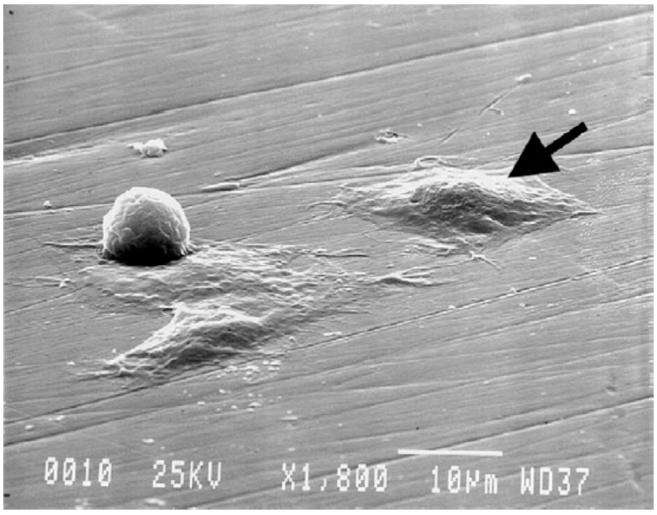

Fig. 8. SEM image of MC3T3-E1 cells at various stages of adherence on titanium substrate. The round cell is detached from the substrate, whereas the flattened ones are well attached [69].

4. Biological behavior of untextured metallic glass surfaces

This chapter addresses the biological behavior of various metallic glass systems reported in the literature for which the surface has not been textured. Antibacterial and biocompatibility properties are discussed, and conclusions on interesting metallic glass compositions are given.

4.1. Antibacterial activity

This section aims to provide an overview and a critical review of the various studies performed in recent years on the antibacterial activity of metallic glasses. Table 1 provides the compositions studied and in which form (BMG or TFMG), the bacteria and analytical methods used, the antibacterial properties and their proposed origin, and the corrosion resistance of the alloy when it was studied. The publications are listed in chronological order.

Some trends can be deduced from Table 1. The majority of metallic glasses are Zr-based and contain a significant amount of Cu. The secondary elements include Ti, Ag, Al, and Ni. Marginal amounts of Ta, Si, and Co are also added to some alloys. The interest of adding elements like Cu, Al, Ni or Be is often to improve the GFA of the metallic glasses thanks to the smaller atomic sizes of these elements allowing a more disordered state [1]. Compositions devoid from Cu or Ag have very poor antibacterial properties, indicating the necessity of at least one of these elements. However, a high Cu concentration is not sufficient on its own to achieve a strong bactericidal effect [90]. Most papers attribute the antibacterial properties to a release ion phenomenon, usually of Cu or Ag or even Al. The low surface roughness of TFMGs is also cited as a favorable bactericidal factor. In fact, TFMGs are characterized by a very smooth surface (Ra roughness most often below 10 nm), which is especially linked to the sputtering deposition process, leading neither to grain boundaries, nor to preferential columnar growth [54,56,84]. This low roughness contributes to a good hydrophobicity of the surface, affecting the bacterial adhesion and biofilm formation [20], which is commonly called antifouling. As an example, a study on Zr-Cu-Ti TFMGs

Table 1
Summary of metallic glasses studied for antibacterial applications.

Composition	BMG TFMG	Bacteria (gram)	Analysis technique	Results (AR = antibacterial rate)	Proposed mechanism	Corrosion resistance	Ref. Year
$Zr_{53}Cu_{33}Al_9Ta_5$ (ZrCuAlTa) $Cu_{48}Zr_{42}Ti_4Al_6$ (CuZrTiAl)	TFMG	*E. coli* (−) *S. aureus* (+)	Plate counting	*E. coli*: AR = 96 % for ZrCuAlTa; 98 % for CuZrTiAl *S. aureus*: AR = 98 % for ZrCuAlTa; 47 % for CuZrTiAl	Metallic ion releaseHydrophobic surface		[82] 2014
$Zr_{51.4}Cu_{29.5}Ni_{12.3}Al_{6.8}$ $Zr_{52.0}Cu_{29.3}Ni_{12.0}Al_{6.7}$ $Zr_{52.2}Cu_{29.2}Ni_{11.7}Al_{6.9}$ $Zr_{51.3}Cu_{29.6}Ni_{12.2}Al_{6.9}$ $Zr_{51}Cu_{30.9}Ni_{11.1}Al_{7.0}$	TFMG	*E. coli* (−) *S. aureus* (+)	Plate counting	Fully bactericidal	Surface roughness Hydrophobic surface Cu-ion release		[83] 2014
$Al_{48}Ag_{37}Ti_{15}$ (AlAgTi) $Zr_{54}Ti_{35}Si_{11}$ (ZrTiSi) $Zr_{59}Ti_{22}Ag_{19}$ (ZrTiAg)	TFMG	*E. coli* (−) *S. aureus* (+) *P. aeruginosa* (−)	Plate counting	ZrTiSi: poor bactericidal effectAlAgTi & ZrTiAg: high bactericidal effect	Ag-ion release		[84] 2014
$Zr_{44.0}Cu_{38.5}Al_{11.0}Ag_{6.5}$ (Zr1) $Zr_{43.2}Cu_{39.8}Al_{10.6}Ag_{6.4}$ (Zr2) $Zr_{41.4}Cu_{43.7}Al_{8.4}Ag_{6.5}$ (Zr3) $Zr_{42.7}Cu_{41.8}Al_{8.6}Ag_{6.9}$ (Zr4)	TFMG	*E. coli* (−) *P. aeruginosa* (−)	Growth area	*P. aeruginosa*: complete inhibition in 24 h *E.coli*: complete inhibition in 24 h for Zr1 & Zr2	Low roughnessCu- & Ag-ion release		[85] 2014
$Zr_{55}Cu_{30}Al_{10}Ni_5$ $(Zr_{55}Cu_{30}Al_{10}Ni_5)_{99}Y_1$	BMG	*S. aureus* (+)	Plate counting	Low bactericidal effect	Cu-ion release		[86] 2014
ZrCuAlAg 20–55 %Zr 30–38 %Cu 8–40 %Al4-25 %Ag	TFMG	*E. coli* (−)	Optical density	High ($Zr_{38}Cu_{36}Al_{18}Ag_8$) to low ($Zr_{23}Cu_{36}Al_{29}Ag_{12}$) antibacterial activity	Cu- & Ag-ion release		[42] 2016
$Cu_{50}Zr_{44}Al_6$ (Cu1) $Cu_{53}Zr_{41.4}Al_{5.6}$ (Cu2) $Cu_{56}Zr_{38.7}Al_{5.3}$ (Cu3)	BMG	*E. coli* (−) *B. subtilis* (+)	Plate counting Time kill assay	Cu1: no bactericidal effect Cu2 & Cu3: complete inhibition in 250 min *E. coli* less resistant than B. subtilis	Cu+ & Cu2 + release		[87] 2017
$Zr_{39}Cu_{39}Ag_{22}$	TFMG	*S. aureus* (+)	Plate counting			Na_2SO_4, 10 g/L, pH = 6.6Good corrosion resistance	[88] 2017
$Zr_{52}Cu_{48}$ (Ag0) $Zr_{86}Cu_8Ag_6$ (Ag6) $Zr_{73}Cu_{16}Ag_{11}$ (Ag11) $Zr_{47}Cu_{28}Ag_{25}$ (Ag25)	TFMG	*E. coli* (−) *S. aureus* (+)	Plate counting	Fully bactericidal when % Ag ≥ 11 %	Cu- & Ag-ion release	Saline solution: Ag25: high corrosionAg11: good corrosion resistance	[89] 2018
$Cu_{85}Zr_{15}$	TFMG	*E. coli* (−) *S. aureus* (+)	Plate counting SEM	Mild bactericidal effect	Cu-ion release, partial lysis	Few pitting	[90] 2018
$Zr_{46}Ti_{40}Ag_{14}$ (ZrTiAg) $Zr_{46}Ti_{43}Al_{11}$ (ZrTiAl)	TFMG	*S. aureus* (+)	Plate counting	ZrTiAg: high bactericidal effectZrTiAl: low bactericidal effect	Low roughness High Ag & mild Al toxicity.Ion release	PBS & Na_2SO_4, 10 g/L, pH = 6.6 More corrosion resistantthan 316L SS & cp-Ti	[20] 2019
$Cu_{55}Zr_{40}Al_5$	BMG	*E. coli* (−)	Plate counting SEM	Mild bactericidal effect	Cu-ion releaseNo effect of roughness (Ra = 70–600 nm)		[91] 2019
ZrCuAg Zr/Cu: 65/35, 50/50, 35/651 % ≤ %Ag ≤ 16 %	TFMG	*E.coli* (−)	Live/Dead	Bactericidal when %Ag ≥ 12 % Resurgence of bactericidal properties when%Ag ≤ 4 % for Zr/Cu = 65/35	High Ag toxicity. Ion release Synergy between Cu & Ag when %Ag ≤ 4 % for Zr/Cu = 65/35	Higher corrosion when: Low Zr/Cu ratioHigh %Ag	[43] 2021
$Zr_{58.6}Al_{15.4}(Co_{1-x}Cu_x)_{26}$x = 0, 0.2, 0.3, 0.4, 0.5, 0.6, 0.7, 0.8	BMG	*E.coli* (−)	Plate counting	Fully bactericidal ($Zr_{58.6}Al_{15.4}Co_{18.2}Cu_{7.8}$)		PBS: Excellent corrosion resistance of $Zr_{58.6}Al_{15.4}Co_{18.2}Cu_{7.8}$	[92] 2021
$Zr_{53,7}Ti_{33,1}Si_{6,2}N_7$ $Zr_{45,5}Ti_{42}Si_{4,4}N_{8,1}$	TFMG	*E.coli* (−)	SEM	Not antibacterial: original structure of bacteria is maintained			[93] 2021
$Ti_{40}Zr_{10}Cu_{36}Pd_{14}$	BMG and TFMG	*Aggregatibacter actinomycetemcomitans* (−) Oral plaque	Live/Dead Plate counting SEM	Bactericidal effect seen after 24 h compared to the Ti-6Al-4 V	Cu-ion release Hydrophobic surface even after oxidation	SBF: formation of oxide layer leading to higher Ecorr and smaller Icorr	[94] 2022

highlights the correlation between the surface roughness, its affinity with water and the bacterial adhesion [95]. It is clearly shown that the bacteria population significantly decreases for smoother surfaces and higher water contact angles.

In terms of bacteria, *E. coli* and *S. aureus* are the most commonly used. Given the difference in membrane thickness, it is important to test the antibacterial properties on both gram-positive and gram-negative bacteria. The majority of the studies have been carried out on TFMGs, which may be linked to the difficulty of synthesizing large BMGs, making the use of TFMGs in the medical field more plausible than that of

BMGs. Studies on corrosion resistance are emerging in the most recent research. Indeed, the satisfactory antibacterial properties of metallic glasses bring them closer to use for medical applications, and it has thus become essential to measure their corrosion resistance, ideally in simulated body fluid.

To evaluate the ideal compositions for antibacterial applications, it is necessary to define the interest and effect, positive as well as negative, of the various metallic elements used in the compositions in Table 1.

Ag: Very good antibacterial properties on many organisms. The human body is marginally affected by the absorption of silver in the blood when it remains under a certain threshold (otherwise risk of argyria), and the element is easily eliminated by the body. Often used in medicine as an alloy, for example for catheters. Biocompatible in small amounts; the main drawback is its high cost [93].
Al: Clearly toxic at high concentration; thus, its percentage in the alloy must remain low, as in the conventional Ta–6Al–4 V alloy. Non-carcinogenic but sometimes associated with Alzheimer's disease. Biocompatible in small amounts but to be avoided when possible [93].
Be: Causes toxic reaction with human body, added to improve GFA [1].
Co: Sometimes used as a supplement in some implant alloys. Rapidly eliminated by the organism but can remain there for many years in the case of punctual overdose. Biocompatible in small amounts [93].
Cu: Known for its intrinsic antimicrobial properties against many microorganisms (bacteria, viruses, or fungi). Used among other things on hospital knobs and anything else that is regularly touched. Generally low toxicity but too high concentrations can lead to poisoning. Copper is widely used for intrauterine devices (IUDs) but is not recommended for people with liver and kidney problems [96].
Ni: Often added to improve corrosion resistance. However, many people have a sensitivity to nickel, which can lead to inflammation. Can become toxic even at low concentrations. Element to avoid [93].
Si: Causes respiratory problems in powder form. However, in the context of an implant, it is relatively inert, but some studies have shown its positive effect on bone formation and corrosion resistance [97].
Ta: Biocompatible but slightly expensive and uncommon. Can increase corrosion resistance [98].
Ti: Biocompatible, regularly used in biomedical applications for decades thanks to its good corrosion resistance to body fluids and light weight [96].
Zr: Biocompatible, often used in dentistry for its good mechanical properties and outstanding corrosion resistance [43].

However, it is necessary to examine the nuances of the effect of these metals of the human body. Indeed, the vast majority of studies regarding the toxicity of these elements have been performed on crystalline materials. Metallic glasses have an amorphous structure and are thus potentially less prone to corrosion and therefore to ion release. For future studies, it would be ideal to perform measurements of ion release in simulated body fluid to quantify ion release and thus to define potential toxicity levels. The matter of the biocompatibility of metallic glasses has been extensively studied, as highlighted in the following section.

4.2. Biocompatibility

This section details different metallic glass systems that exhibit cytocompatibility or biocompatibility. Two types of metallic glasses can be distinguished for biomedical applications: (1) bioinert compositions that remain intact in contact with the biological environment or that exhibit an ion release so low that it is not considered harmful, and (2) biodegradable metallic glasses, which are extremely interesting in the context of implants that would not need to be removed later (these metallic glasses can be resorbed in the organism once their goal is fulfilled, without any toxicity).

4.2.1. Bioinert

Bioinert metallic glasses are particularly interesting for biomedical applications, such as implants and surgical devices. Because of the prolonged contact of these medical objects with the human body, it is necessary to develop metallic glass compositions that do not (or only very slightly) degrade over time. The metallic glass must also not be harmful to human cells. Table 2 summarizes several compositions whose biocompatibility properties were observed, either as a BMG or TFMG. The type of cells used for the cytocompatibility tests as well as the various analysis techniques used are reported. The *in vitro* results, and *in vivo* results when performed, are briefly described as well as the corrosion resistance of these compositions.

Table 2 shows that the majority of the bioinert metallic glasses studied are Zr-based. There are also several Ti-based ones, whereas Fe-based ones are marginal. Studies of metallic glasses in the form of TFMGs became more prevalent in recent years. Indeed, it is essential to move toward thin films, especially for large implants and surgical tools. Studies on BMGs remain relevant, for example for direct applications such as small implants. It would be extremely interesting to perform research to determine if a BMG and TFMG of the same chemical composition have identical biological properties. Several different cells are used for *in vitro* cytocompatibility testing. MC3T3-E1 cells tend to be slightly more popular.

There are several levels of cytocompatibility assessment depending on the study. The vast majority of studies monitor the evolution of cell viability as well as the cell morphology. This is indeed the first step to obtain information about the cytocompatibility of the surface, as described in the ISO 10993–5 standard. However, to date, there are too few articles investigating the cytocompatibility properties in depth. From an animal welfare perspective, it is preferable to define the biocompatibility of a material as much as possible through *in vitro* tests before moving on to *in vivo* trials. Furthermore, because the final goal is to produce implants and surgical tools for humans, the biological properties of promising compositions must be fully known. To achieve this goal, several analyses can be conducted before the *in vivo* tests, *i.e.* hemolysis, cell mineralization, toxicology of leachable extracts, or cell gene expression. Several studies have already conducted *in vivo* tests. The results are very promising, as the implants were shown to be corrosion resistant and did not cause inflammation or affect the blood composition and thus possess good biocompatibility. According to Table 2, only two studies have evaluated a TFMG tested *in vivo* [113,118]. The TFMG didn't exhibit clear indications of toxicity, there were no erythema or oedema observed during intracutaneous (intradermal) reactivity test for dermal reactions. But the behavior of the material was not very good, as it exhibited a low bone affinity despite good cytocompatibility *in vitro*[113]. As its composition is similar to that of some BMGs with a good *in vivo* response, it is possible that the very low roughness of the TFMG may generate this unsatisfactory result. In this case, it would be necessary to texture the surface of the TFMGs to improve their bone affinity, for example by a laser post-irradiation treatment, as developed in Chapter 6.

To ensure the biocompatibility of a metallic glass, it is also necessary to evaluate its corrosion rate to ensure that it would not be harmful to human beings because of an excessive ion release. Fig. 9 presents the corrosion rate values (in μm/year) obtained for various bioinert metallic glasses as well as for some biocompatible materials regularly used in the medical field. The fluids used for the corrosion tests in Table 2 and Fig. 9 are saliva, simulated body fluid SBF (mineral composition similar to that of blood plasma: 142 mM Na^+, 5 mM K^+, 1.5 mM Mg^{2+}, 2.5 mM Ca^{2+}, 103 mM Cl^-, 27 mM HCO^{3-}, 1 mM HPO_4^{2-}, and 0.5 SO_4^{2-}), phosphate-buffered saline PBS (137 mM NaCl, 2,7 mM KCl, 8 mM Na_2HPO_4, and 2 mM KH_2PO_4, pH = 7.4), and Hank's balanced salt solution HBSS (140 mM NaCl, 5 mM KCl, 1 mM $CaCl_2$, 0.4 mM $MgSO_4{\cdot}7H_2O$, 0.5 mM

Table 2
Summary of bioinert metallic glasses studied for biocompatible applications.

Composition	BMG TFMG	Cells	Analysis technique	*In vitro* results	*In vivo* results	Corrosion resistance	Ref. Year
Zr-Ti-Co-Be Pd-Ag-P-Si	BMG	L929	ISO 10993–5 (Test on extracts)	Cytocompatible	Non-irritant Pd-Ag-P-Si: biocompatible		[99] 2010
$Zr_{60.14}Cu_{22.31}Fe_{4.85}Al_{9.7}Ag_3$	BMG	MG63	Cell Counting Kit-8	Cytocompatibility (88 % after 5 days)		SBF: Higher than Ti6Al4V and pure Zr	[100] 2013
$Zr_{61}Cu_{25}Al_{12}Ti_2$	BMG	HUVECs	Cell Counting Kit-8 qPCR Blood analysis Mucosa irritation test	Cytocompatible High gene expression of VEGF & vWF	Small amount of inflammatory cells Normal blood analysis Biocompatible		[101] 2014
$Zr_{46}(Cu_{4.5/5.5}Ag_{1/5.5})_{46}Al_8$ $Zr_{51.9}Cu_{23.3}Ni_{10.5}Al_{14.3}$ $Zr_{51}Ti_5Ni_{10}Cu_{25}Al_9$ $Ti_{40}Zr_{25}Ni_{12}Cu_3Be_{20}$	BMG	L929	MTT assay Optical density SEM & EDX	Cytocompatible	ZrCuAlAg: No inflammation High bone attachment Biocompatible	HBSS: High Highest for ZrCuAlAg	[102] 2015
$Zr_{62.5}Al_{10}Fe_5Cu_{22.5}$	BMG	HAECs HASMs	LIVE/DEAD	Cytocompatible		PBS: High	[103] 2015
$Zr_{48}Cu_{36}Al_8Ag_8$	TFMG	L929	LIVE/DEAD	Cytocompatible		SBF: High	[104] 2015
$Ti_{40}Cu_{36}Pd_{14}Zr_{10}$	TFMG BMG	L929 Human gingival fibroblast cells (HGF)	LIVE/DEAD MTT assay	Cytocompatibility (>80 %)		SBF: High	[105] 2015 [94] 2022 [106] 2017 [107] 2017
$Ti_{47}Cu_{38}Zr_{7.5}Fe_{2.5}Sn_2Si_1Ag_2$	BMG	MC3T3-E1	SEM Image processing	Cytocompatible		SBF: Higher than Ti-6Al-4 V	[108] 2015
$Fe_{60}Cr_{10}Mo_{10}P_{13}C_7$ $Fe_{50}Cr_{20}Mo_{10}P_{13}C_7$ $Fe_{55}Cr_{20}Mo_5P_{13}C_7$	BMG	NIH 3 T3	Cell Counting Kit-8 SEM	Cytocompatible		HBSS & saliva: High, similar to Ti-6Al-4 V	[109] 2015
$Ti_{40}Cu_{34}Pd_{14}Zr_{10}Sn_2$	BMG		Blood analysis SEM & EDX		No inflammation High bone attachment No diffusion of ions Biocompatible		[110] 2015
$Zr_{65}Al_{7.5}Ni_{10}Cu_{17.5}$	BMG		Blood analysis SEM & EDX		No increase of Cu & Ni in blood No inflammatory cells No corrosion	No pitting corrosion	[111] 2016
$Zr_{50}Ti_{32}Cu_{13}Ag_5$ $Zr_{40}Ti_{37}Co_{12}Ni_{11}$	TFMG	MC3T3-E1	MTS assay test	Cytocompatible		PBS: Higher than 316SS and cp-Ti	[112] 2019
$Zr_{48}Cu_{36}Al_8Ag_8$	TFMG BMG	MC3T3-E1 L929	Cell Counting Kit-8 Platelet adhesion test μCT SEM	Hemocompatible Cytocompatible Mineralization	Slow osseointegration Bone implant contact = 15.32 % Small portion of cells survived after 24 h, <5% after 5 day (cytotoxic)	SBF: Higher than pure Ti Cu ion release of > 20000 ppb after 1 day and 80000 ppb after 3 days and release of Al, Zr and Ag.	[113] 2020 [107] 2017
Ti-Cu-Pd-Zr:B %B = 0, 4, 8, 14	TFMG	MC3T3-E1	MTT assay Platelet adhesion test Fluorescence microscopy	Hemocompatible Cytocompatible		SBF: Higher for 8 % B	[37] 2021
$Ti_{47}Cu_{40}Zr_{7.5}Fe_{2.5}Sn_2Si_1$ $Ti_{47}Cu_{38}Zr_{7.5}Fe_{2.5}Sn_2Si_1Ag_2$ $Ti_{48}Cu_{37}Zr_{7.5}Fe_{2.5}Sn_2Si_1Ag_2$	BMG	MC3T3-E1	WST-1 assay	Cytocompatible Cell differentiation Mineralization		PBS: High	[114] 2021
$Fe_{50}Cr_{18}Mo_{10}C_{20}Si_2$	BMG	NIH 3 T3	MTT assay Hemolysis test	Hemocompatible Cytocompatible		HBSS: Higher than 316L SS	[115] 2022
$Zr_{40}Ti_{15}Cu_{10}Ni_{10}Be_{25}$ $Zr_{50}Ti_5Cu_{10}Ni_{10}Be_{25}$ $Zr_{40}Ti_{15}Cu_{10}Ni_5\ Si_5Be_{25}$	BMG	IMR90	MTT assay	Cytocompatible		SBF: Higher than Ti-6Al-4 V	[116] 2022
$Ti_{53}Cu_{36}Ni_{11}$	TFMG	C2C12 myoblasts.	LIVE/DEAD	Cytocompatible Proliferation of cells			[117] 2014
$Ti_{60}Nb_{15}Zr_{10}Si_{15}$	TFMG	Blood SaOS2 L929 MC3T3-E1	Hemolysis test LIVE/DEAD ISO 10993–05 MTT assay	Hemocompatible Cytocompatible Mineralization	No inflammation	SBF: Higher than the Ti6Al4V	[118] 2019
Zr-Ti-Fe 29,8 ≤ Zr ≤ 35,3 at.% 17,3 ≤ Ti ≤ 40,9 at.% 17,8 ≤ Fe ≤ 49,8 at.%	TFMG	MG-63 cells	MTS assay	Noncytotoxic			[119] 2017

(*continued on next page*)

Table 2 (*continued*)

Composition	BMG TFMG	Cells	Analysis technique	*In vitro* results	*In vivo* results	Corrosion resistance	Ref. Year
$Zr_{53,7}Ti_{33,1}Si_{6,2}N_7$ $Zr_{45,5}Ti_{42}Si_{4,4}N_{8,1}$	TFMG	Human gingival fibroblast cells (HGF)	SEM Live/Dead	Biocompatible (cell growing)			[120] 2021
$Ti_{47}Zr_{41}Si_{12}$ $Ti_{58}Zr_{33}Si_9$ $Ti_{66}Zr_{25}Si_9$ $Ti_{75}Zr_{19}Si_6$	TFMG	No cell involved	Bio-corrosion	Good bio-corrosion resistance, best one seems to be $Ti_{66}Zr_{25}Si_9$		SBF: Good resistance, better than	[1] 2014
$Zr_{54}Ti_{35}Si_{11}$	TFMG	MG63 L929	MTT assay Live/Dead	Hemocompatible Cell proliferation Cytocompatible		SBF: Good resistance	[121] 2023

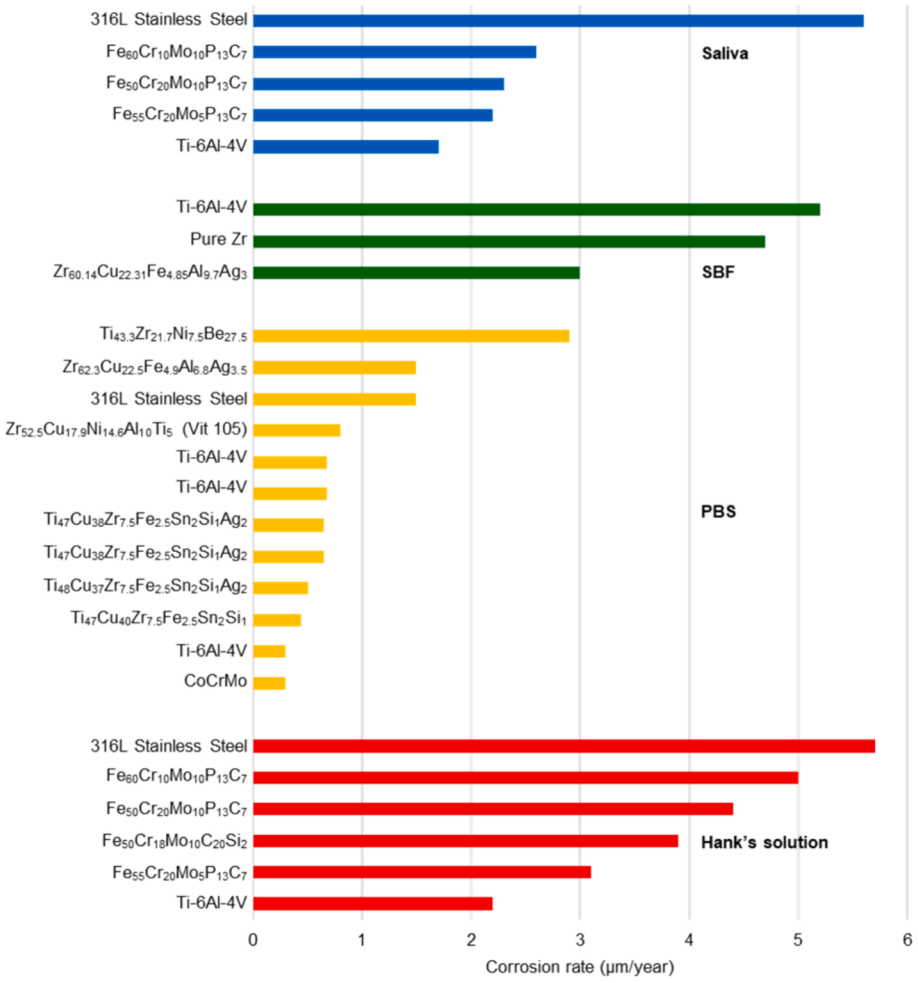

Fig. 9. Corrosion rate (μm/year) of various BMGs and materials commonly used in the medical field. Data obtained from [100,108,109,114,115,122,123].

MgCl2·•6H2O, 0.3 mM $Na_2HPO_4{\cdot}2H_2O$, 0.4 mM KH_2PO_4, 6 mM D-Glucose, and 4 mM $NaHCO_3$). All of these fluids were at 37 °C for the corrosion tests. SBF, PBS, and HBSS were the most widely used fluids for these experiments.

First of all, it should be noted that the corrosion rate of Ti–6Al–4 V differs depending on the solution used. It is therefore difficult to compare two metallic glasses that have not been tested in the same solution. However, they may be compared by observing their corrosion rate compared with that of Ti-6Al–4 V. Overall, all the metallic glasses studied have a low corrosion rate. Fe-based metallic glasses tend to exhibit more corrosion than Zr-based and Ti-based metallic glasses. Besides their use is limited owing to a too important mismatch between the mechanical properties of the bone (Young's modulus of about 200 GPa for Fe-based BMGs to compare with 20 for bones)[124]. Moreover Fe-based TFMGs could be more difficult to obtain via magnetron co-sputtering because of the magnetic property of Fe, making it not an ideal candidate for these TFMGs. Zr- and Ti-based metallic glasses have a corrosion rate close to or lower than that of Ti–6Al–4 V, except for $Ti_{43.3}Zr_{21.7}Ni_{7.5}Be_{27.5}$, which may be caused by the absence of Cu or high amount of Be. To obtain easily comparable results, it would be necessary to always perform the corrosion rate measurements in the same solution or in the three most commonly used solutions (SBF, PBS, and HBBS). Because SBF is the closest solution to the human organic environment, it is most likely the most representative of the actual corrosion rate that a bone implant would experience.

Zr-based and Ti-based metallic glasses appear to be the most

interesting for bioinert medical implants and tools. The presence of at least two elements among Zr, Cu, and Ti is an important condition because of their good biocompatibility and corrosion resistance. According to the data compiled in Table 2 and Fig. 9, the compositions that induce good cytocompatibility or biocompatibility properties obey the following law: at.% Zr + at.% Cu + at.% Ti $\geq$ 65 %. Ti-based metallic glasses may be the most promising and simple to implement in practice, given that many of the implants currently used are already Ti-based, e.g., Ti–6Al–4 V. The biocompatibility of potential alloying elements for Ti-based metallic glasses has been previously reviewed in the literature [125]. The presence of Pd provides good biocompatibility; however, it is relatively expensive and should thus be avoided [126]. Because of safety concerns, some other elements should also be avoided, including Ni and Be, or limited like Al. Moreover, cytocompatible compositions without these elements are achievable [127]. Quaternary alloys are interesting to study, as they can be synthesized in the form of TFMGs, especially by adopting the combinatorial approach. The biological applications of these metallic glasses restrict the possible compositions, which makes TFMGs even more interesting compared with BMGs, as their rapid quenching allows for a wider range of compositions. However, sputtering on complex shapes is difficult, and it remains to be defined whether the *in vitro* and *in vivo* biocompatibility properties of a BMG and TFMG of the same composition are similar.

4.2.2. Biodegradable

There is less scientific work exploring biodegradable metallic glasses compared with bioinert ones. Most of the studied compositions are Mg-based and contain elements such as Zn, Ca, and Sr as well as rare earths. There are also some metallic glasses that are Ca-based, Zn-based, and Sr-based. These compositions are studied for low and mild load bearing implants that could be harmlessly absorbed by the human body once their goal is fulfilled. Table 3 summarizes the compositions studied and their shape (BMG or TFMG), the cells used for the cytocompatibility tests, the analysis techniques used, and the *in vitro* and *in vivo* results.

Several trends can be identified in Table 3. Recently, Mg-based metallic glasses have been the most studied for biodegradable implants. There are also Ca-based metallic glasses and, to a lesser extent, Sr-based metallic glasses. The most frequently studied system is Mg–Zn–Ca, which is composed of inexpensive elements and whose biodegradability is already well known. Moreover, Ca and Mg are already naturally present in large quantities in the human body (approximately 1100 and 25 g, respectively [151]). A metallic glass in the form of a TFMG was studied in only one of the papers discussed in Table 3; therefore, many of the properties of biodegradable TFMGs remain to be explored.

The cytocompatibility of studied systems is not necessarily estimated, most likely because they are considered to be biocompatible regarding their composition. In fact, some articles only address the dissolution of the metallic glass and the release of H_2, which are also important criteria. The dissolution rate is used to estimate the lifetime of an implant according to its dimensions (often given in mm/year). The release of H_2 is a well-known problem of Mg dissolution, which produces H_2, becoming harmful by creating subcutaneous gas bubbles.

Fig. 10 compares the corrosion rate (in mm/year) of biodegradable metallic glasses in various solutions. These solutions include the previously presented ones (SBF, PBS, and HBSS), 0.05 M Na_2SO_4, and Ringer's solution (125 mM NaCl, 1.5 mM $CaCl_2{\cdot}2H_2O$, 5 mM KCl, and 0.8 mM Na_2HPO_4 [152]). These solutions were maintained at 37 °C for the experiments.

On average, biodegradable metallic glasses have a corrosion rate that is 1000 times greater than that of bioinert metallic glasses (Fig. 9). For bioinert metallic glasses, the results differ depending on the solutions used for the corrosion rate tests. Here again, it would be preferable to perform them in several solutions, or always in SBF, to easily compare the different compositions studied. For Ca-based metallic glasses, it is possible to strongly vary the corrosion rate only through small variations of compositions.

Among the biodegradable metallic glasses, the Mg–Zn–Ca system stands out because it exhibits very good biocompatibility and its elements are present in great quantity in the human body. Compositions containing Sr are also possible. Elements such as Li or Yb are sometimes added to metallic glasses. Although these elements are biocompatible, they are rather expensive, and their presence does not lead to more efficient biodegradable materials than those of the ternary system Mg–Zn–Ca. This system has been studied extensively and offers excellent biocompatibility, as proven through *in vivo* trials. Adding the low cost of the raw materials, this system is very interesting for low and mild load bearing biodegradable implants. Exploration of the Mg–Zn–Ca system remains ongoing, and studies on the best glass-forming compositions have already been conducted [157,158]. For further information on Mg-based BMGs, including the synthesis process and mechanical properties, Bin *et al.* published a review on the recent developments of these systems [159].

The TFMG which aims to be biodegradable requires good biocompatibility, adequate corrosion kinetics combined with good mechanical properties.

To study the biocompatibility, it is important to consider its cytotoxicity, absorbability and bone-regeneration capacity. In terms of osteointegration, the activity of osteoblasts, which indicates bone formation, and the activity of osteoclasts, which indicates bone resorption, are important to take into account. As the TFMG should be resorbable it has to have a certain rate of corrosion in relation to the rate of bone generation. Also, the product issued of this corrosion should not be harmful for the human body. To ensure human tolerance the H_2 gas evolution from the degradation of the implant must be lower than 0.01 $mL/cm^2/day$. The desired corrosion rate of biodegradable implants is 0.5 mm/y in simulated body fluid (SBF) at 37 °C, whereas 0.2 to 0.5 mm/year is considered a suitable corrosion rate *in vivo*. However, depending on the application, the corrosion rate can require to be different and this corrosion rate depends on the materials and the implant characteristics (size, stress-condition, microenvironment). Similarly, the corrosion of screws should not reduce their cross-section by more than 5 %, providing a maximum acceptable corrosion rate of 0.4 mm/year. In addition, the bio-functionality of the implants must be confirmed through cell-adhesion, cell-spreading, and cell-proliferation tests [160].

In terms of mechanical properties these films should have properties close to the bones' ones, especially to ensure a good osseointegration. These recommended key-properties can be found in Table 4 [160]. However, these characteristics are, most often, not all tested in published studies. If we refer to BMGs mentioned in Table 3 for instance, it is worth mentioning that the compressive (or tensile) strength criteria is most of the time validated. Moreover, concerning TFMGs, biodegradable films are part of the light-metallic glass family, characterized by similar densities of the one of bones [140,141]. In addition, Young's modulus of Mg, Zn or Ca-based TFMGs are quite low compared to conventional non-biodegradable TFMGs [145,146]. Among all required parameters, the elongation is by far the most difficult to fulfill, even if metallic glasses are known for their significant elongation before rupture (in the range of several %) [129,130]. This characteristic has nevertheless not to be strictly considered as limitative for the bone reconstruction application, since, in that case, discontinuous porous materials are expected.

5. Effect of surface texture on biological behavior

Despite all the studies performed on numerous metallic glass systems, there are still no perfect compositions that achieve both biocompatibility and antibacterial behavior. The main problem is that the increase in antibacterial properties is related to ion release, which compromises the biocompatibility. Surface texturing may be a potential solution to this problem. The idea is to provide an antibacterial effect by modifying the surface topography [169], while the biocompatibility is

Table 3
Summary of biodegradable metallic glasses studied for biocompatible applications.

Composition	BMG TFMG	Cells	Analysis technique	*In vitro* results (DR = degradation rate)	*In vivo* results	Ref. Year
$Mg_{60+x}Zn_{35-x}Ca_5$ x = 0, 3, 6, 7, 9, 12, 14, 15	BMG		Hydrogen evolution Immersion test in Hank's, MEM, Ringer's and SBF solution	High Zr amount ($0 \leq x \leq 7$): Nearly no H evolution Corrosion rate between 0.1554 and 1.17 mm/year	$Mg_{60}Zn_{35}Ca_5$: No hydrogen evolution No inflammation	[128] 2009 [129] 2022
$Mg_{60+x}Zn_{34-x}Ca_6$ x = 0, 2, 4, 6	BMG		Immersion test in SBF and Ringer's solution	Corrosion rate between 0.06 and 1.67 mm/year		[130] 2018 [131] 2016
$Mg_{65+x}Zn_{32-x}Ca_3$ x = 0, 2, 4	BMG		Immersion test in Ringer's solution	Corrosion rate between 0.43 and 1.33 mm/year		[132] 2016 [130] 2018
$Mg_{65}Zn_{30}Ca_5$	BMG		Immersion test in MEM	Corrosion rate of 0.63 mm/year		[133] 2013 [134] 2013 [130] 2018
$Mg_{64+x}Zn_{32-x}Ca_4$ x = 0, 2, 3, 4, 5, 7, 8, 9	BMG		Immersion test in Hank's, PBS, Ringer's, SBF and MEM solution	Corrosion rate between 0.21 and 0.88 mm/year $Mg_{69}Zn_{27}Ca_4$		[135] 2019 [132] 2016 [136] 2015 [137] 2013 [138] 2019 [131] 2016
$Sr_{60}Mg_{18}Zn_{22}$ $Sr_{60}Li_{11}Mg_9Zn_{20}$ $Sr_{60}Li_5Mg_{15}Zn_{20}$ $Sr_{60}Mg_{20}Zn_{15}Cu_5$ $Sr_{40}Yb_{20}Mg_{20}Zn_{15}Cu_5$	BMG		Immersion test	$Sr_{40}Yb_{20}Mg_{20}Zn_{15}Cu_5$: no degradation Others: extremely fast degradation		[139] 2009
$Zn_{40}Mg_{11}Ca_{31}Yb_{18}$ (Zn) $Ca_{65}Mg_{15}Zn_{20}$ (Ca)	BMG		Immersion test	Zn: No degradation Ca: fully degraded in 2 days		[140] 2010
$Ca_{65}Zn_{20}Mg_{15}$	BMG	L929 VSMC ECV304 MG63	MTT assay Cytoskeleton organization Apoptosis ALP activity	Cytocompatibility at low concentration (<30 %) High ALP activity (linked to mineralization activity)	No inflammation Some osteolysis caused by rapid degradation	[141] 2011
$Ca_{65}Zn_{20}Mg_{15}$ $Ca_{48}Zn_{30}Mg_{14}Yb_8$ $Ca_{32}Zn_{38}Mg_{12}Yb_{18}$	BMG	MG63	MTT assay Immersion test	Cytocompatible Low H release rate Low DR = 0.25 mm/year		[142] 2011
$Ca_{57.5}Mg_{15}Zn_{27.5}$ $Ca_{55}Mg_{17.5}Zn_{27.5}$ $Ca_{52.5}Mg_{20}Zn_{27.5}$ $Ca_{52.5}Mg_{17.5}Zn_{30}$ $Ca_{52.5}Mg_{22.5}Zn_{25}$ $Ca_{50}Mg_{20}Zn_{30}$	BMG		Immersion test Hydrogen evolution Electrochemical testing	Rapid rate of dissolution Regulation of dissolution with Zn content Incongruent dissolution		[143] 2012
$Sr_{40}Mg_{20}Zn_{15}Yb_{20}Cu_5$	BMG	MG63	MTT assay Immersion test ALP activity	Cytocompatibility Good ALP activity Very low H_2 generation rate		[144] 2012
$Ca_{20}Mg_{20}Zn_{20}Sr_{20}Yb_{20}$	BMG	MG63	MTT assay Immersion test ALP activity Radiography and μCT	Cytocompatibility Cell differentiation	Bone formation Biocompatibility Slow degradation	[145] 2013
$Mg_{66}Zn_{30}Ca_4$ $Mg_{66}Zn_{29}Ca_4Ag_1$ $Mg_{66}Zn_{27}Ca_4Ag_3$	BMG	MC3T3-E1	MTT assay SEM Hydrogen evolution Immersion test in PBS solution	Cytocompatibility Lower H_2 generation with Ag Corrosion rate between 0.265 and 0.308 mm/year		[136] 2015
$Mg_{66}Zn_{30}Ca_4$ (Sr0) $Mg_{66}Zn_{30}Ca_3Sr_1$ (Sr1) $Mg_{66}Zn_{30}Ca_{2.5}Sr_{1.5}$ (Sr1.5)	BMG	MC3T3-E1	MTT assay SEM ALP activity	Cytocompatible Cell differentiation (for 5 % Sr1 only) Mineralization (for 5 % Sr1 only)		[146] 2016
$Mg_{65.2}Zn_{30}Ca_4Mn_{0.8}$	BMG		Immersion test in PBS solution	Corrosion rate of 2.40 mm/year		[147] 2018

(*continued on next page*)

Table 3 (*continued*)

Composition	BMG TFMG	Cells	Analysis technique	*In vitro* results (DR = degradation rate)	*In vivo* results	Ref. Year
$Mg_{64.9}Zn_{30}Ca_4Mn_{0.8}Sr_{0.3}$ $Mg_{64.7}Zn_{30}Ca_4Mn_{0.8}Sr_{0.5}$ $Mg_{64.4}Zn_{30}Ca_4Mn_{0.8}Sr_{0.8}$	BMG		Immersion test in PBS solution	Corrosion rate between 0.36 and 1.81 mm/year		[147] 2018
MgCaZn 35.9 % ≤ %Mg ≤ 63 % 4.1 % ≤ %Ca ≤ 21 % 17.9 % ≤ %Zn ≤ 58.3 %	TFMG	MG63	Cell viability (fluorescence microscope)	Higher Zn content = lower cell viability		[148] 2017
$Mg_{60}Zn_{35}Ca_5$	BMG	Primary rabbit osteoblasts	MTT assay Live/Dead ALP activity SEM μCT Blood analysis	Cytocompatible (similar to Ti-6Al-4 V) High ALP activity Mineralization	Bone formation High bone mineral density No inflammation Normal blood analysis Biocompatible	[149] 2019
$Mg_{60}Ca_5Zn_{35}$ $Mg_{72}Ca_{12}Zn_{16}$ $Mg_{63}Ca_{15}Zn_{22}$	BMG	MC3T3-E1	MTT assay Immersion test Hydrogen evolution	Cytocompatible		[150] 2020

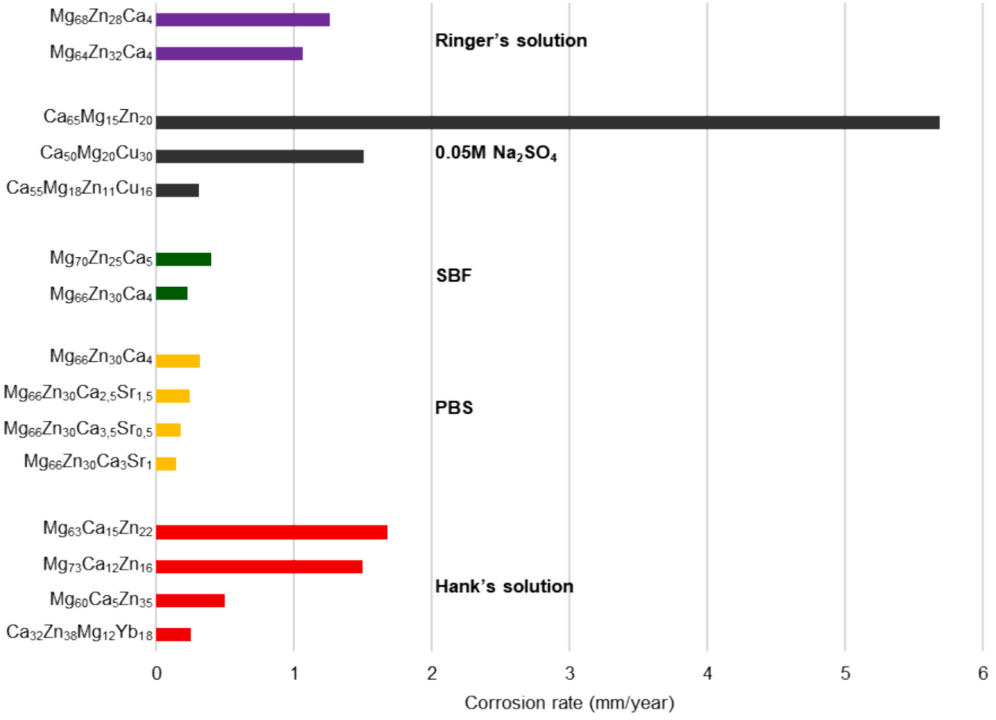

Fig. 10. Corrosion rate (mm/year) of various BMGs. Data obtained from [142,150,153–156].

provided by the alloy composition and may be improved by texturing. This is critical for artificial implants. Indeed, when placing an implant, it is essential to obtain good osseointegration, *i.e.* the establishment of a strong and viable direct connection at the interface between the implant and bone. The implant surface state is thus of great interest. This chapter focuses on the effect of surface topography patterns on the behavior of prokaryotic bacterial cells (called "bacteria") and eukaryotic cell adhesion (called "cells"). The results specifically obtained through surface modification using lasers are discussed in Chapter 6.

5.1. Bacterial adhesion

As presented previously, some bacteria represent a danger for human health. Antibiotic treatments have been widely used to treat the action of bacteria; however, this is no longer sufficient because of their increasing resistance to these treatments [65,170,171]. One approach to solve this problem is to focus on surface structuring, either to induce the death of the bacteria or to prevent their adhesion and thus their proliferation [63]. Many coatings, including bactericidal substances such as silver, copper, or zinc, have been synthesized in the form of "release-based coatings". The bactericidal agent is thus released at the extreme surface of the coating and prevents microbial infection [172]. However, the control of the release is complex and often leads to cytotoxicity and inflammatory responses. The ideal solution is thus to prevent bacterial adhesion by modifying the surface state of a material, to create an antifouling (preventing initial adhesion) or bactericidal effect. Another strategy takes profit of the surface texture to change its wettability, which, indirectly, may also influence the bacteria adhesion. From a general viewpoint, an hydrophobic texture would be able to prevent the adhesion of bacteria and thus the formation of biofilm, whereas an hydrophilic texture would be more prone to favor cell adhesion [173,174]. When surface topography is used to control bacteria adhesion, it is usually difficult to estimate whether the bactericidal effects are primarily due to the surface texturing or to the chemical composition of the material. The texturing will have a greater impact as the contact surface between the material and bacteria decreases, at the

Table 4
Desirable mechanical properties of biodegradable implants for orthopedic applications [160].

Property	Value	Ref
Density	1.8–2.0 (g/cm^3)	[161] 2005 [162] 2009
Tensile strength	≥ 300 (MPa)	[163] 2015
Tensile yield stress	≥ 200 (MPa)	[164] 2009
Young's modulus	17–22 (GPa)	[161] 2005 [165]
Compressive strength	≥ 230 (MPa)	Based on value for human cortical bone
Compressive yield stress	≥ 182 (MPa)	Based on value for human cortical bone
Elongation (strain %)	≥ 10 %	[166] 2014
Mechanical integrity	≥ 24 weeks based on longest healing time of neck femur	[167] 2014 [163] 2015
Fracture toughness	Minimum 12 MPa.m$^{1/2}$	Based on value for human cortical bone
Mechanical integrity	Fixation screw must maintain 95 % of original load-bearing capability for at least 6 weeks after implantation	[168] 2015

detriment of the chemical composition, and conversely [175].

Bacteria tend to react in a very conventional way to certain surface irregularities. For example, they will be retained in distributed pits whose diameter is larger than that of the bacteria [176]. Bacteria preferentially colonize recessed regions with dimensions larger than themselves, such as pits and grooves, as observable in Fig. 11 [175]. In contrast, their adhesion is limited on a topography with smaller dimensions, such as on the surfaces shown in Fig. 12c [177]. Even if the main roughness parameter Ra (quadratic mean roughness) is the most represented in the literature, recent works also refer to other less common key parameters, such as the skewness and kurtosis of the surface, or the furrow density. In particular, these innovative roughness parameters are correlated with bactericidal properties of laser textured surfaces and could be considered in the evaluation of the influence of surface textures on their bacterial activity [178].

NB: The texture of surfaces generated by pulsed lasers can cover several scales, from 10 nm up to hundred micrometres. In order to encompass this large diversity of textures resulting from laser irradiation, it is often found in the literature the « micro-nanotexture » vocable, which will then be used in the following.

Micro-nanotexturing of the surface may achieve a bactericidal effect by stretching the membrane, leading to its rupture and thus to the death of the bacteria (a phenomenon called "lysis") [180]. Definitely, the stretching is strongly dependent on the surface roughness, *i.e.* the height, spacing, and periodicity of the structures, as well as on the width and shape of the contact area [175,178]. Fig. 13 shows the adsorption of a bacterial cell on nanopillars and its lysis caused by membrane stretching.

Studies conducted on titanium alloys have shown that surfaces with micrometric or sub-micrometric patterns result in lower bacterial adhesion compared with rougher surfaces. Similarly, extremely smooth surfaces (<30 nm) do not prevent bacteria from adhering to the surface [181]. Surface irregularities leading to good antibacterial properties are

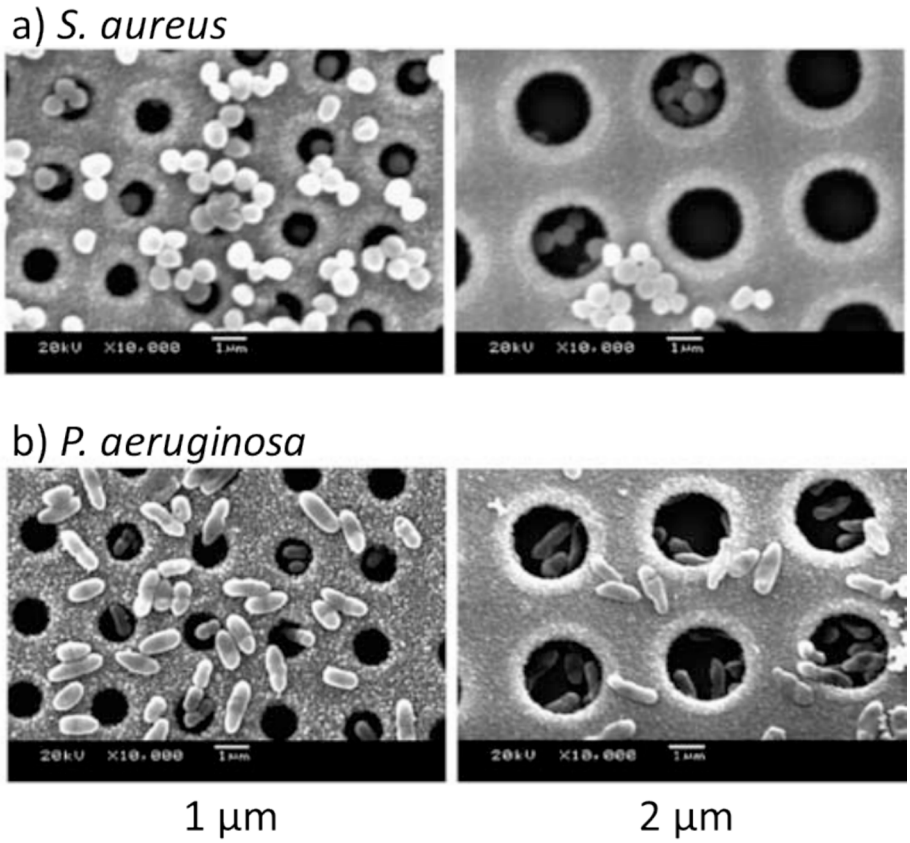

Fig. 11. SEM images of a) S. aureus and b) P. aeruginosa retained on pitted surfaces of titanium with pit diameters of 1 and 2 µm [176].

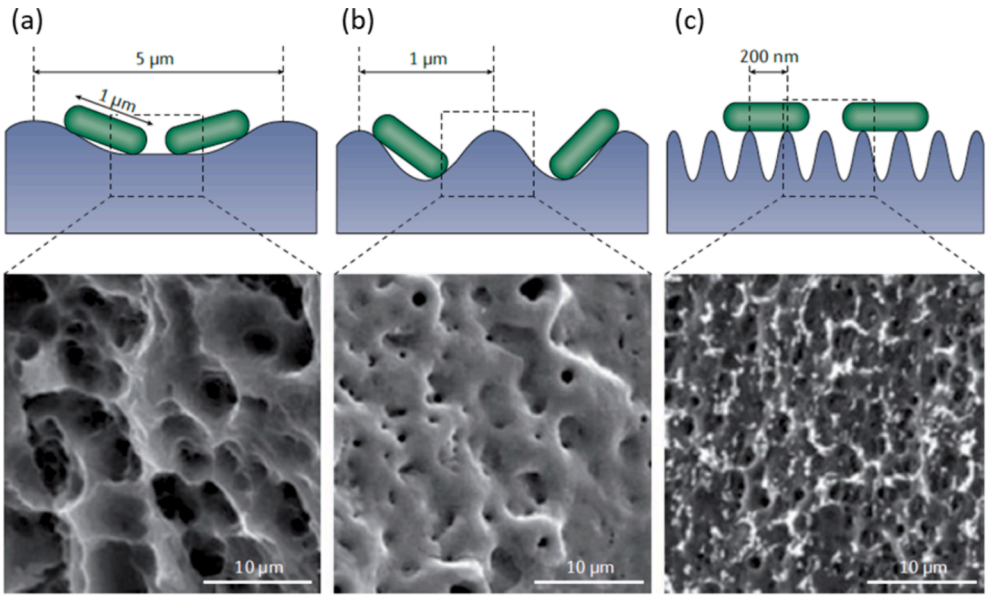

Fig. 12. Preferential attachment of bacteria on micro and nanopatterned surfaces, with SEM images of equivalent textured surfaces of titanium [175,179].

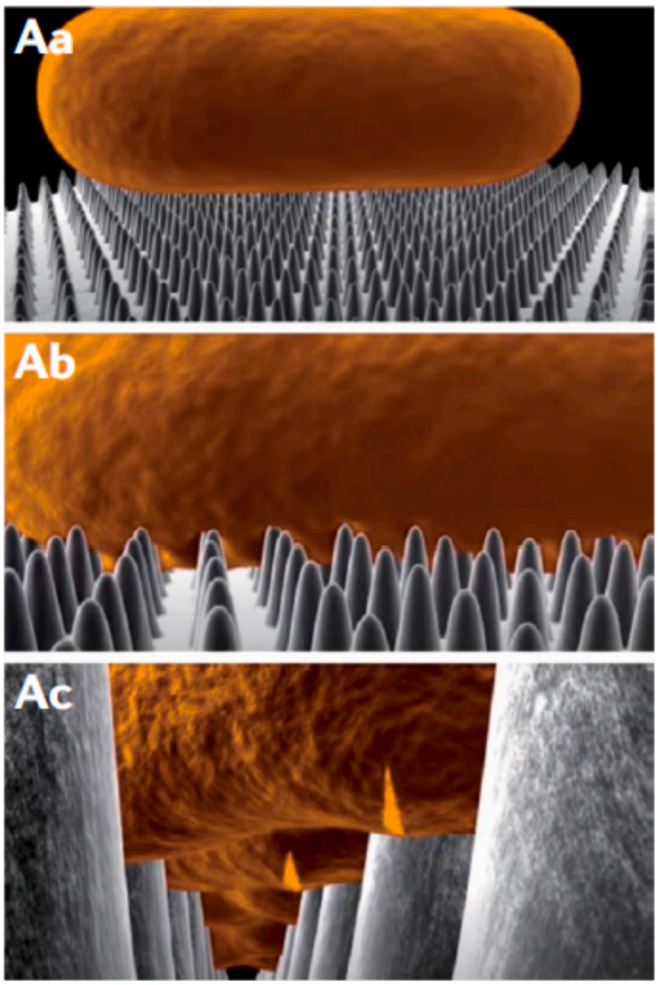

Fig. 13. Membrane rupture by stretching on nanopillars [175].

of the same order of magnitude as the bacteria, *i.e.* approximately 1 µm. Depending on the type of bacteria considered, it is therefore possible to obtain relatively different results in bactericidal tests depending on the dimensions of the bacteria compared to the surface structure [175,182]. Moreover, as the death of bacteria occurs because of the rupture of their protective membrane due to a mechanical–bactericidal effect of the roughness, the bacteria will not react in the exact same way depending on whether they are gram-positive or gram-negative. Indeed, gram-positive bacteria (with a thicker and more rigid membrane) would require a stronger mechanical stress to reach rupture and bacterial cell lysis than gram-negative bacteria.

5.2. *Cell proliferation*

To improve the efficiency and rate of osseointegration (direct structural and functional connection between living bone and the surface of an implant), several surface modification methods have been employed over the past decades. Indeed, the good integration of an implant starts not only from the chemical composition of the surface but also from its wettability and topography. This latter characteristic can also be used to orient the cells in a preferential direction.

The main surface textures susceptible to modify the behavior of cells are dots (or protrusions) [183,184], pillars (or posts) [74,185,186], pits [187], and grooves (or gratings) [185,188,189]. Several methods can be used to create these patterns, including anodization and colloidal lithography for partially ordered patterns, and more advanced techniques for ordered patterns such as photolithography, electron beam lithography, additive manufacturing, and femtosecond laser lithography [190]. These patterns can be either microscopic, nanoscopic, or both at the same time, which is called a multi-scale, or multi-hierarchical, pattern. Indeed, as illustrated in Fig. 14 (with bone cells as an example), the interactions between cells and topography occur over several scales. The prediction of the behavior of cells on a given textured surface is then very complex, as it depends on the topographic properties of the surface and on the cell properties at micro and nano scales.

Many works have focused on microscopic, nanoscopic, or multi-scale patterns to study the behavior of cells on these engineered surfaces. The results have been previously summarized in reviews that classify the studies based on the cells used [191], the topographic patterns [190,192,193], or the potential applications [194].

It is important to highlight that the behavior of cells on surfaces strongly depends on the parameters of the pattern, including the height, width, or diameter and periodicity. Overall, cells tend to easily find anchorage points on a textured material and can grow on it as long as its chemical composition is not toxic. This adhesion is achieved through the

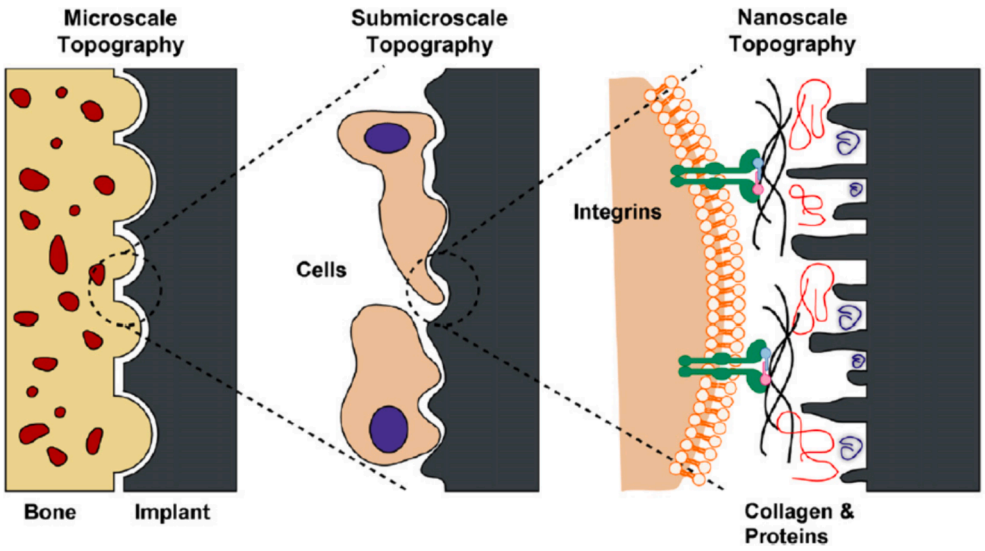

Fig. 14. Interactions between bone and implant surfaces from micro to nanoscale topography [184].

cell filopodia, which are membrane extensions that act like antennae probing the environment to find a suitable location for migration [195]. Figs. 15 and 16 present perfect examples of how micro- or nano-textured surfaces can affect cell behavior. The cell is aligned parallelly for a microgroove pattern, whereas it is oriented perpendicularly for a nanogroove pattern [189]. As for pillars, cells can propagate on top of them if the width and spacing are optimal.

In vivo experiments with Pd-based BMGs have also demonstrated that nanopatterning may have a positive effect on the biocompatibility of the bone implant [126]. There is therefore a consensus that surface texturing, whether in the form of a micropattern, nanopattern, or multi-scale pattern, generally tends to improve cell adhesion and align cells depending on the size of the pattern compared to the size of the cells. The use of hierarchical structures with micro- and nano-topographical features appears to be the most promising route for further development. Therefore, the use of lasers for surface texturing is of great interest and will be discussed in the next chapter. However, given the number of cells, culture conditions, materials, and observation methods used, it remains complex to state with certainty the exact relationship between surface topography and cell evolution.

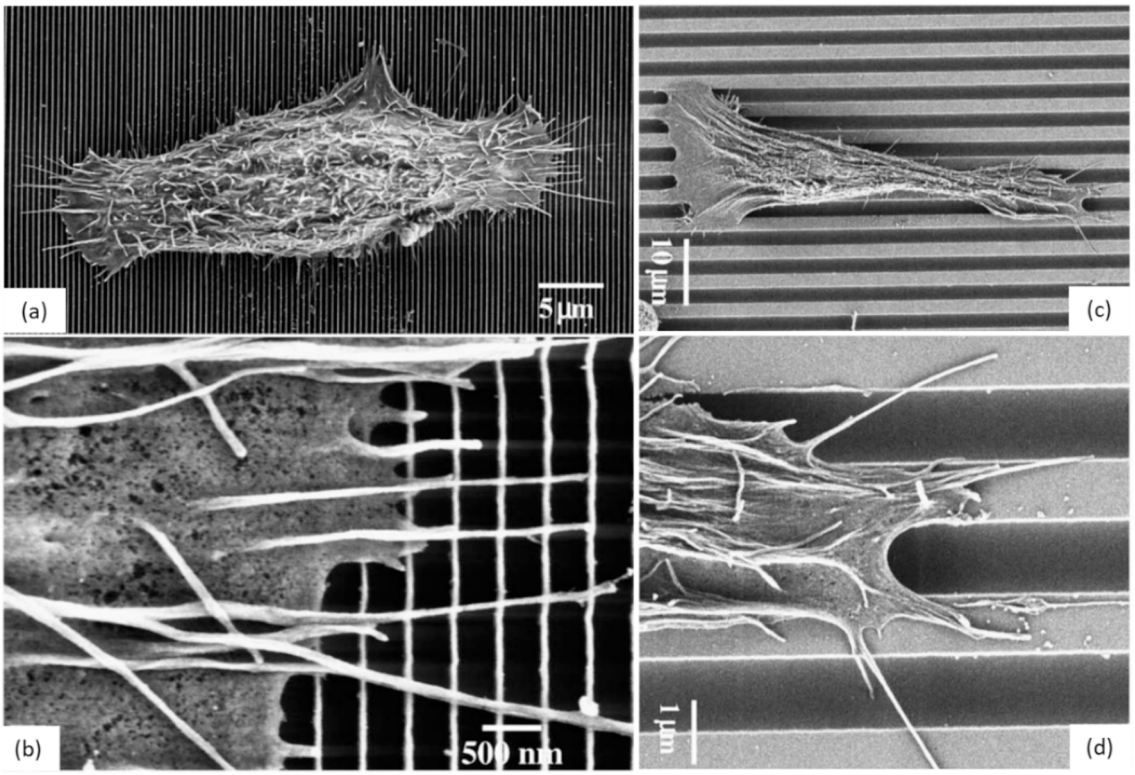

Fig. 15. SEM images of human corneal epithelial cells cultured on micro- and nanopatterned substrates of silicon: a) perpendicular alignment on 70-nm ridges with a 400-nm pitch, b) expanded view on filopodia of previous cell, c) parallel alignment on 850-nm ridges with a 2000-nm pitch, d) expanded view on filopodia of previous cell [189].

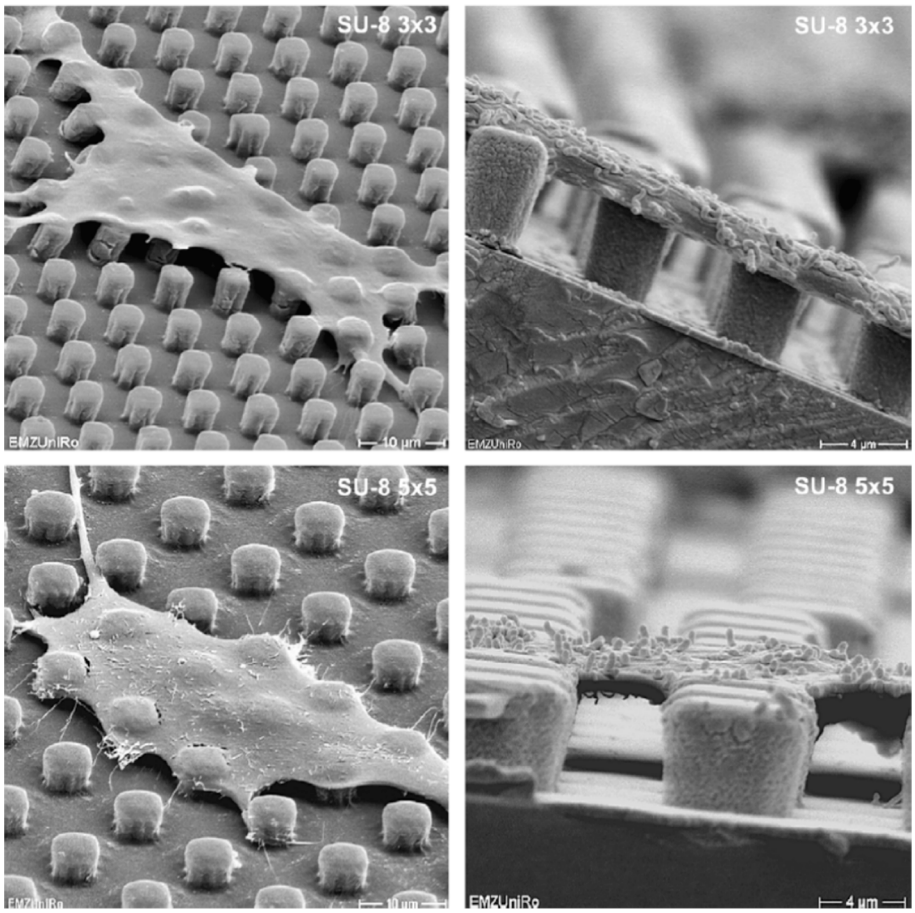

Fig. 16. MG63 osteoblasts adhering on top of micropillars realized on pure titanium [196].

6. Laser surface texturing

This chapter focuses on the use of various laser irradiation conditions to modify the surface state via irradiation and laser–matter interactions. The first part addresses surface textures realized thanks to laser ablation techniques. The associated surface patterns have an order of magnitude of at least a few microns. The second part discusses the fabrication of sub-micron structures generated by ultrashort pulse lasers. As exposed in the previous chapter, surface patterns of this size are favorable to bactericidal effects and cell proliferation. For a given material to be textured, in addition to its surface properties (thermal, optical, structural), there are many laser parameters that may affect the final result, including the fluence, polarization, wavelength, spot size, pulse frequency, pulse duration, time delay (for double/multi pulses), number of pulses, and overlapping of the pulses [197]. These different parameters determine the type of surface texturing achieved.

6.1. Micrometric structures

Laser ablation is a process that alters the surface properties of a material by changing its texture and roughness. The laser beam creates topography of different shapes on the material surface through ablation that removes a certain thickness [198]. This ablation can be achieved either with a continuous or pulsed laser depending on the required structure and irradiated material [199]. Precision in the tens of microns and excellent repeatability can be achieved. However, this destructive technique is complex to use on thin films, which require very low fluence and pulsed lasers to avoid damage to the substrate. Frequently produced shapes include grooves and holes. These patterns may improve properties such as the adhesion, wettability, friction, or cell adhesion. The energy, and therefore the laser parameters required to cause evaporation or ablation, are highly dependent on the material, including its chemical composition, thermal properties (e.g., conductivity, specific heat) [200], and optical properties (e.g., reflectivity, absorbance, transmittance) [201].

The ablation threshold is generally used to define the boundary between the ablative and non-ablative regimes. At a certain incident beam energy (fluence), the binding energy of the material is exceeded by the radiant energy, resulting in decomposition, often in the form of vaporization [202]. To avoid unwanted material damage during ablation and to form fairly fine structures, pulsed lasers are generally used. Indeed, for continuous radiation, the heat accumulated by the material does not have time to dissipate and thus accumulates, leading to thermal effects and substantial structural changes extending beyond the point of impact (*i.e.* during laser welding). Pulsed lasers allow good heat dissipation to avoid these problems, explaining why nanosecond lasers are extensively used for this purpose; however, picosecond and femtosecond lasers can also be used if the material is prone to damage [203]. Shorter pulses allow easier control of the energy delivered to the material surface, as visible in Fig. 17.

6.2. Submicrometric and nanometric structures

Different mechanical, chemical and physical processes can be used to modify the surface at a submicrometer scale. Nevertheless, among all the texturing techniques, the use of lasers, and of femtosecond laser in particular, is the most flexible, and the most documented [204]. This micro- and nano-structuring technique has some advantages compared with other techniques, such as nanolithography (*i.e.* photolithography, X-ray lithography, electron beam lithography, micro-contact printing,

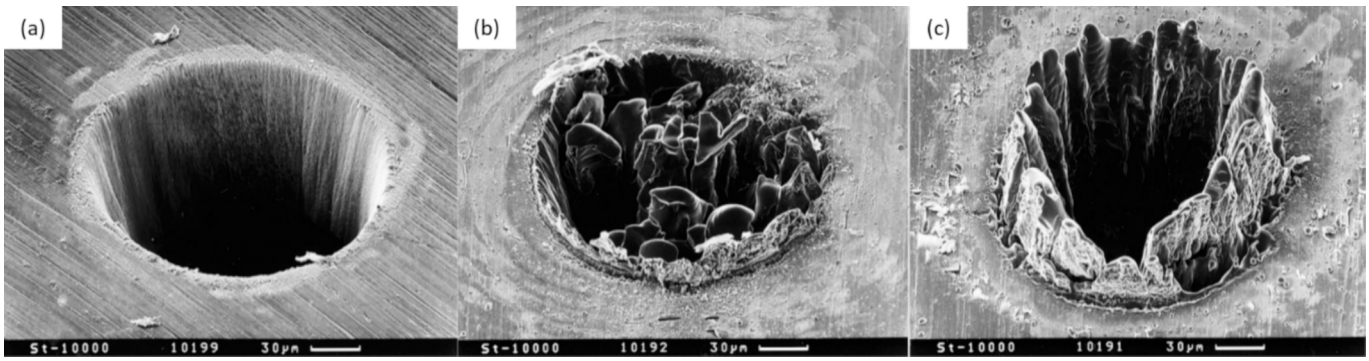

Fig. 17. SEM images of pulsed laser ablation on a thick steel foil ($\lambda = 780$ nm) with femtosecond, picosecond, and nanosecond pulses: a) 200 fs, 120 µJ, F = 0.5 J/cm^2; b) 80 ps, 900 µJ, F = 3.7 J/cm^2; c) 3.3 ns, 1 mJ, F = 4.2 J/cm^2 [203].

nano-imprint lithography, or scanning-probe lithography) [205,206] or reactive-ion etching [207]. Indeed, the use of a femtosecond laser does not require polluting chemicals, can avoid heat-induced surface damaging, and is promising for large-scale industrial uses [208,209].

Femtosecond lasers, known as ultrafast lasers, are now commonly used to functionalize surfaces. Due to their ultrashort pulses, their thermal effect is very limited, causing no detrimental effects regarding residual stresses, as it is often the case for more conventional lasers. Moreover, their very located volume of interaction allows the treatment of thin films, where the other lasers are rather adapted to bulk materials. Indeed, the ultra-short pulses created by these lasers enable the generation of unique morphological, topological, and chemical modifications on the surface of materials. Surface nanostructuring provides very interesting optical, wetting, tribological, and biological properties, which explains its use in various fields such as aeronautics, renewable energies, nanofluidics, and medicine [210–214]. The repeated cycles of fast melting and solidification on a consequent number of pulses enables the drawing of surface morphologies impossible to obtain by other techniques. These morphologies can be controlled by modifying the wavelength, polarization, pulse duration or fluence and can thus promote specific shapes, orientations, or depths [215,216]. These modifications can lead to the enhancement of different surface properties, *i.e.* optical properties, hydrophobicity, or cell adhesion.

Femtosecond lasers can create laser-induced periodic surface structures (LIPSS) on various materials such as semiconductors, metals, polymers, or metallic glasses. These structures, observed for the first time in 1965 on semiconductors, resemble rectilinear ripples [217]. Two types of LIPSS can be distinguished according to their periodicity. Low-spatial-frequency LIPSS (LSFL) generally appear for ultrashort laser fluences slightly above the damage threshold of the material and after several pulses. Their period is slightly shorter than the wavelength of the laser beam, and they appear oriented perpendicularly to the electric polarization field [218]. A femtosecond laser with an emitting wavelength of 1064 nm would create a LSFL with a periodicity of nearly 1 µm. LSFL are generated by interference between the incident laser and a surface electromagnetic wave created by surface defects (roughness), which may include the excitation of surface plasmon polaritons (SPPs). High-spatial-frequency LIPSS (HSFL) are the second most common type of LIPSS. They have a periodicity between half and one tenth of the incident laser wavelength. Their orientation can be either perpendicular or parallel to the electrical polarization. Their origin remains under discussion in the literature, with different formation mechanisms proposed, such as second-harmonic generation, the involvement of specific types of plasmon modes, or self-organization [219,220]. The physical effects inducing different types of LIPSS during femtosecond laser irradiation has been thoroughly investigated [221].

Because the orientation of LIPSS is directly related to the polarization direction of the laser beam, it is possible to obtain more complex structures than classical ripples by changing the polarization direction between pulses. Moreover, double pulses can be easily generated by temporal shaping, *i.e.* a second ultrafast pulse generated after a few picoseconds or nanoseconds after the first one. This induces relatively different LIPSS structures depending on the time delay and polarization states, such as those shown in Fig. 18.

The challenge in ultrafast laser texturing remains to reach ultimate scale at nanometers, well below the diffraction limit. Nakhoul *et al.* [222] reported recently high aspect-ratio nanopatterns driven by inhomogeneous local absorption sustained by nanoscale convection and architectured by timely-controlled polarization pulse shaping (Fig. 19). Such high aspect-ratio surface nanotopography is expected to have great potential for innovative applications in biomedecine, nanocatalysis, and metaphotonic [222,223].

6.3. Structural and chemical atomic-scale impact of the laser treatment

Metallic glasses are intrinsically characterized by a perfect homogeneity of their constitutive chemical elements. That's why recent studies do not focus on such a purely chemical approach. However, the metallic glass character of a material must be considered as a metastable state, which can be disrupted by any external stress. In this sense, a thermal treatment is the most conventional way to destabilize the amorphous structure. XRD in heating mode and DSC technics allow then to determine the critical key-parameters T_g and T_x (glass transition and crystallization temperatures respectively), and their difference, which defines the super-plastic domain range [54].

Within the context of this paper, the laser beam is the energy source capable of affecting the disordered structure of the metallic glass. If well-controlled through an ultrashort pulsed laser, such a structural modification can be deliberate. This process is referred to as devitrification, susceptible to form a hardened surface and subsurface. These studies are in general two-fold with a first part dedicated to a simulation of the temperature–time depth profile [224,225], associated, sometimes, with an experimental proof of the local crystallization by TEM. Antonowicz *et al.*, for instance, have shown that each pulse provoked a heating up to 1500 K during some tens of ns (Fig. 20) [226]. When repeated, this laser irradiation became prone to strongly transform the Zr-Cu TFMG into an unexpected cubic form of zirconia top-layer first, followed by a subsequent inner crystallization of a copper sub-layer. Another strategy to solve the crystallization of a TFMG was recently proposed by Dasson-neville *et al.* adopting an *in situ* approach in heating mode [227]. They have used the same Zr-Cu film model to suggest, at the TEM-scale, a scenario for the film crystallization: some nanometric monoclinic zirconia clusters first appear, where the metallic crystallization initiates. The whole crystallization of the film is then conducted behind a propagating transformation front resulting mainly in the transformation of the amorphous matrix into Zr_7Cu_{10} intermetallics.

Studies associating laser treatment with metallic glasses are mainly related to a modification of their surface texture, but the concomitant

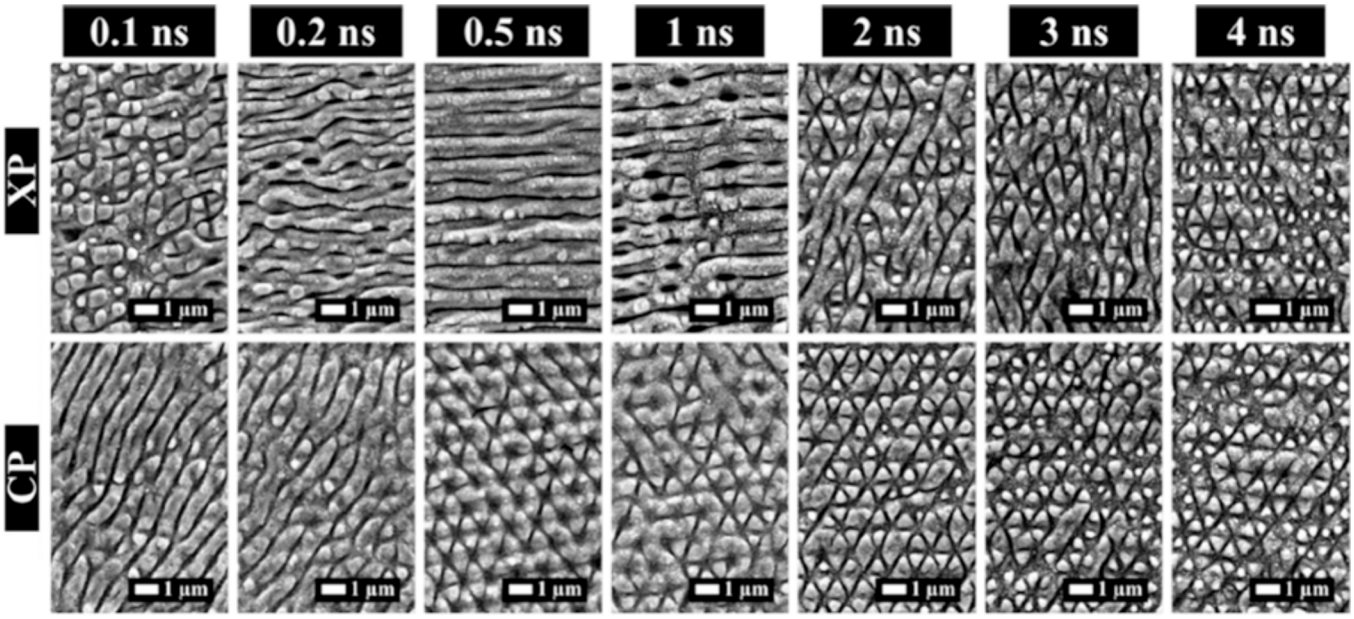

Fig. 18. SEM images of stainless steel irradiated at a fluence of 0.1 J/cm^2 and a pulse duration of 350 fs with double pulse for different interpulse delays and two different polarization configurations (XP = crossed polarization and CP = circular polarization) [216].

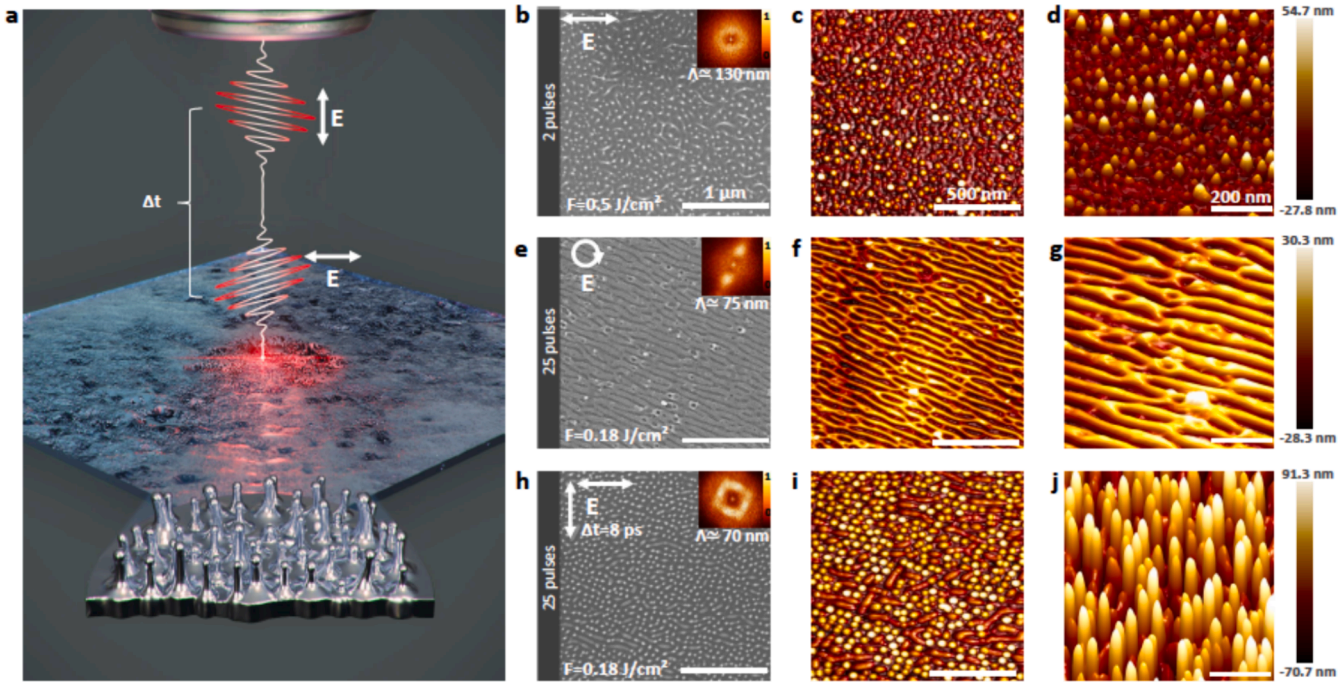

Fig. 19. A) schematic illustration of nanopeaks formation by femtosecond laser using double pulses. b,e,h) scanning electron microscopy with 2d fourier transform (ft). c,f,i) 2d atomic force microscopy. d,g,j) 3d atomic force microscopy of various surface morphologies of ni(0 0 1) crystal irradiated with different laser parameters and polarizations [222].

effects on chemistry are also of prime interest. It was recently proved that the atmosphere under which the laser process is conducted had an important impact on the top-layer chemical composition. As an example, P. Dominic *et al.* clearly showed, by XPS analysis of tungsten treated areas under vacuum the absence of peaks attesting oxidized species in opposition to treated zone in ambient air (Fig. 21) [228]. This difference in the surface composition was correlated with opposite wettability behaviours (Fig. 21 a,b).

However, most often, the fs-laser texturing is carried out in ambient air, provoking a superficial oxidation of the treated material. This oxidation is proved qualitatively by Raman spectroscopy of the $Ti_{47.5}Zr_{25}Cu_{22.5}Ni_5$ BMG [229], or more locally by ToF-SIMS imaging [230] (Fig. 22). XPS spectroscopy is also often reported to precise the fine composition of this oxide [231] or mixed oxide [232]. Moreover, a further carbon pollution linked to the adsorption of hydro-carbonated species may be also revealed on top-surface [233].

The next step has consisted to determine the thickness and nature of this thin oxide layer, estimated indirectly by sputter-depth-profile spectroscopic analyses (GD-OES [234], AES [235], ToF-SIMS [232], XPS [21] …) or directly by TEM EDX [236,237] (with an example in

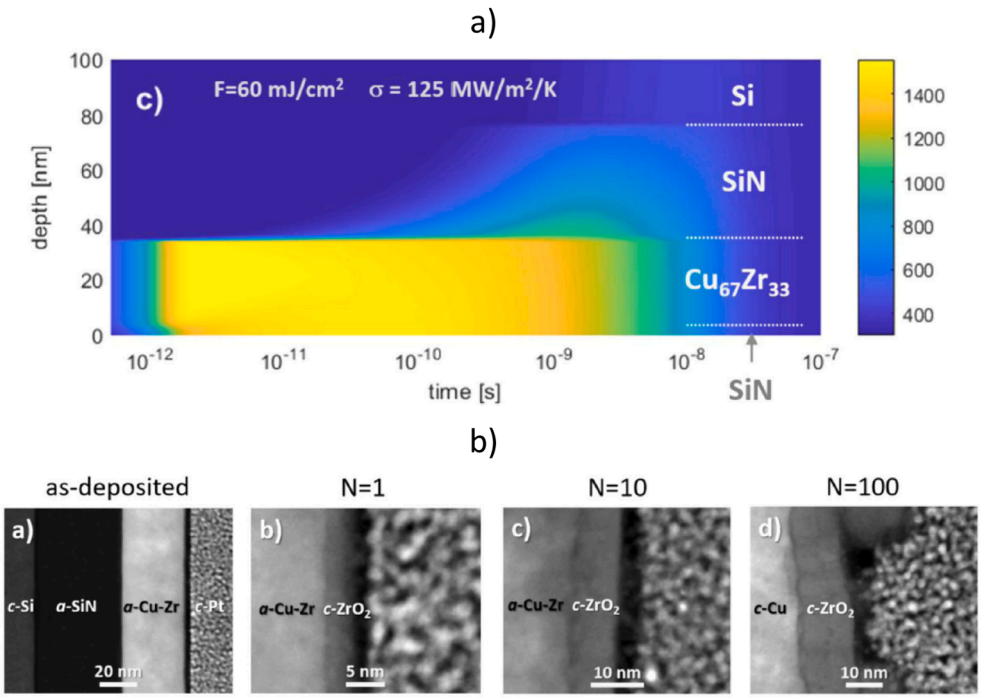

Fig. 20. Laser irradiation of a Zr-Cu TFMG with a 60 mJ/cm^2 fluence laser: a) temporal temperature-depth distribution, b) TEM cross section highlighting the nature of transformed layer for different (0, 1, 10, 100) pulses [226].

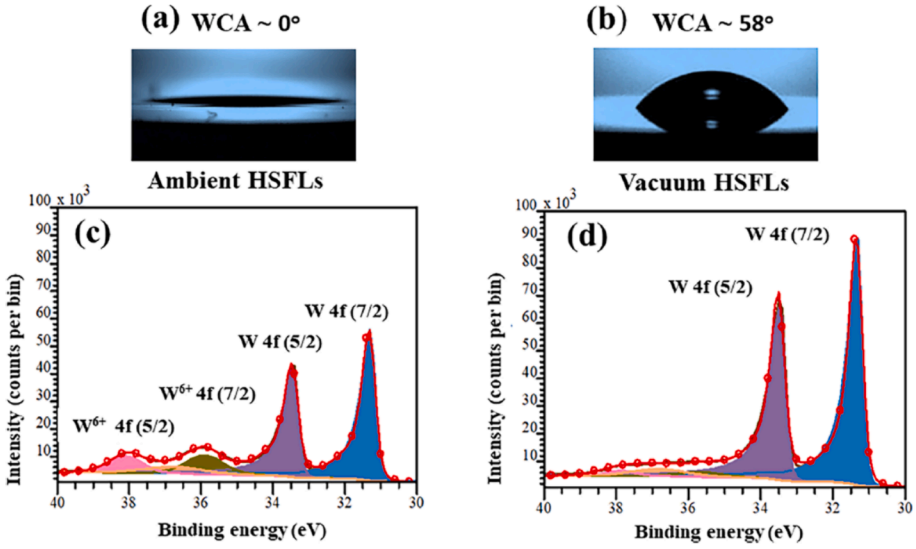

Fig. 21. Camera images of contact angles measured after 10 min of fabrication for (a) ambient HSFLs (b) and vacuum HSFLs generated by fs laser with Fp = 0.32 J/cm2 and N = 20. (c & d) HR XPS peaks for W 4f spectra one hour after fs-laser irradiation. (c) Ambient HSFLs show the doublet peaks corresponding to oxidation which are absent in the (d) [228].

Fig. 23) or EELS [235]. Whatever the technics considered for its analysis, the thickness reported involving a fs-laser texturing treatment is most often ranging from 10 and 30 nm.

Prudent *et al.* [237] show a flexible one-step ultrafast laser process coupling structural modifications consisting in turning of a ZrCu metallic glass to a composite material of monoclinic zirconia crystallites embedded inside amorphous metallic glass associated with nano-topography modifications with the generation of highly concentrated 20 nm diameter nanowells on the surface (Fig. 24).

6.4. *Laser surface texturing of metallic glasses*

Laser surface texturing is therefore widely used on many materials. As metallic glasses are relatively new materials, studies on their formulation and physicochemical properties are still in progress. In parallel, some researchers have studied the effect of laser irradiation on metallic glasses. Table 5 provides a summary of papers addressing laser-induced surface structures on metallic glasses.

The majority of the compositions studied are Zr-based because of their commercial availability, stemming from their excellent GFA, especially with Vitreloy105® ($Zr_{52.8}Cu_{17.6}Ni_{14.8}Al_{9.9}Ti_{4.9}$) and Vitreloy1® ($Zr_{41.2}Ti_{13.8}Cu_{12.5}Ni_{10}Be_{22.5}$). Many different structures can be

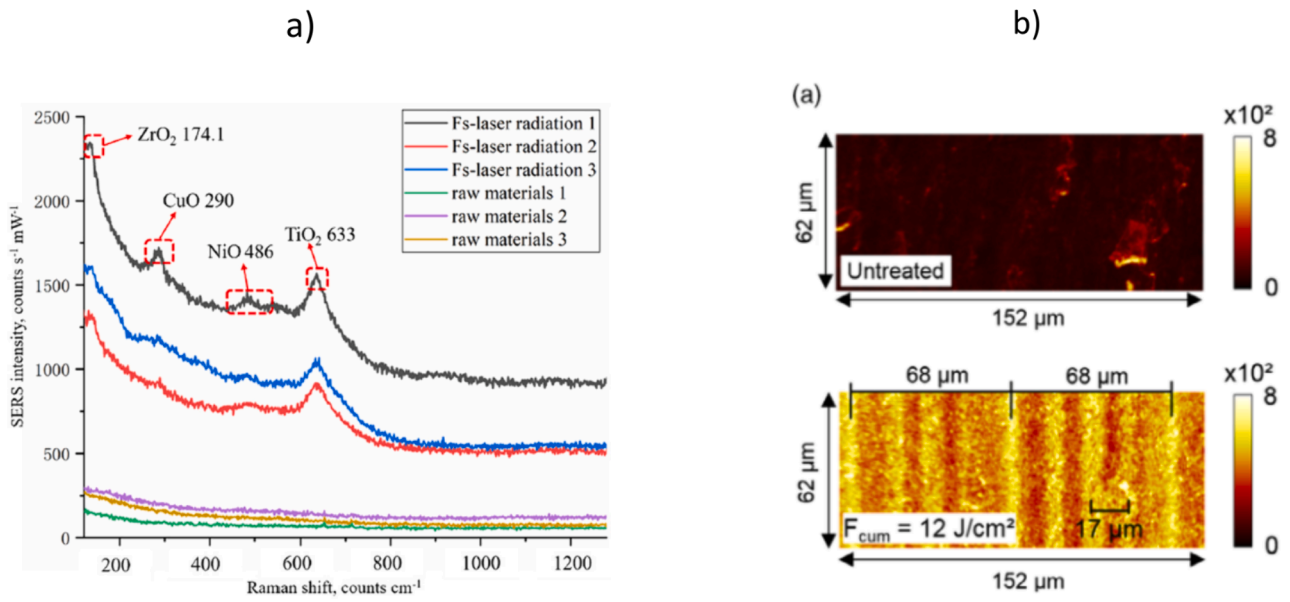

Fig. 22. A) raman spectrum of untreated and laser treated $ti_{47.5}Zr_{25}Cu_{22.5}Ni_5$ BMG showing oxide crystalline peaks after the irradiation process [229] b) Top view ToF-SIMS integrated images of oxygen distribution of untreated and laser textured titanium alloy [230].

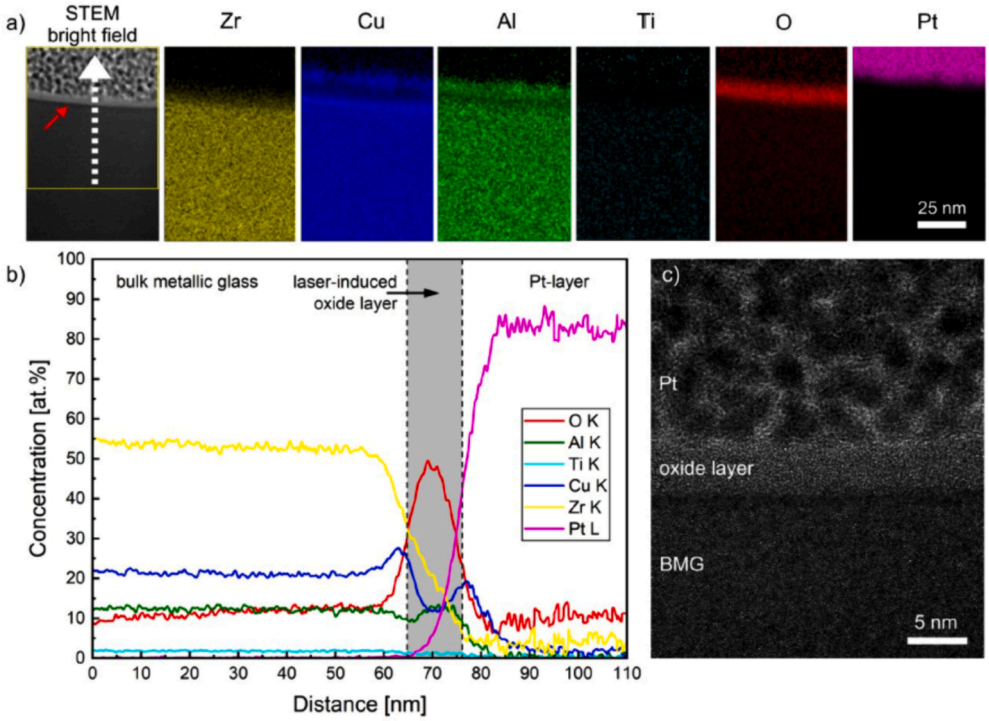

Fig. 23. A) stem images of sur surface of $zr_{61}Cu_{25}Al_{12}Ti_2$ BMG with LIPSS and EDX maps of the different elements. b) Line-scan EDX profile by EDX of the different elements (following the white arrow of the STEM-image in a)). c) HRTEM image of the interface of the BMG centered at the oxide layer [236].

realized with nanosecond lasers, the most common being grooves. These structures have a significant effect on the hydrophilicity of the surface. In addition, this property appears to evolve over time and is dependent on the storage conditions [244]. Using femtosecond laser irradiation, metallic glasses form very similar structures, whether they are Zr-based, Ti-based, or Fe-based. Although the laser parameters differ due to the compositional variation, the formation of LIPSS is always observed. Metallic glasses behave relatively similarly to other materials (Table 5) in terms of their femtosecond-laser-induced structure. TFMGs are very rarely studied [249], whereas femtosecond irradiation only slightly attacks the surface. As exposed previously, the composition range achievable with TFMGs is broader than that for BMGs; therefore, TFMGs are good candidates for future femtosecond irradiation research. Femtosecond laser irradiation can induce a type of periodic structure other than LIPSS, whose period is greater than the laser wavelength, that is to say about a few micrometers. These structures are called “SWPSS” (for “super-wavelength periodic structure” or “supra-wavelength periodic structure”), “parallel ridges”, “micro-ripples”, or “grooves” (not to be confused with the grooves produced by ablation, which are several tens of micrometers wide). These structures are less studied and less well

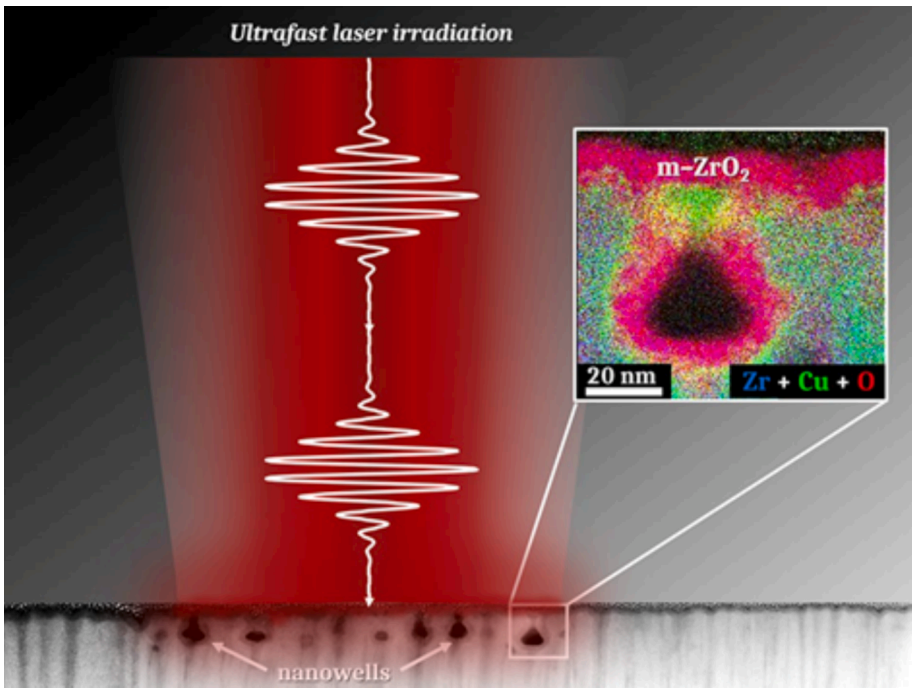

Fig. 24. Double ultrafast pulses scheme irradiation of ZrCu TFMG leading to subsurface nanowells formation MEB image). Inset: EDX TEM mapping of the different elements showing ZrO_2 monoclinic crystallites layer [237].

known than LIPSS; however, they are observed on other materials such as semiconductors [252], dielectrics [253], and metal alloys [254]. These supra-wavelength surface structures appear at higher fluences than LIPSS or with a higher number of pulses [245,246,250].

It is therefore possible to create different surface structures on metallic glasses using lasers. Laser-textured metallic glasses are thus very promising surfaces for biomedical applications.

7. Biological behavior of laser textured surfaces

This final chapter focuses on the use of laser texturing for the realization of antibacterial and biocompatible surfaces. The results obtained on various materials, in particular metallic materials, are presented first to demonstrate the effectiveness of this process. Then, the studies performed on the behavior of metallic glass under different laser irradiations are presented. This includes works on the generation of micrometric (grooves, dimples…) and submicrometric structures (LIPSS). Finally, the few studies exploring the relationship between laser texturing of metallic glasses and their promising biological properties are exposed.

7.1. Biological properties of various laser textured materials

Papers on the effect of laser surface texturing on the antibacterial and biocompatible properties of various materials are summarized in Table 6. Some characteristic laser textured surfaces gathered in this table were selected, and illustrated through their SEM images in Fig. 25. The materials and lasers used are displayed along with the obtained structures. These papers also investigated the effect of the formed structures on cells or bacteria.

Analysis of Table 6 leads to some trends. Ti and its alloys (especially Ti–6Al–4 V) are generally used to observe the effect of surface laser texturing. Indeed, the biocompatibility of these materials is already well established, and they are widely used in biomedical applications. Laser ablation texturing is often used to create grooves, on which the viability and behavior of cells is regularly tested. The antibacterial effect of these structures is not observed, most likely because their dimensions are much larger than those of the bacteria. Eventually, the laser texturing may affect the surface chemistry, modifying the antibacterial behavior; however, this is not related to the topography itself. The results obtained on various grooves indicates that it is difficult to define the precise behavior of the cells, in particular because those used are very often different and thus most likely do not behave in the same way. It remains possible to define the main outlines of their behavior. The cells tend to align themselves in the direction of the grooves, if their dimensions are similar. It also appears that the grooves must have a minimum depth of 5 μm to induce orientation of the cells; otherwise, the cells are not affected [259].

Moreover, Table 6 also shows that LIPSSs formed on titanium-based alloys are always formed using femtosecond lasers, although it is also possible to make them using picosecond lasers on other materials [266]. These LIPSSs exhibit effects on both bacteria and cells through chemical or topographical modifications. The adhesion of the *E. coli* bacteria is reduced on LIPSS due to their rod shape and their size, which is slightly larger than the spatial period of the LIPSS. This induces the rupture of the membrane by elongation and, thus, its subsequent lysis. The behavior of *S. aureus* on LIPSS is more complex to describe, as shown by some contrasting results [214,260]. Slight variations in the LIPSS synthesis parameters can result in reduced or increased adhesion of S. aureus. Identical LIPSS can therefore have a positive or negative effect on bacterial adhesion depending on the shape and size of the bacteria. LIPSSs may also affect the behavior of cells, even though they are at least ten times larger. This type of surface texturing provides anchorage points for the cells, which allows their good adhesion and spreading (Fig. 26). In fact, the LIPSS topography can lead to a change in wettability, a more hydrophilic surface is for example known to allow proteins from saliva to adhere on the surface, improving protein adsorption, and therefore cell adhesion. Proteins are usually sensible to small structure such as pits or pillars in the range of 1–10 nm but cells are attracted to feature of a higher range of 15 nm-100 μm [264]. In addition, a textured surface will exhibit a larger surface area than a smooth surface allowing more links between cell and surface [267]. Several other intrinsic criteria linked to the cells themselves have also to be taken into account, such as for instance the capacity of the cell to spread and differentiates

Table 5
Summary of laser surface textured metallic glasses.

Composition	BMGTFMG	Laser	Obtained structures	Ref. Year
Cu_xZr_{1-x} x = 0.33, 0.5, 0.67	BMG	Simulation	Determination of ablation threshold	[238] 2015
$Zr_{41.2}Ti_{13.8}Cu_{12.5}Ni_{10}Be_{22.5}$	BMG	Nanosecond laser Nd:YAG, λ = 1064 nm Pulse duration: 8 ns	• Periodic ripples on the edge of ablated area Lower periodicity when moving away from the pulse center	[239] 2016
$Zr_{41.2}Ti_{13.8}Cu_{12.5}Ni_{10}Be_{22.5}$	BMG	Nanosecond laser Nd:YAG, λ = 532 nm Pulse duration: 15.4 ns	• Micro grooves • Submicron cross-shaped protrusions • Nanoparticles	[240] 2017
$Zr_{52.8}Cu_{17.6}Ni_{14.8}Al_{9.9}Ti_{4.9}$	BMG	Nanosecond laser 20-W Yb fiber laser λ = 1064 nm Pulse duration: 65 ns, 140 ns, 220 ns	• Micro grooves Width = 30 μm Depth = 8–30 μm Protrusions at grooves' edges Resolidified droplets	[241] 2019
$Zr_{52.8}Cu_{17.6}Ni_{14.8}Al_{9.9}Ti_{4.9}$	BMG	Nanosecond laser 20-W Yb fiber laser λ = 1064 nm Pulse duration: 220 ns	• Grooves: Width = 25–30 μm Depth = 5–28 μm Increased hydrophilicity • Dimples: Diameter = 30 μm Decreased hydrophilicity	[242] 2020
$Zr_{41.2}Ti_{13.8}Cu_{12.5}Ni_{10}Be_{22.5}$	BMG	Nanosecond laser λ = 1064 nm Pulse duration: 7 ns	• Leaf-shaped structures (ripples + vein-like structures) Increased hydrophilicity	[243] 2021
$Zr_{41.2}Ti_{13.8}Cu_{12.5}Ni_{10}Be_{22.5}$	BMG	Nanosecond laser λ = 1064 nm Pulse duration: 7 ns	• Micro-convex structures Pitch = 45, 90, 150 μm Increased hydrophilicity post-process Decrease hydrophilicity after 100 days	[244] 2021
$Ti_{40}Zr_{10}Cu_{36}Pd_{14}$	BMG	Femtosecond laser Ti:Sapphire, λ = 775 nm Pulse duration: 150 fs	• LIPSS: Λ = 600 nm • Parallel ridges: Λ = 2000 nm	[245] 2009
$Zr_{44}Ti_{11}Cu_{10}Ni_{10}Be_{25}$	BMG	Femtosecond laser Ti:Sapphire, λ = 800 nm Pulse duration: 120 fs	• LIPSS: Λ = 720 nm • Parallel ridges: Λ = 1600 nm	[246] 2014
$Zr_{41.2}Ti_{13.8}Cu_{12.5}Ni_{10}Be_{22.5}$	BMG	Femtosecond laser Ti:Sapphire, λ = 800 nm Pulse duration: 50 fs	• LIPSS: Λ = 730 nm	[247] 2016
$Fe_{82}Si_{11}C_7$	BMG	Femtosecond laser Ti:Sapphire, λ = 800 nm Pulse duration: 50 fs	• LIPSS: Λ = 722 nm; depth = 115 nm	[248] 2020
$Zr_{65}Cu_{35}$	TFMG	Femtosecond laser Ti:Sapphire, λ = 800 nm Pulse duration: 60 fs	• LIPSS: Λ = 630–650 nm	[249] 2021
$Zr_{64.13}Cu_{15.75}Ni_{10.12}Al_{10}$	BMG	Femtosecond laser λ = 1030 nm Pulse duration: 300 fs	• LIPSS: Λ = 700–928 nm • SWPSS: Λ = 1500–2000 nm	[250] 2021
$Fe_{52}Cr_{13}Mo_{12}C_{15}B_6Er_2$	BMG	Nanosecond laser λ = 532 nm Pulse duration: 15.4 ns	• Nanoparticles • Nanonetwork structure	[251] 2021

[268].

Some researchers have also succeeded in creating multiscale textures by combining grooves with LIPSS with a single femtosecond laser treatment [259,261]. In these cases, the LIPSS can be oriented in different directions depending on the laser irradiation conditions. The cells are oriented along the grooves when the depth of the microstructure is sufficient (>1 μm) or along the LIPSS when the depth is too small.

It has therefore been repeatedly demonstrated that laser irradiation, whether to create grooves, LIPSS, or multi-scale textures, modifies the antibacterial properties and cytocompatibility of surfaces on conventional biomedical materials. The final parts of this paper discuss the possibility of texturing metallic glasses using a laser and the results obtained in terms of biological response.

7.2. Biological properties of laser textured metallic glasses

Despite the positive effect of laser texturing on the antibacterial and biocompatible aspects that has been demonstrated previously on various materials, there has been relatively little research conducted to date on metallic glasses that combine laser surface texturing and biological properties. Given the limited existing research, the results presented in this final section will be detailed.

Villapún *et al.* used a femtosecond laser to texture a BMG of $Cu_{55}Zr_{40}Al_5$ composition [269]. Several laser fluences were tested: 0.70 J/cm^2 (T1), 1.39 J/cm^2 (T2), and 2.82 J/cm^2 (T3). These high fluences resulted in ablation texturing. From a topographic viewpoint, increasing the fluence led to a greater surface roughness. In addition to the grooves created by the laser ablation, LIPSS appeared, which induced a multiscale structure. At the chemical level, the high fluences led to crystallization of the surface and modification of the composition, in particular because of the oxidation of Cu and Zr and the formation of intermetallics. The antibacterial properties of the samples were examined using bioluminescence and plate counting of *E. coli* bacteria. A mild bactericidal effect was observed, which was stronger for high fluences (Fig. 27). Given the effect of laser texturing on both topography and chemical composition, it was difficult to define the exact source of the improved antibacterial properties of the BMG.

Jiao *et al.* studied the *in vitro* cytocompatibility of a $Zr_{52.8}Cu_{17.6}Ni_{14.8}Al_{9.9}Ti_{4.9}$ BMG (Vit 105) before and after nanosecond laser texturing [270]. They machined the surface at a high fluence of 30 J/

Table 6
Summary of surface structures produced on metallic surfaces through laser irradiation.

Composition	Laser	Structures	Cells Bacteria	Results	Ref. Year
Ti-6Al-4 V	Nanosecond laser Nd:YVO4, λ = 355 nm	• Grooves:Width = 11.0–12.7 μmHight = 9.0–10.2 μmSpacing = 20, 40, 60 μm	HOS	Better cell adhesion and spreading Alignment along the grooves	[255] 2009
Ti-6Al-4 V	ArF Excimer, λ = 193 nm	• Grooves:Width = 25 μmSpacing = 20 μm• Dimples: Diameter = 60 μm	MC3T3-E1	Higher nanohardness Higher wear resistance Better corrosion resistance Same cell viability Alignment along the grooves	[256] 2015
Ti-6Al-4 V	2-kW Yb fiber laser λ = Undisclosed	• Grooves:Width = 200–250 μmDepth = 20–90 μm	MG63	Better cell viability and spreading for features of similar dimensions	[257] 2015
Ti-6Al-4 V	Picosecond laser λ = 1064 nm	• Grooves:Width = 30 μmSpacing = 75, 150 μmDepth = 1, 2.5, 4 μm	Rat BM-MSC	Better cell adhesion Better cell contact guidance with increasing groove depth	[258] 2018
Ti-6Al-4 V	Femtosecond laser Yb:YAG, λ = 1030 nm Pulse duration: 400 fs	Multiscale structure• Grooves:Width = 25–75 μmDepth = 1–10 μm• LIPSS:Λ = 700–900 nm	C3H10T1/2	Cells are more sensitive to LIPSS, except if the grooves and cells dimensions are close Alignment of cells if width = 25–50 μm and depth > 5 μm	[259] 2016
Titanium Grade 2	Femtosecond laser Yb:KYW, λ = 1030 nm Pulse duration: 500 fs	• LIPSS:Λ = 710 nm• Nanopillars:Diameter = 750 nmHeight = 175 nm	*S. aureus* (+)	Reduced bacterial adhesion thanks to lower contact area	[214] 2016
S235JRC steel 316Ti SS	Femtosecond laser Ti:sapphire, λ = 790 nm Pulse duration: 30 fs	• LIPSS:Λ = 700 nm	*E. coli* (−) *S. aureus* (+)	*E. coli*: reduced adhesion *S. aureus*: increased adhesion	[260] 2017
Titanium Grade 2	Femtosecond laser Yb:KGW, λ = 1030 nm Pulse duration: 300 fs	• LIPSS:Λ = 340, 637, 751 nm	Saos-2	Better cytocompatibility for 637 nm More elongated shape of the cells Perpendicular alignment of cells	[235] 2018
TZ-3Y20AB (ATZ)	Femtosecond laser Yb:KYW, λ = 1030 nm Pulse duration: 560 fs	Multiscale structure• Grooves:Width = 10 μm• LIPSS:Λ = 300–400 nmPerpendicular to grooves	HBMSCs	Higher metabolic activity Increased proliferation Cell mineralization Alignment along the grooves	[261] 2018
99.7 % pure Ti	Femtosecond laser λ = 1030 nm Pulse duration: 300 fs	• LIPSS:Λ = 400 nm• Columns withoverlapped LIPSS:Λ = 500 nmColumns spacing = 1 μm	*E. coli* (−) MSCs	Good antibacterial behavior, especially columns with overlapped LIPSS Cytocompatible Better cell spreading	[262] 2020
TiAl alloy	Femtosecond laser λ = 1030 nm Pulse duration: 40 fs Repetition rate: 50 kHz	• Grooves:Λ = 25 μm, 5 μm, 15 μm• Holes:Λ = 20 μmDiameter = 5 μm	*S. aureus* *S. epidermidis*	Reduce bacteria adhesion Biocide effect	[263] 2022
Ti-6Al-4 V	Femtosecond laser λ = 1030 nm and 515 nm Pulse duration: 400 fs	• LSFL:Λ = 761 nm, 392 nm	HGF *Streptococcus mutans* *Porphyromonas gingivalis*	Reduce bacteria adhesion Enhance adhesion of HGF	[264] 2022
Ti-6Al-4 V	Femtosecond laser λ = 1030 nm Pulse duration: 400 fs	• LSFL:Λ = 761 nm• Radial LIPSS	hMSCs	Radial LIPSS promote osteoblastic differentiation	[265] 2022

cm^2 to create two different surface patterns: grooves and dimples. The grooves had an average width and depth of approximately 28.6 and 10.2 μm, respectively, and the dimples had an average diameter and depth of approximately 32.23 and 2.44 μm, respectively. The laser treatments induced a slight change in the surface composition, especially by removing the oxide layer. The cell viability of MG63 osteoblasts on the as-cast and both textured samples was evaluated by measuring the optical density (cell counting kit-8 assay). The as-cast BMG, as well as the dimpled textured surface exhibited the same optical density as the positive control sample, indicating their good cytocompatibility. The grooves textured sample exhibited a 22 % optical density increase, synonymous with even better cytocompatibility. Regarding the cell morphology, the microstructure had a strong impact. As observed in Fig. 28, cell attachment was significantly decreased on the dimple-textured surfaces. Although the cells were randomly dispersed on the as-cast surface, they were preferentially orientated along the grooves.

Huang *et al.* observed the effect of femtosecond laser irradiation (λ = 1030 nm, pulse duration of 300 fs) on surface texturing and antibacterial properties of a $Zr_{55}Cu_{16}Ni_{15}Ti_{10}Al_4$ BMG [271]. Different surface structures were obtained: LIPSS, SWPSS, and pore structure. LIPSS and SWPSS exhibited a periodicity of approximately 830 and 2930 nm, respectively. The pore structure was composed of arranged columns containing a series of microholes. The columns had a periodicity of 10.12 μm, and the microholes had a diameter of 2.3 μm with a distance between them of approximately 4.3 μm along each column. The bacterial adhesion of *E. coli* was observed on polished and textured surfaces

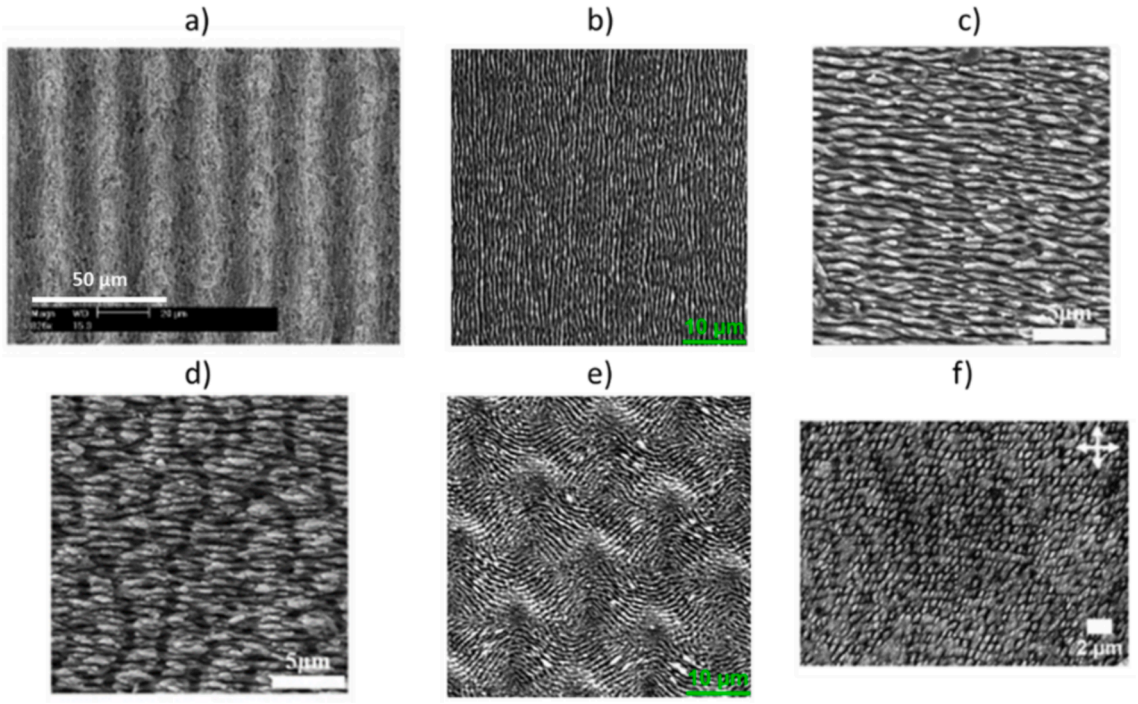

Fig. 25. SEM images of a) Grooves [255], b) LSFL [265], c) Nano-ripples [262], d) Overlapped LIPSS structure [262], e) Radial LIPSS [265] and f) Nanopillars [214].

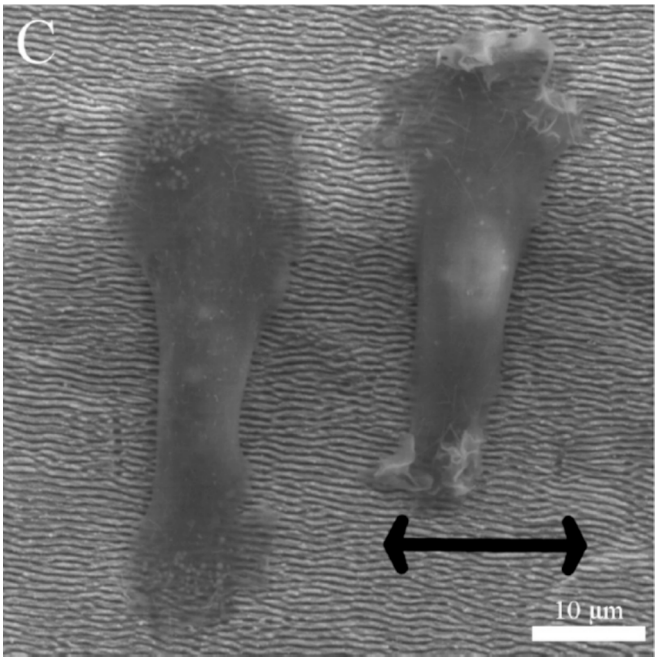

Fig. 26. SEM image of adhesion of Saos-2 cells on femtosecond laser-textured titanium (the double-sided arrows indicate the direction of the periodic patterns of 620 nm of period) [235].

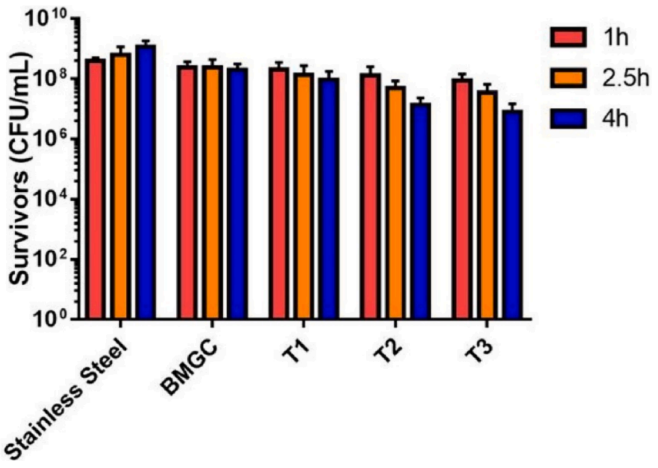

Fig. 27. Colony forming units of E. coli for all laser textured samples after 1, 2.5, and 4 h of contact compared with those for as-cast $Cu_{55}Zr_{40}Al_5$ BMG (BMGC) and stainless steel [269].

using fluorescence microscopy (Fig. 29). The LIPSS exhibited lower adhesion than the polished sample; however, the SWPSS led to a better bactericidal effect. The pore structure exhibited an adhesion rate that was a bit lower than that of the SWPSS.

Du *et al.* textured the surface of different Zr-based BMGs with a femtosecond laser ($\lambda = 1030$ nm) to improve their antibacterial and cytocompatible properties [272]. All four tested BMGs were industrial grade: V105s ($Zr_{43.3}Cu_{27.8}Ni_{15.2}Al_{9.1}Ti_{4.6}$), V105 ($Zr_{57.5}Cu_{21.1}Ni_{14.2}Al_{3.7}Ti_{3.5}$), 106c ($Zr_{63.2}Cu_{21.4}Ni_{11.3}Al_{4.1}$), and Zum ($Zr_{58.9}Cu_{33.2}Ni_{4.2}Al_{3.7}$). For each of these BMGs, three surface textures were realized: polished (before laser irradiation), LIPSS at low fluence (0.23 J/mm^2), and nanoparticles at high fluence (2.3 J/mm^2). Fig. 30 shows the nanoparticles and LIPSS textured obtained on V105s (the results for the other BMGs were similar). For the LIPSS, in addition to having a given periodicity (of approximately 800 nm), they also had a certain nanoscale roughness due to the presence of many nanometric particles, as visible in Fig. 30b.

To determine the antibacterial character of the textured surfaces, the adhesion of *E. coli* and *S. aureus* bacteria was observed using fluorescence microscopy. Fig. 31 presents the results obtained for the four BMGs for each surface. The surface coverage rate was also calculated to observe the differences more quantitatively.

It should be noted that no crystallization appeared during irradiation; therefore, the variations observed were caused by the topography. The laser irradiation thus induced a bactericidal effect, particularly with

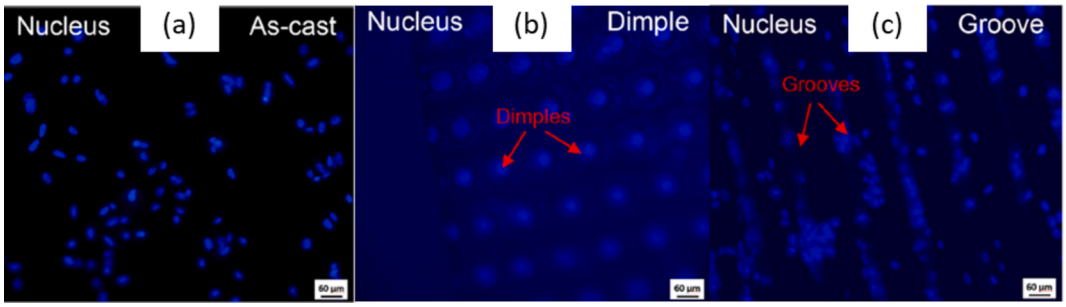

Fig. 28. Morphologies of MG63 cell nucleus cultured on $Zr_{52.8}Cu_{17.6}Ni_{14.8}Al_{9.9}Ti_{4.9}$ surfaces for different surface patterns: a) as-cast, b) pit-textured, c) groove-textured [270].

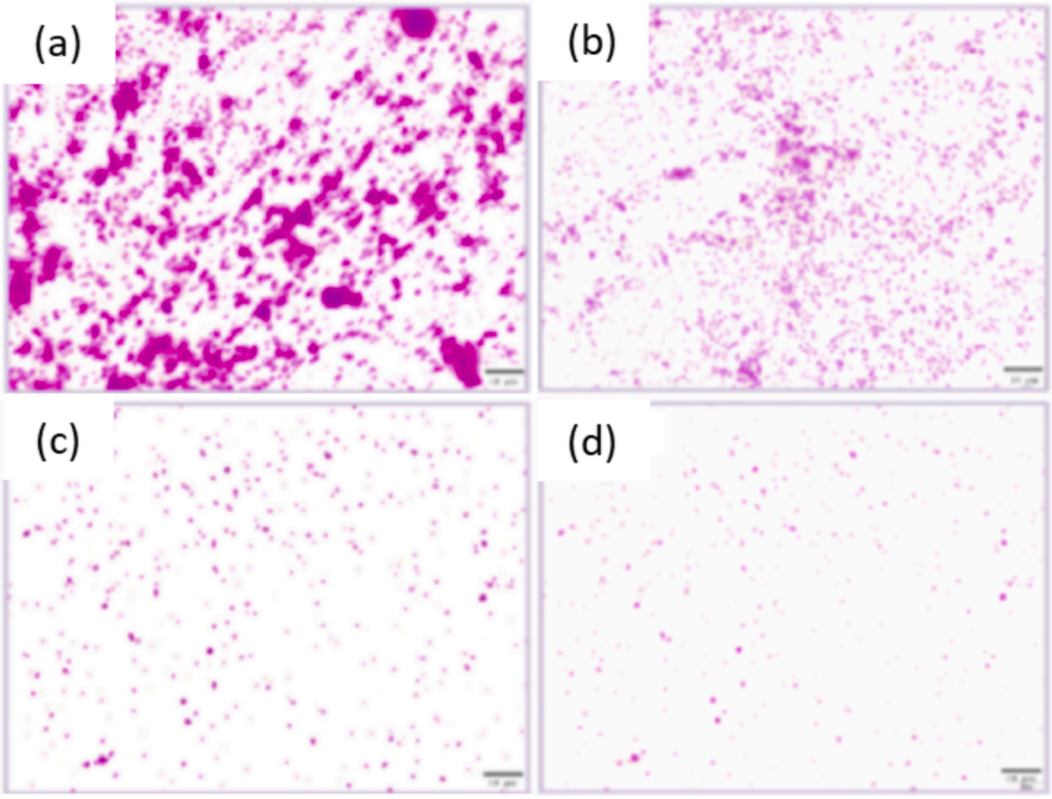

Fig. 29. Fluorescence microscopy images of E.coli adhesion on different surfaces: a) polished, b) LIPSS, c) SWPSS, d) microholes [271].

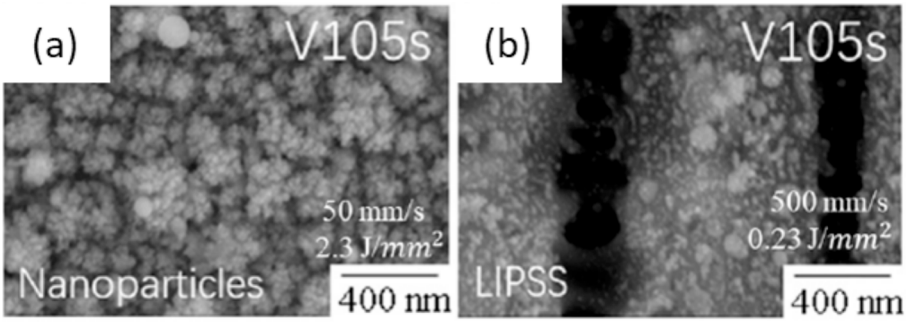

Fig. 30. SEM images of V105s BMG after laser irradiation: a) Nanoparticle texture; b) LIPSS texture [272].

the LIPSS texture. The results slightly fluctuated depending on the BMG, although the compositions were quite close. The texturing also appeared to have a more important bactericidal effect on *E. coli* than on *S. aureus*, a phenomenon that has already been observed on other materials with LIPSS textures [260]. These results can be easily understood from Fig. 32 [272]. For a polished surface, Du *et al.* show that bacteria have a large contact area with the surface, and this area is smaller for a nanoparticle surface, which reduces bacterial adhesion. LSFL, due to their submicron

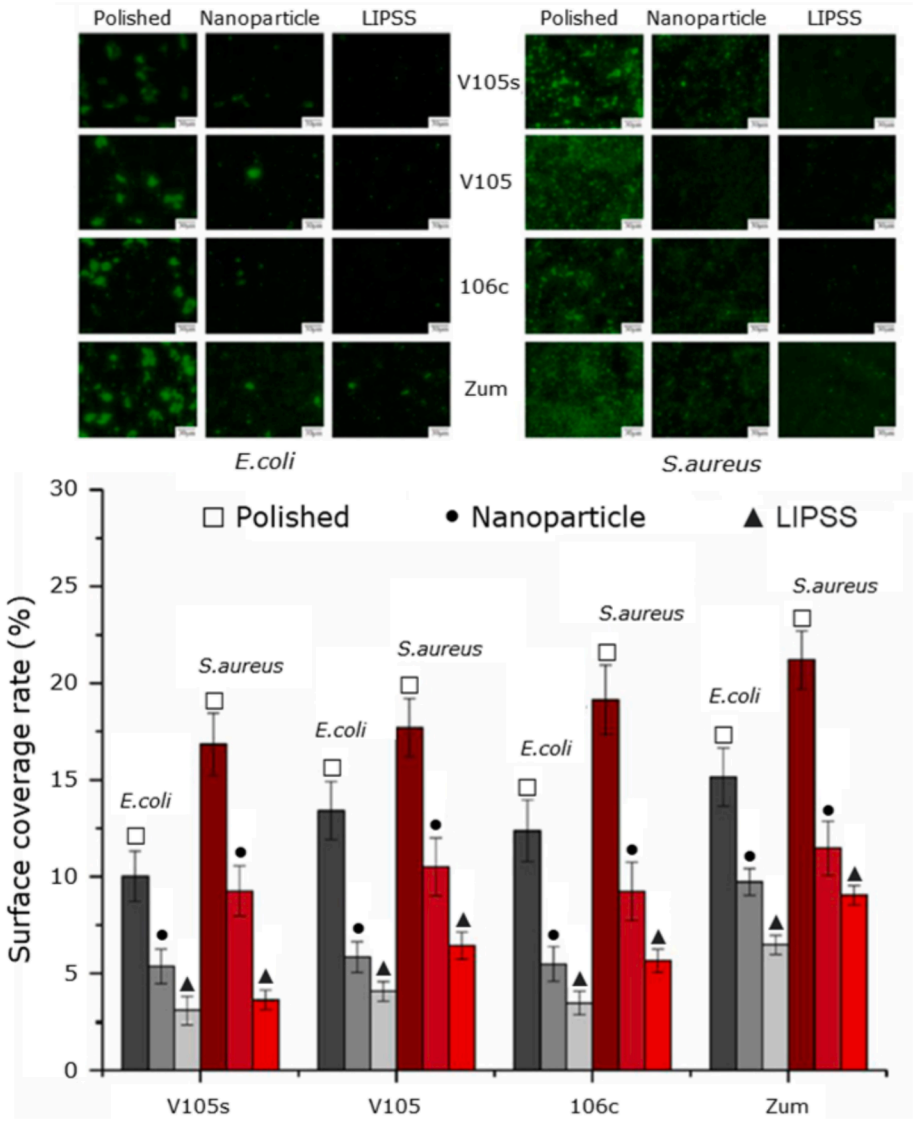

Fig. 31. Adhesion of E. coli and S. aureus after 24 h incubation: Top) fluorescence microscopy images for different surface structures and BMGs; Bottom) surface coverage of bacteria [272].

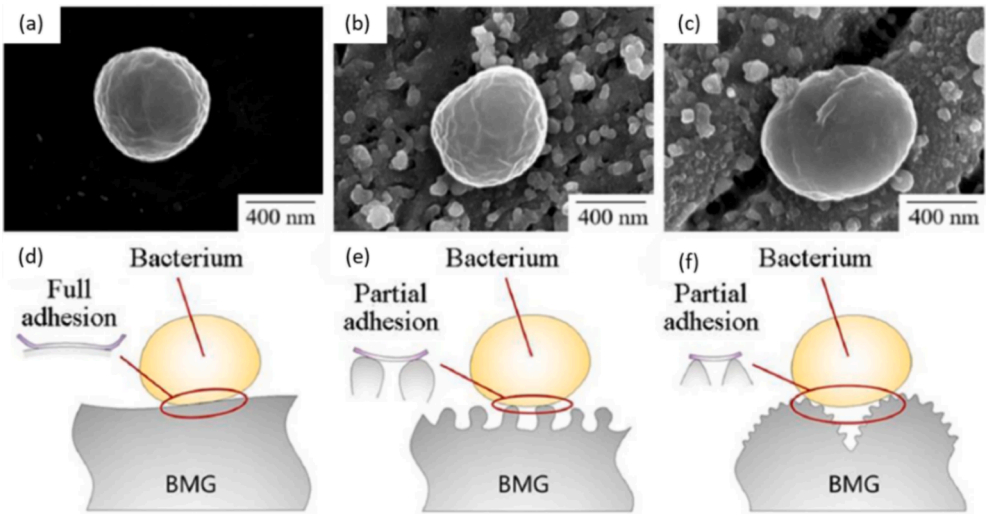

Fig. 32. Adhesion of S. aureus on $Zr_{43.3}Cu_{27.8}Ni_{15.2}Al_{9.1}Ti_{4.6}$ (V105s): a) SEM image on polished surface, b) SEM image on nanoparticle surface, c) SEM image on LIPSS surface, d) adhesion on polished surface, e) adhesion on nanoparticle surface, f) adhesion on LIPSS surface [272].

periodicity and nanoscale roughness, further decrease the contact between the bacteria and surface and, thus, their adhesion. Because *E. coli* is rod-shaped, it is more sensitive to deformation due to partial adhesion than *S. aureus*, which explains the greater antibacterial effect for *E. coli*.

In addition, they conducted cytocompatibility tests using fluorescence microscopy with MC3T3-E1 cells [272]. The cell viability was slightly lower than for the polished surface, especially for the nanoparticle texture; however, the viability rate remained high enough to consider the surface as cytocompatible. The laser surface texturing thus had a very low impact on the cell viability. More recently they studied the impact of biomimetic surfaces on adhesion and antibacterial tests [273] on $Zr_{43}Cu_{28}Ni_{15}Al_9Ti_5$ metallic glass. They show that the shark skin-like structure [197], that has the highest roughness, presents the most important changes compared to the polished surface.

Some other recent work from H. Huang *et al.* also studied the impact of laser texturing of Ti and Zr-based metallic glasses on the adhesion of cells and bacteria. They show that the adhesion of MC3T3-E1 cells is enhanced on textured Ti-based metallic glass ($Ti_{47.5}Zr_{25}Cu_{22.5}Ni_5$), with the higher adhesion obtained with SWPSS structures. This characteristic is also seen of Ti6Al4V titanium alloy with lower increasing of adhesion (Fig. 33) [229]. In comparison of these tests, a bacteria adhesion comparison have been made on Zr-based metallic glasses ($Zr_{53\text{-}56}Cu_{15\text{-}19}Ni_{12\text{-}16}Ti_{8\text{-}11}Al_4$) and shown that, contrarily to cell adhesion test on Ti-based metallic glass, the femtosecond laser texture of the surface reduces the adhesion of bacteria (*E. Coli* and *S. aureus*) (Fig. 34) [174].

These studies indicate that laser irradiation to modify the biological properties of metallic glasses is a very promising technique that leads to good antibacterial and cytocompatible properties. However, these studies are not very numerous, whereas there is a very large number of metallic glasses systems. Moreover, the biological properties of laser-textured TFMGs have not yet been studied. Given their thin-film form, the use of a femtosecond laser to nanotexture their surface, *i.e.* in the form of LIPSS, is possible and remains to be explored.

8. Conclusions and perspectives

This review presented the state-of-the-art research on metallic glasses, microorganisms, and surface texturing by laser as well as the interactions between these three fields. For metallic glasses, the history of the different compositions and synthesis techniques from their discovery until today, in the form of BMGs and TFMGs, was discussed along their main properties. The characteristics of bacteria, how they behave on textured surfaces, and the importance of fighting against their proliferation were covered. Eukaryotic cells were also described, as well as their behavior in contact with surfaces. For laser texturing, two main axes were defined: the ablative regime and the formation of LIPSS by ultrafast pulsed laser.

A review of the last years' scientific research concerning the interaction between metallic glasses and microorganisms was performed. In terms of antibacterial properties, *E. coli* and *S. aureus* are the most commonly used because of their prevalence in hospital-acquired infections. Ideal compositions are Zr- and Ti- based because of their high stability and good biocompatibility. The elements that create this bactericidal effect are typically Cu, Ag, and Al. These elements must be present in sufficient quantity in metallic glasses to decrease bacterial adhesion without exceeding a certain threshold. Above this limit, the obtained material may rapidly corrode and therefore become toxic. An element to avoid would be Ni, to which a significant part of the population is hypersensitive[274]. Ti has no bactericidal effect but is critical because of its well-known intrinsic biocompatibility. It is extensively

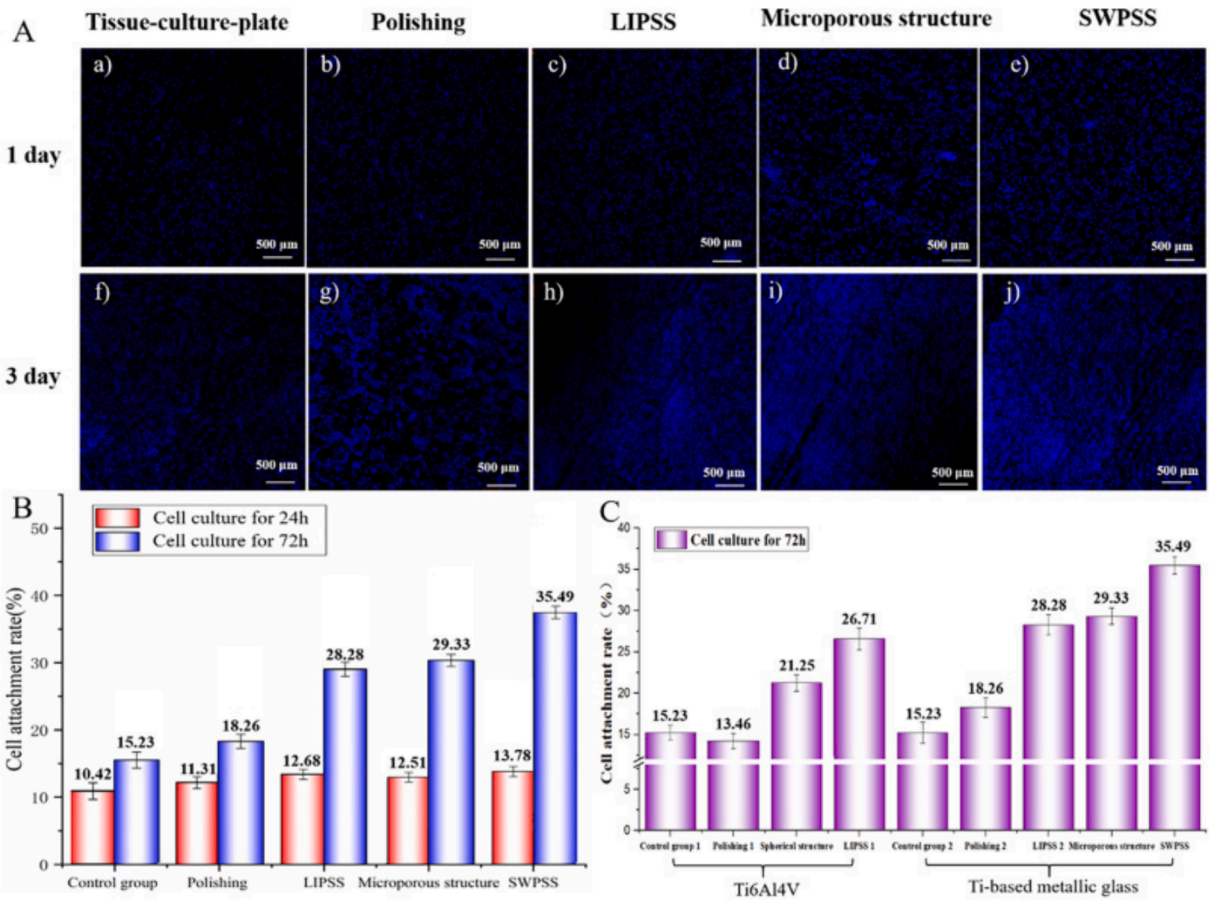

Fig. 33. (a) Adhesion of MC3T3-E1 cells (in fluorescence microscopy) and (b) cell adhesion percentage on polished and textured $Ti_{47.5}Zr_{25}Cu_{22.5}Ni_5$ metallic glass. (c) Comparison of the MC3T3-E1 cells adhesion percentage on Ti6Al4V and $Ti_{47.5}Zr_{25}Cu_{22.5}Ni_5$ metallic glass [229].

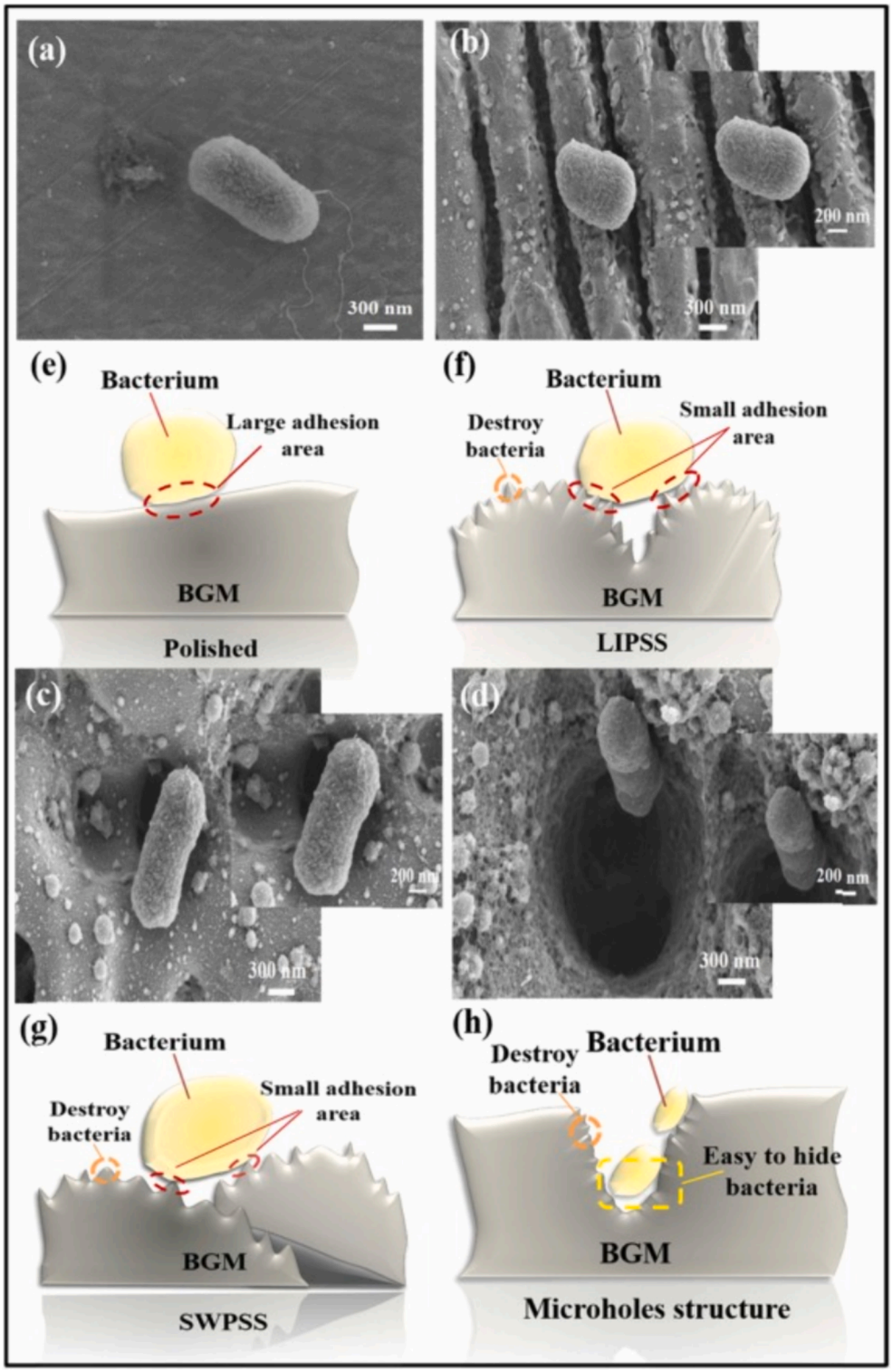

Fig. 34. Changes of bacterial adhesion ((a)-(d) SEM images of E. Coli, (e)-(h) schemes) depending of the surface texture of a $Zr_{53\text{-}56}Cu_{15\text{-}19}Ni_{12\text{-}16}Ti_{8\text{-}11}Al_4$ BMG [174].

used in the biomedical field (generally as Ti–6Al–4 V), and its presence in a metallic glass can be reassuring for professionals in the medical field.

Biocompatible metallic glasses have been separated into two categories: bioinert and biodegradable materials. Most common bioinert metallic glasses are Zr- and Ti-based. The compositions studied are not very different from those for antibacterial properties. For example, Cu, Al, or Ag are also usually found in investigated compositions. According to the literature review, compositions with good cytocompatibility or biocompatibility would obey the law: at.% Zr + at.% Cu + at.% Ti $\geq$ 65 %. Tests performed *in vivo* indicate that BMGs can have very good biocompatibility. However, it remains some doubt about TFMGs, as the only *in vivo* study has given mixed results with slow osseointegration, although the *in vitro* cytocompatibility has been attested. There is a good

balance between the number of studies dedicated to BMGs and TFMGs; however, the latter are more promising for large implants and surgical tools. For biodegradable alloys, Mg-based and Ca-based metallic glasses are the most common. The addition of Zn, and sometimes Sr, results in alloys with very biocompatible alloys. Most of the compositions studied belong to the Mg–Zn–Ca system. Because of their dissolution, the main issue of these materials is related to the H_2 release, which is therefore a fundamental criterion to be studied. It is also critical to measure the corrosion rate of these alloys to estimate their lifetime before complete resorption. To do this, studies in solutions that are similar to the human body are essential. SBF solution is the most representative when working on bone implants because its composition is similar to that of blood plasma.

Numerous promising studies have been performed on metallic glasses. The performance of these materials, particularly for biomedical applications, can still be improved through a further surface treatment. For example, laser texturing can be used to modify the surface affinity toward microorganisms. The biologic effect can indeed be directly linked to a modification of the surface chemistry with in particular formation of a thin oxide film, or correlated with the structure of the subsurface susceptible to be locally devitrified. The activity of both cells and bacteria can also be indirectly influenced by the microstructure of the laser textured surface, which the wetting properties are most often drastically changed. Laser ablation, which produces structures with dimensions larger than 10 μm (often grooves), leads to better cell viability and cell adhesion, as observed with various eukaryotic cells. These cells also tend to align along grooves when they are close in width and deeper than 5 μm, which would therefore promote the osseointegration of implants. The formation of LIPSS by a femtosecond laser has also been shown to be effective in improving the cytocompatibility of the surface. In addition, these structures exhibit a strong bactericidal effect.

To conclude, many advances have recently been made in the synthesis of BMGs and TFMGs, the study of the interaction between microorganisms and textured surfaces, and surface structuration by a laser. It is thus now possible to combine these three fields to engineer multifunctional durable surfaces with very good antibacterial and biocompatibility properties. The path toward such biomedical devices has already been paved by several scientific studies, which have demonstrated that these materials fulfill tomorrow's biomaterials requirements.

CRediT authorship contribution statement

N. Lebrun: Writing – original draft, Methodology, Investigation. **F. Dupla:** Writing – original draft, Methodology, Investigation. **H. Bruhier:** Writing – original draft, Methodology, Investigation. **M. Prudent:** Validation. **A. Borroto:** Validation. **C. Der Loughian:** Writing – original draft, Methodology. **F. Bourquard:** Validation. **J-M. Pelletier:** Validation, Resources. **M. Rousseau:** Validation. **J.-P. Colombier:** Validation. **J.-F. Pierson:** Validation. **F. Garrelie:** Writing – original draft, Validation. **P. Steyer:** Writing – review & editing, Visualization, Validation, Supervision, Project administration, Methodology, Funding acquisition.

Declaration of competing interest

The authors declare that they have no known competing financial interests or personal relationships that could have appeared to influence the work reported in this paper.

Data availability

Data will be made available on request.

Acknowledgements

This work is supported by the ANR projects MEGALIT (ANR-18-CE08-0018) and AWOCAT (ANR-22-CE08-0030) of the French Agence Nationale de la Recherche, and the projet SAFE within Investment for the future program (PIA): EUR Manutech Sleight – ANR – 17 -EURE – 0026.

References

[1] J.L. Ke, C.H. Huang, Y.H. Chen, W.Y. Tsai, T.Y. Wei, J.C. Huang, In vitro biocompatibility response of Ti–Zr–Si thin film metallic glasses, Appl. Surf. Sci. 322 (2014) 41–46, https://doi.org/10.1016/j.apsusc.2014.09.204.
[2] M. Chen, A brief overview of bulk metallic glasses, NPG Asia Mater. 3 (2011) 82–90, https://doi.org/10.1038/asiamat.2011.30.
[3] I. Shivakoti, G. Kibria, R. Cep, B.B. Pradhan, A. Sharma, Laser surface texturing for biomedical applications: A review, Coatings 11 (2021) 1–15, https://doi.org/10.3390/coatings11020124.
[4] W. Klement, R.H. Willens, P. Duwez, Non-crystalline structure in solidified gold-silicon alloys, Nature 187 (1960) 869–870, https://doi.org/10.1038/187869b0.
[5] R.C. Ruhl, Cooling rates in splat cooling, Mater. Sci. Eng. 1 (1967) 313–320, https://doi.org/10.1016/0025-5416(67)90013-4.
[6] H.S. Chen, D. Turnbull, Formation, stability and structure of palladium-silicon based alloy glasses, Acta Metall. 17 (1969) 1021–1031, https://doi.org/10.1016/0001-6160(69)90048-0.
[7] R.C. Budhani, T.C. Goel, K.L. Chopra, Melt-spinning technique for preparation of metallic glasses, Bull. Mater. Sci. 4 (1982) 549–561, https://doi.org/10.1007/BF02824962.
[8] A. Inoue, H.S. Chen, J.T. Krause, T. Masumoto, Young's modulus sound velocity and Young's modulus of Ti-, Zr- and Hf-based amorphous alloys, J. Non Cryst. Solids 68 (1984) 63–73, https://doi.org/10.1016/0022-3093(84)90034-6.
[9] A. Peker, W.L. Johnson, A highly processable metallic glass: Zr41.2Ti13.8Cu12.5Ni10.0Be22.5, Appl. Phys. Lett. 63 (1993) 2342–2344, https://doi.org/10.1063/1.110520.
[10] N. Nishiyama, K. Takenaka, H. Miura, N. Saidoh, Y. Zeng, A. Inoue, The world's biggest glassy alloy ever made, Intermetallics 30 (2012) 19–24, https://doi.org/10.1016/j.intermet.2012.03.020.
[11] Q. Halim, N.A.N. Mohamed, M.R.M. Rejab, W.N.W.A. Naim, Q. Ma, Metallic glass properties, processing method and development perspective: a review, Int J Adv Manuf Technol 112 (2021) 1231–1258, https://doi.org/10.1007/s00170-020-06515-z.
[12] W. Wu, X. Li, Q. Liu, J.Y. Hsi Fuh, A. Zheng, Y. Zhou, L. Ren, G. Li, Additive manufacturing of bulk metallic glass: Principles, materials and prospects, Materials Today Advances 16 (2022) 100319, https://doi.org/10.1016/j.mtadv.2022.100319.
[13] A. Inoue, A. Takeuchi, Recent development and application products of bulk glassy alloys, Acta Mater. 59 (2011) 2243–2267, https://doi.org/10.1016/j.actamat.2010.11.027.
[14] J. Qiao, H. Jia, P.K. Liaw, Metallic glass matrix composites, Mater. Sci. Eng. R. Rep. 100 (2016) 1–69, https://doi.org/10.1016/j.mser.2015.12.001.
[15] C. Chattopadhyay, K.S.N.S. Idury, J. Bhatt, K. Mondal, B.S. Murty, Critical evaluation of glass forming ability criteria, Mater. Sci. Technol. 32 (2016) 380–400, https://doi.org/10.1179/1743284715Y.0000000104.
[16] A. Inoue, T. Zhang, A. Takeuchi, Ferrous and nonferrous bulk amorphous alloys, Mater. Sci. Forum 269–272 (1998) 855–864, https://doi.org/10.4028/www.scientific.net/msf.269-272.855.
[17] D. Ma, H. Tan, D. Wang, Y. Li, E. Ma, Strategy for pinpointing the best glass-forming alloys, Appl. Phys. Lett. 86 (2005) 1–3, https://doi.org/10.1063/1.1922570.
[18] F. Ren, L. Ward, T. Williams, K.J. Laws, C. Wolverton, J. Hattrick-Simpers, A. Mehta, Accelerated discovery of metallic glasses through iteration of machine learning and high-throughput experiments, Sci. Adv. 4 (2018), https://doi.org/10.1126/sciadv.aaq1566.
[19] Y. Douest, R.M. Forrest, B. Ter-Ovanessian, N. Courtois, F. Tancret, A.L. Greer, J. Chevalier, D. Fabrègue, Machine learning-guided exploration and experimental assessment of unreported compositions in the quaternary Ti-Zr-Cu-Pd biocompatible metallic glass system, Acta Biomater. 175 (2024) 411–421, https://doi.org/10.1016/j.actbio.2023.12.028.
[20] A. Jabed, M.M. Khan, J. Camiller, M. Greenlee-Wacker, W. Haider, I. Shabib, Property optimization of Zr-Ti-X (X = Ag, Al) metallic glass via combinatorial development aimed at prospective biomedical application, Surf. Coat. Technol. 372 (2019) 278–287, https://doi.org/10.1016/j.surfcoat.2019.05.036.
[21] A. Liens, A. Etiemble, P. Rivory, S. Balvay, J.-M. Pelletier, S. Cardinal, D. Fabrègue, H. Kato, P. Steyer, T. Munhoz, J. Adrien, N. Courtois, D. Hartmann, J. Chevalier, On the potential of bulk metallic glasses for dental implantology: case study on Ti40Zr10Cu36Pd14, Materials 11 (2018) 249, https://doi.org/10.3390/ma11020249.
[22] P. Ramasamy, A. Szabo, S. Borzel, J. Eckert, M. Stoica, A. Bárdos, High pressure die casting of Fe-based metallic glass, Sci. Rep. 6 (2016), https://doi.org/10.1038/srep35258.
[23] K.J. Laws, B. Gun, M. Ferry, Large-scale production of Ca65Mg15Zn20 bulk metallic glass samples by low-pressure die-casting, Mater. Sci. Eng. A 475 (2008) 348–354, https://doi.org/10.1016/j.msea.2007.04.059.
[24] R. Nowosielski, R. Babilas, Fabrication of bulk metallic glasses by centrifugal casting method, Journal of Achievements in Materials and Manufacturing Engineering 20 (2007) 487–490.

[25] Z. Liu, W. Chen, J. Carstensen, J. Ketkaew, R.M.O. Mota, J.K. Guest, J. Schroers, 3D metallic glass cellular structures, Acta Mater. 105 (2016) 35–43, https://doi.org/10.1016/j.actamat.2015.11.057.

[26] A. Akbarpour, D.A. Milkova, E.N. Zanaeva, M.S. Parkhomenko, V.V. Cheverikin, A. Lubenchenko, A.I. Bazlov, Influence of cold rolling process and chemical composition on the mechanical properties and corrosion behavior of Zr-based metallic glasses, Metals 11 (2021), https://doi.org/10.3390/met11101514.

[27] J. Kim, T. Lee, Brazing method to join a novel Cu54Ni6Zr22Ti18 bulk metallic glass to carbon steel, Sci. Technol. Weld. Join. 22 (2017) 714–718, https://doi.org/10.1080/13621718.2017.1306155.

[28] A.A. Aliyu, A.M. Abdul-Rani, T.V.V.L.N. Rao, E. Axinte, S. Hastuty, R. P. Parameswari, J.R. Subramaniam, S.P. Thyagarajan, Characterization, adhesion strength and in-vitro cytotoxicity investigation of hydroxyapatite coating synthesized on Zr-based BMG by electro discharge process, Surface and Coatings Technology 370 (2019) 213–226, https://doi.org/10.1016/j.surfcoat.2019.04.084.

[29] L. Zhang, H. Huang, Micro machining of bulk metallic glasses: a review, Int. J. Adv. Manuf. Technol. 100 (2019) 637–661, https://doi.org/10.1007/s00170-018-2726-y.

[30] P. Zhang, J. Tan, Y. Tian, H. Yan, Z. Yu, Research progress on selective laser melting (SLM) of bulk metallic glasses (BMGs): a review, Int. J. Adv. Manuf. Technol. (2021) 2017–2057, https://doi.org/10.1007/s00170-021-07990-8.

[31] L. Deng, S. Wang, P. Wang, U. Kühn, S. Pauly, Selective laser melting of a Ti-based bulk metallic glass, Mater. Lett. 212 (2018) 346–349, https://doi.org/10.1016/j.matlet.2017.10.130.

[32] C. Zhang, D. Ouyang, S. Pauly, L. Liu, 3D printing of bulk metallic glasses, Mater. Sci. Eng. R. Rep. 145 (2021) 100625, https://doi.org/10.1016/j.mser.2021.100625.

[33] N. Sohrabi, J. Jhabvala, R.E. Logé, Additive manufacturing of bulk metallic glasses—process, challenges and properties: A review, Metals 11 (2021), https://doi.org/10.3390/met11081279.

[34] H.F. Li, Y.F. Zheng, Recent advances in bulk metallic glasses for biomedical applications, Acta Biomater. 36 (2016) 1–20, https://doi.org/10.1016/j.actbio.2016.03.047.

[35] Y. Gu, X. Han, F. Yan, L. Li, The strain rate sensitivity of heterogeneous thin film metallic glasses: interplay between nanoscale heterogeneity and dynamic plasticity, Front. Mater. 9 (2022) 925096, https://doi.org/10.3389/fmats.2022.925096.

[36] N. Bönninghoff, W. Diyatmika, J.P. Chu, S. Mráz, J.M. Schneider, C.-L. Lin, F. Eriksson, G. Greczynski, ZrCuAlNi thin film metallic glass grown by high power impulse and direct current magnetron sputtering, Surf. Coat. Technol. 412 (2021) 127029, https://doi.org/10.1016/j.surfcoat.2021.127029.

[37] S. Thanka Rajan, M. Das, P.S. Kumar, A. Arockiarajan, B. Subramanian, Biological performance of metal metalloid (TiCuZrPd:B) TFMG fabricated by pulsed laser deposition, Colloids Surf. B Biointerfaces 202 (2021), https://doi.org/10.1016/j.colsurfb.2021.111684.

[38] A. Obeydavi, A. Shafyei, A. Rezaeian, P. Kameli, J.W. Lee, Microstructure, mechanical properties and corrosion performance of Fe44Cr15Mo14Co7C10B5Si5 thin film metallic glass deposited by DC magnetron sputtering, J. Non Cryst. Solids 527 (2020) 119718, https://doi.org/10.1016/j.jnoncrysol.2019.119718.

[39] J. Lee, K.H. Huang, K.C. Hsu, H.C. Tung, J.W. Lee, J.G. Duh, Applying composition control to improve the mechanical and thermal properties of Zr-Cu-Ni-Al thin film metallic glass by magnetron DC sputtering, Surf. Coat. Technol. 278 (2015) 132–137, https://doi.org/10.1016/j.surfcoat.2015.07.015.

[40] Y.H. Liu, T. Fujita, A. Hirata, S. Li, H.W. Liu, W. Zhang, A. Inoue, M.W. Chen, Deposition of multicomponent metallic glass films by single-target magnetron sputtering, Intermetallics 21 (2012) 105–114, https://doi.org/10.1016/j.intermet.2011.10.007.

[41] M.M. Khan, I. Shabib, W. Haider, A combinatorially developed Zr-Ti-Fe-Al metallic glass with outstanding corrosion resistance for implantable medical devices, Scr. Mater. 162 (2019) 223–229, https://doi.org/10.1016/j.scriptamat.2018.11.011.

[42] Y. Liu, J. Padmanabhan, B. Cheung, J. Liu, Z. Chen, B.E. Scanley, D. Wesolowski, M. Pressley, C.C. Broadbridge, S. Altman, U.D. Schwarz, T.R. Kyriakides, J. Schroers, Combinatorial development of antibacterial Zr-Cu-Al-Ag thin film metallic glasses, Sci. Rep. 6 (2016) 1–8, https://doi.org/10.1038/srep26950.

[43] S. Comby-Dassonneville, T. Venot, A. Borroto, E. Longin, C. Der Loughian, B. Ter Ovanessian, M.A. Leroy, J.F. Pierson, P. Steyer, ZrCuAg thin-film metallic glasses: Toward biostatic durable advanced surfaces, ACS Appl. Mater. Interfaces 13 (2021) 17062–17074, https://doi.org/10.1021/acsami.1c01127.

[44] M. Apreutesei, P. Djemia, L. Belliard, G. Abadias, C. Esnouf, A. Billard, P. Steyer, Structural-elastic relationships of Zr-TL (TL = Cu Co, Ni) thin films metallic glasses, J. Alloy. Compd. 707 (2017) 126–131, https://doi.org/10.1016/j.jallcom.2016.12.208.

[45] M. Ghidelli, A. Orekhov, A.L. Bassi, G. Terraneo, P. Djemia, G. Abadias, M. Nord, A. Béché, N. Gauquelin, J. Verbeeck, J.P. Raskin, D. Schryvers, T. Pardoen, H. Idrissi, Novel class of nanostructured metallic glass films with superior and tunable mechanical properties, Acta Mater. 213 (2021), https://doi.org/10.1016/j.actamat.2021.116955.

[46] B. Zhang, X. Yang, G. Cao, G. Liu, Z. Wei, H. Zong, Y. Yin, H. Bala, Characteristic studies on the ZrCuAlSi multi-component thin-film metallic glasses fabricated by pulsed laser deposition, Applied Physics A: Materials Science and Processing 126 (2020) 3–9, https://doi.org/10.1007/s00339-020-03631-1.

[47] J. Rivory, J.M. Frigerio, M. Harmelin, A. Quivy, Y. Calvayrac, J. Bigot, Preparation of CuxZr1-x metallic glasses by sputtering and their thermal stability, electrical and optical properties, Thin Solid Films 89 (1982) 323–327, https://doi.org/10.1016/0040-6090(82)90608-3.

[48] K. Shimamura, K. Miura, K. Kawashima, K. Asami, K. Hashimoto, The corrosion behavior of sputter-deposited amorphous copper-valve metal alloys in 12 N HCl, in: Proceedings of the Symposium on Corrosion, Electrochemistry, and Catalysis of Metallic Glasses, The electrochemical Society, 1988: pp. 232–237.

[49] M. Nastasi, F.W. Saris, L.S. Hung, J.W. Mayer, Stability of amorphous Cu/Ta and Cu/W alloys, J. Appl. Phys. 58 (1985) 3052–3058, https://doi.org/10.1063/1.335855.

[50] Q.M. Chen, F.Z. Cui, Y.D. Fan, H. De Li, Metastable bismuth-iron alloy films synthesized with ion mixing and magnetron cosputtering, J. Appl. Phys. 63 (1988) 2452–2453, https://doi.org/10.1063/1.341019.

[51] M. Apreutesei, P. Steyer, L. Joly-Pottuz, A. Billard, J. Qiao, S. Cardinal, F. Sanchette, J.M. Pelletier, C. Esnouf, Microstructural, thermal and mechanical behavior of co-sputtered binary Zr–Cu thin film metallic glasses, Thin Solid Films 561 (2014) 53–59, https://doi.org/10.1016/j.tsf.2013.05.177.

[52] A. Bagherpour, E. Haye, P. Moskovkin, S. Lucas, Vein pattern vs. columnar fracture shape in Cu-Zr thin film metallic glasses: Driving force and mechanism, Materialia 32 (2023) 101914, https://doi.org/10.1016/j.mtla.2023.101914.

[53] P. Yiu, W. Diyatmika, N. Bönninghoff, Y.C. Lu, B.Z. Lai, J.P. Chu, Thin film metallic glasses: Properties, applications and future, J. Appl. Phys. 127 (2020), https://doi.org/10.1063/1.5122884.

[54] S. Comby-Dassonneville, G. Tiphéne, A. Borroto, G. Guillonneau, L. Roiban, G. Kermouche, J.F. Pierson, J.L. Loubet, P. Steyer, Real-time high-temperature scanning indentation: Probing physical changes in thin-film metallic glasses, Appl. Mater. Today 24 (2021), https://doi.org/10.1016/j.apmt.2021.101126.

[55] J.P. Chu, W. Diyatmika, Y.J. Tseng, Y.K. Liu, W.C. Liao, S.H. Chang, M.J. Chen, J. W. Lee, J.S.C. Jang, Coating cutting blades with thin-film metallic glass to enhance sharpness, Sci. Rep. 9 (2019), https://doi.org/10.1038/s41598-019-52054-3.

[56] [57] P. Zeman, M. Zítek, Zuzjaková, R. Čerstvý, Amorphous Zr-Cu thin-film alloys with metallic glass behavior, Journal of Alloys and Compounds 696 (2017) 1298–1306. doi: 10.1016/j.jallcom.2016.12.098.

[57] M. Jain, A. Sharma, K. Pajor, K. Wieczerzak, N.M. della Ventura, X. Maeder, J. J. Kruzic, B. Gludovatz, J. Michler, Mechanical properties and thermal stability of thin film metallic glass compared to bulk metallic glass from ambient to elevated temperatures, J. Alloy. Compd. 960 (2023) 170728, https://doi.org/10.1016/j.jallcom.2023.170728.

[58] D.W. Grogan, Physiology of prokaryotic cells, in: Cell Physiology Source Book, Fourth Edi, Elsevier Inc., 2012, pp. 891–906, https://doi.org/10.1016/B978-0-12-387738-3.00050-0.

[59] D.P. Clark, N.J. Pazdernik, M.R. McGehee, Cells and organisms, Mol. Biol. (2019) 2–37, https://doi.org/10.1016/b978-0-12-813288-3.00001-x.

[60] World Health Organization, Report on the burden of endemic health care-associated infection worldwide, World Health Organization, 2011.

[61] R.B. Moyes, J. Reynolds, D.P. Breakwell, Differential staining of bacteria: Gram stain, Curr. Protoc. Microbiol. (2009) 1–8, https://doi.org/10.1002/9780471729259.mca03cs15.

[62] T.J. Silhavy, D. Kahne, S. Walker, The bacterial cell envelope, Cold Spring Harb. Perspect. Biol. 2 (2010), https://doi.org/10.1101/cshperspect.a000414.

[63] F. Song, H. Koo, D. Ren, Effects of material properties on bacterial adhesion and biofilm formation, J. Dent. Res. 94 (2015) 1027–1034, https://doi.org/10.1177/0022034515587690.

[64] J.B. Kaper, J.P. Nataro, H.L.T. Mobley, Pathogenic Escherichia coli, Nature Reviews Microbiology 2 (2004) 123–140, https://doi.org/10.1038/nrmicro818.

[65] A. Gnanamani, P. Hariharan, M. Paul-Satyaseela, Staphylococcus aureus: Overview of bacteriology, clinical diseases, epidemiology, antibiotic resistance and therapeutic approach, Frontiers in Staphylococcus Aureus (2017), https://doi.org/10.5772/67338.

[66] L.G. Harris, S.J. Foster, R.G. Richards, P. Lambert, D. Stickler, A. Eley, An introduction to Staphylococcus aureus, and techniques for identifying and quantifying S. aureus adhesins in relation to adhesion to biomaterials: Review, Eur. Cell. Mater. 4 (2002) 39–60, https://doi.org/10.22203/ecm.v004a04.

[67] T. Ciociola, L. Giovati, A. Giovannelli, S. Conti, M. Castagnola, A. Vitali, The activity of a mammalian proline-rich peptide against Gram-negative bacteria, including drug-resistant strains, relies on a nonmembranolytic mode of action, Infection and Drug Resistance 11 (2018) 969–979, https://doi.org/10.2147/IDR.S165179.

[68] J. Sun, S. Zhang, X. Chen, J. Chen, B. Han, Growth properties of Staphylococcus aureus in biofilm formed on polystyrene plate, Afr. J. Microbiol. Res. 6 (2012) 3284–3291, https://doi.org/10.5897/AJMR12.147.

[69] S.A. Hacking, A. Khademhosseini, Cells and surfaces in vitro, in: Biomaterials Science: an Introduction to Materials in Medicine, Third Edit, Elsevier, 2013, pp. 408–427, https://doi.org/10.1016/B978-0-08-087780-8.00037-1.

[70] D.A. Towler, R.St. Arnaud, Use of cultured osteoblastic cells to identify and characterize transcriptional regulatory complexes, in: J.P. Bilezikian, L.G. Raisz, G.A. Rodan (Eds.), Principle of Bone Biology Vol.1, 2002.

[71] M.D. Yazid, S.H.Z. Ariffin, S. Senafi, M.A. Razak, R.M.A. Wahab, Determination of the differentiation capacities of murines' primary mononucleated cells and MC3T3-E1 cells, Cancer Cell Int. 10 (2010) 1–12, https://doi.org/10.1186/1475-2867-10-42.

[72] N. Price, S.P. Bendall, C. Frondoza, R.H. Jinnah, D.S. Hungerford, Human osteoblast-like cells (MG63) proliferate on a bioactive glass surface, J. Biomed. Mater. Res. 37 (1997) 394–400, https://doi.org/10.1002/(SICI)1097-4636(19971205)37:3<394::AID-JBM10>3.0.CO;2-C.

[73] M. Aivazi, M. Fathi, F. Nejatidanesh, V. Mortazavi, B.H. Beni, J.P. Matinlinna, Effect of surface modification on viability of L929 cells on zirconia nanocomposite substrat, Journal of Lasers in Medical Sciences 9 (2018) 87–91, https://doi.org/10.15171/jlms.2018.18.

[74] C.R. Pedrosa, C. Chanseau, C. Labrugère, S. Krishnamoorthy, M.C. Durrieu, Mesenchymal stem cell differentiation driven by osteoinductive bioactive nanoscale topographies, Appl. Sci. 11 (2021), https://doi.org/10.3390/app112311209.

[75] A.J. Dulgar-Tulloch, R. Bizios, R.W. Siegel, Human mesenchymal stem cell adhesion and proliferation in response to ceramic chemistry and nanoscale topography, Journal of Biomedical Materials Research - Part A 90 (2009) 586–594, https://doi.org/10.1002/jbm.a.32116.

[76] J.P. Fan, P. Kalia, L. Di Silvio, J. Huang, In vitro response of human osteoblasts to multi-step sol-gel derived bioactive glass nanoparticles for bone tissue engineering, Mater. Sci. Eng. C 36 (2014) 206–214, https://doi.org/10.1016/j.msec.2013.12.009.

[77] N. Jiménez, V.J.D. Krouwer, J.A. Post, A new, rapid and reproducible method to obtain high quality endothelium in vitro, Cytotechnology 65 (2013) 1–14, https://doi.org/10.1007/s10616-012-9459-9.

[78] N. Kaga, T. Akasaka, T. Matsuura, A. Yokoyama, Y. Yoshida, Proliferation of Saos-2 and Ca9-22 cells on grooved and pillared titanium surfaces, Biomed. Mater. Eng. 30 (2020) 559–567, https://doi.org/10.3233/BME-191074.

[79] M. Goto, T. Tsukahara, K. Sato, T. Kitamori, Micro- and nanometer-scale patterned surface in a microchannel for cell culture in microfluidic devices, Anal. Bioanal. Chem. 390 (2008) 817–823, https://doi.org/10.1007/s00216-007-1496-4.

[80] E.I. Akpan, O.P. Gbenebor, S.O. Adeosun, O. Cletus, Chitin and chitosan composites for bone tissue regeneration. Handbook of Chitin and Chitosan Volume 3: Chitin and Chitosan Based Polymer Materials for Various Applications, Elsevier, Chennai, 2020.

[81] Biological evaluation of medical devices — Part 5: Tests for in vitro cytotoxicity, ISO 10993-5 (2009).

[82] J.P. Chu, T.Y. Liu, C.L. Li, C.H. Wang, J.S.C. Jang, M.J. Chen, S.H. Chang, W. C. Huang, Fabrication and characterizations of thin film metallic glasses: Antibacterial property and durability study for medical application, Thin Solid Films 561 (2014) 102–107, https://doi.org/10.1016/j.tsf.2013.08.111.

[83] J.H. Chu, J. Lee, C.C. Chang, Y.C. Chan, M.L. Liou, J.W. Lee, J.S.C. Jang, J.G. Duh, Antimicrobial characteristics in Cu-containing Zr-based thin film metallic glass, Surf. Coat. Technol. 259 (2014) 87–93, https://doi.org/10.1016/j.surfcoat.2014.05.019.

[84] Y.Y. Chu, Y.S. Lin, C.M. Chang, J.K. Liu, C.H. Chen, J.C. Huang, Promising antimicrobial capability of thin film metallic glasses, Mater. Sci. Eng. C 36 (2014) 221–225, https://doi.org/10.1016/j.msec.2013.12.015.

[85] H.W. Chen, K.C. Hsu, Y.C. Chan, J.G. Duh, J.W. Lee, J.S.C. Jang, G.J. Chen, Antimicrobial properties of Zr-Cu-Al-Ag thin film metallic glass, Thin Solid Films 561 (2014) 98–101, https://doi.org/10.1016/j.tsf.2013.08.028.

[86] L. Huang, E.M. Fozo, T. Zhang, P.K. Liaw, W. He, Antimicrobial behavior of Cu-bearing Zr-based bulk metallic glasses, Mater. Sci. Eng. C 39 (2014) 325–329, https://doi.org/10.1016/j.msec.2014.03.017.

[87] V.M. Villapún, H. Zhang, C. Howden, L.C. Chow, F. Esat, P. Pérez, J. Sort, S. Bull, J. Stach, S. González, Antimicrobial and wear performance of Cu-Zr-Al metallic glass composites, Mater. Des. 115 (2017) 93–102, https://doi.org/10.1016/j.matdes.2016.11.029.

[88] A. Etiemble, C. Der Loughian, M. Apreutesei, C. Langlois, S. Cardinal, J. M. Pelletier, J.F. Pierson, P. Steyer, Innovative Zr-Cu-Ag thin film metallic glass deposed by magnetron PVD sputtering for antibacterial applications, J. Alloy. Compd. 707 (2017) 155–161, https://doi.org/10.1016/j.jallcom.2016.12.259.

[89] G.I. Nkou Bouala, A. Etiemble, C. Der Loughian, C. Langlois, J.F. Pierson, P. Steyer, Silver influence on the antibacterial activity of multi-functional Zr-Cu based thin film metallic glasses, Surf. Coat. Technol. 343 (2018) 108–114, https://doi.org/10.1016/j.surfcoat.2017.10.057.

[90] V.M. Villapún, C.C. Lukose, M. Birkett, L.G. Dover, S. González, Tuning the antimicrobial behaviour of Cu85Zr15 thin films in “wet” and “dry” conditions through structural modifications, Surface and Coatings Technology 350 (2018) 334–345, https://doi.org/10.1016/j.surfcoat.2018.06.094.

[91] V.M. Villapún, S. Tardío, P. Cumpson, J.G. Burgess, L.G. Dover, S. González, Antimicrobial properties of Cu-based bulk metallic glass composites after surface modification, Surf. Coat. Technol. 372 (2019) 111–120, https://doi.org/10.1016/j.surfcoat.2019.05.041.

[92] K. Han, H. Jiang, Y. Wang, J. Qiang, C. Yu, Antimicrobial Zr-based bulk metallic glasses for surgical devices applications, J. Non Cryst. Solids 564 (2021), https://doi.org/10.1016/j.jnoncrysol.2021.120827.

[93] P. Dolara, Occurrence, exposure, effects, recommended intake and possible dietary use of selected trace compounds (aluminium, bismuth, cobalt, gold, lithium, nickel, silver), Int. J.of Food Sciences and Nutrition 65 (2014) 911–924, https://doi.org/10.3109/09637486.2014.937801.

[94] A. Rezvan, E. Sharifikolouei, A. Lassnig, V. Soprunyuk, C. Gammer, F. Spieckermann, W. Schranz, Z. Najmi, A. Cochis, A.C. Scalia, L. Rimondini, M. Manfredi, J. Eckert, B. Sarac, Antibacterial activity, cytocompatibility, and thermomechanical stability of Ti40Zr10Cu36Pd14 bulk metallic glass, Materials Today Bio 16 (2022) 100378, https://doi.org/10.1016/j.mtbio.2022.100378.

[95] J.-F. Tang, P.-Y. Huang, J.-H. Lin, T.-W. Liu, F.-C. Yang, C.-L. Chang, Microstructure and Antimicrobial Properties of Zr-Cu-Ti Thin-Film Metallic Glass Deposited Using High-Power Impulse Magnetron Sputtering, Materials 15 (2022) 2461, https://doi.org/10.3390/ma15072461.

[96] Biological responses to metal implants, Food and Drug Administration (FDA) (2019).

[97] W. Götz, E. Tobiasch, S. Witzleben, M. Schulze, Effects of silicon compounds on biomineralization, osteogenesis, and hard tissue formation, Pharmaceutics 11 (2019) 1–27, https://doi.org/10.3390/pharmaceutics11030117.

[98] J. Black, Biological performance of Tantalum, Clin. Mater. 16 (1994) 167–173, https://doi.org/10.1016/0267-6605(94)90113-9.

[99] M.D. Demetriou, A. Wiest, D.C. Hofmann, W.L. Johnson, B. Han, N. Wolfson, G. Wang, P.K. Liaw, Amorphous metals for hard-tissue prosthesis, JOM 62 (2010) 83–91, https://doi.org/10.1007/s11837-010-0038-2.

[100] Y. Liu, Y.M. Wang, H.F. Pang, Q. Zhao, L. Liu, A Ni-free ZrCuFeAlAg bulk metallic glass with potential for biomedical applications, Acta Biomater. 9 (2013) 7043–7053, https://doi.org/10.1016/j.actbio.2013.02.019.

[101] J. Li, H.J. Ai, The responses of endothelial cells to Zr61Ti2Cu25Al12 metallic glass in vitro and in vivo, Mater. Sci. Eng. C 40 (2014) 189–196, https://doi.org/10.1016/j.msec.2014.03.051.

[102] Y. Sun, Y. Huang, H. Fan, Y. Wang, Z. Ning, F. Liu, D. Feng, X. Jin, J. Shen, J. Sun, J.J.J. Chen, In vitro and in vivo biocompatibility of an Ag-bearing Zr-based bulk metallic glass for potential medical use, J. Non Cryst. Solids 419 (2015) 82–91, https://doi.org/10.1016/j.jnoncrysol.2015.03.039.

[103] L. Huang, C. Pu, R.K. Fisher, D.J.H. Mountain, Y. Gao, P.K. Liaw, W. Zhang, W. He, A Zr-based bulk metallic glass for future stent applications: Materials properties, finite element modeling, and in vitro human vascular cell response, Acta Biomater. 25 (2015) 356–368, https://doi.org/10.1016/j.actbio.2015.07.012.

[104] B. Subramanian, S. Maruthamuthu, S.T. Rajan, Biocompatibility evaluation of sputtered zirconium-based thin film metallic glass-coated steels, Int. J. Nanomed. 10 (2015) 17–29, https://doi.org/10.2147/IJN.S79977.

[105] B. Subramanian, In vitro corrosion and biocompatibility screening of sputtered Ti40Cu36Pd14Zr10 thin film metallic glasses on steels, Mater. Sci. Eng. C 47 (2015) 48–56, https://doi.org/10.1016/j.msec.2014.11.013.

[106] S. Thanka Rajan, A.K. Nandakumar, T. Hanawa, B. Subramanian, Materials properties of ion beam sputtered Ti-Cu-Pd-Zr thin film metallic glasses, Journal of Non-Crystalline Solids 461 (2017) 104–112, https://doi.org/10.1016/j.jnoncrysol.2017.01.008.

[107] T.H. Li, P.C. Wong, S.F. Chang, P.H. Tsai, J.S.C. Jang, J.C. Huang, Biocompatibility study on Ni-free Ti-based and Zr-based bulk metallic glasses, Mater. Sci. Eng. C 75 (2017) 1–6, https://doi.org/10.1016/j.msec.2017.02.006.

[108] S. Pang, Y. Liu, H. Li, L. Sun, Y. Li, T. Zhang, New Ti-based Ti-Cu-Zr-Fe-Sn-Si-Ag bulk metallic glass for biomedical applications, J. Alloy. Compd. 625 (2015) 323–327, https://doi.org/10.1016/j.jallcom.2014.07.021.

[109] S. Li, Q. Wei, Q. Li, B. Jiang, Y. Chen, Y. Sun, Development of Fe-based bulk metallic glasses as potential biomaterials, Mater. Sci. Eng. C 52 (2015) 235–241, https://doi.org/10.1016/j.msec.2015.03.041.

[110] R. Kokubun, W. Wang, S. Zhu, G. Xie, S. Ichinose, S. Itoh, K. Takakuda, In vivo evaluation of a Ti-based bulk metallic glass alloy bar, Biomed. Mater. Eng. 26 (2015) 9–17, https://doi.org/10.3233/BME-151546.

[111] K. Imai, In vivo investigation of Zr-based bulk metallic glasses sub-periosteally implanted on the bone surface, Journal of Materials Science and Chemical, Engineering 04 (2016) 46–51, https://doi.org/10.4236/msce.2016.41009.

[112] A. Jabed, Z.U. Rahman, M.M. Khan, W. Haider, I. Shabib, Combinatorial development and in vitro characterization of the quaternary Zr–Ti–X–Y (X–Y = Cu–Ag/Co–Ni) metallic glass for prospective bioimplants, Adv. Eng. Mater. 21 (2019) 1–12, https://doi.org/10.1002/adem.201900726.

[113] S.T. Rajan, A.T. V V, M. Terada-Nakaishi, P. Chen, T. Hanawa, A.K. Nandakumar, B. Subramanian, Zirconium-based metallic glass and zirconia coatings to inhibit bone formation on titanium, Biomedical Materials 15 (2020) 065019. doi: 10.1088/1748-605X/aba23a.

[114] W. Yang, Y. Liu, N. Hua, S. Pang, Y. Li, P.K. Liaw, T. Zhang, Formation and properties of biocompatible Ti-based bulk metallic glasses in the Ti–Cu–Zr–Fe–Sn–Si–Ag system, J. Non Cryst. Solids 571 (2021), https://doi.org/10.1016/j.jnoncrysol.2021.121060.

[115] K. Li, L. Liang, Q. Huang, J. Xiao, Y. Tian, H. Wu, A novel FeCrMoCSi metallic glass with excellent corrosion resistance and in vitro cellular response for biomedical applications, J. Mater. Sci. 57 (2022) 618–632, https://doi.org/10.1007/s10853-021-06511-y.

[116] M. Hasiak, B. Sobieszczańska, A. Łaszcz, M. Biały, J. Chęcmanowski, T. Zatoński, E. Bożemska, M. Wawrzyńska, Production, mechanical properties and biomedical characterization of ZrTi-based bulk metallic glasses in comparison with 316L stainless steel and Ti6Al4V alloy, Materials 15 (2022), https://doi.org/10.3390/ma15010252.

[117] N. Kaushik, P. Sharma, S. Ahadian, A. Khademhosseini, M. Takahashi, A. Makino, S. Tanaka, M. Esashi, Metallic glass thin films for potential biomedical applications: Metallic Glass Thin Films For Potential Biomedical Applications, J. Biomed. Mater. Res. 102 (2014) 1544–1552, https://doi.org/10.1002/jbm.b.33135.

[118] S. Thanka Rajan, A. Bendavid, B. Subramanian, Cytocompatibility assessment of Ti-Nb-Zr-Si thin film metallic glasses with enhanced osteoblast differentiation for biomedical applications, Colloids and Surfaces B: Biointerfaces 173 (2019) 109–120, https://doi.org/10.1016/j.colsurfb.2018.09.041.

[119] B.-S. Lou, Y.-C. Yang, J.-W. Lee, L.-T. Chen, Biocompatibility and mechanical property evaluation of Zr-Ti-Fe based ternary thin film metallic glasses, Surf. Coat. Technol. 320 (2017) 512–519, https://doi.org/10.1016/j.surfcoat.2016.11.039.

[120] P.-H. Kuo, S.-Y. Tsai, J.-G. Duh, Bio-compatible Zirconium-based thin film metallic glasses with nitrogen reinforced by micro-alloying technique, Mater.

Chem. Phys. 272 (2021) 124965, https://doi.org/10.1016/j.matchemphys.2021.124965.
[121] B. Subramanian, P. Sasikumar, S. Thanka Rajan, K. Gopal Shankar, M. Veerapandian, Fabrication of Zr-Ti-Si glassy metallic overlay on 3D printed Ti-6Al4V implant prototypes for enhanced biocompatibility, J. Alloy. Compd. (2023) 170933, https://doi.org/10.1016/j.jallcom.2023.170933.
[122] M.L. Morrison, R.A. Buchanan, R.V. Leon, C.T. Liu, B.A. Green, P.K. Liaw, J. A. Horton, The electrochemical evaluation of a Zr-based bulk metallic glass in a phosphate-buffered saline electrolyte, Journal of Biomedical Materials Research - Part A 74 (2005) 430–438, https://doi.org/10.1002/jbm.a.30361.
[123] S.F. Guo, Z. Liu, K.C. Chan, W. Chen, H.J. Zhang, J.F. Wang, P. Yu, A plastic Ni-free Zr-based bulk metallic glass with high specific strength and good corrosion properties in simulated body fluid, Mater. Lett. 84 (2012) 81–84, https://doi.org/10.1016/j.matlet.2012.06.057.
[124] H.X. Li, Z.C. Lu, S.L. Wang, Y. Wu, Z.P. Lu, Fe-based bulk metallic glasses: Glass formation, fabrication, properties and applications, Prog. Mater Sci. 103 (2019) 235–318, https://doi.org/10.1016/j.pmatsci.2019.01.003.
[125] M. Calin, A. Gebert, A.C. Ghinea, P.F. Gostin, S. Abdi, C. Mickel, J. Eckert, Designing biocompatible Ti-based metallic glasses for implant applications, Mater. Sci. Eng. C 33 (2013) 875–883, https://doi.org/10.1016/j.msec.2012.11.015.
[126] A.M. Loye, H.K. Kwon, D. Dellal, R. Ojeda, S. Lee, R. Davis, N. Nagle, P.G. Doukas, J. Schroers, F.Y. Lee, T.R. Kyriakides, Biocompatibility of platinum-based bulk metallic glass in orthopedic applications, Biomedical Materials (bristol) 16 (2021), https://doi.org/10.1088/1748-605X/abf981.
[127] O. Baulin, D. Fabrègue, H. Kato, T. Wada, S. Balvay, D.J. Hartmann, J. M. Pelletier, A. Ni-, Al-, Be-free Zr-based metallic glass for biomedical applications, J. Non Cryst. Solids 500 (2018) 78–83, https://doi.org/10.1016/j.jnoncrysol.2018.06.026.
[128] B. Zberg, P.J. Uggowitzer, J.F. Löffler, MgZnCa glasses without clinically observable hydrogen evolution for biodegradable implants, Nat. Mater. 8 (2009) 887–891, https://doi.org/10.1038/nmat2542.
[129] C. Jin, Z. Liu, W. Yu, C. Qin, H. Yu, Z. Wang, Biodegradable Mg–Zn–Ca-based metallic glasses, Materials 15 (2022) 2172, https://doi.org/10.3390/ma15062172.
[130] R. Nowosielski, K. Cesarz-Andraczke, Impact of Zn and Ca on dissolution rate, mechanical properties and GFA of resorbable Mg–Zn–Ca metallic glasses, Archives of Civil and Mechanical Engineering 18 (2018) 1–11, https://doi.org/10.1016/j.acme.2017.05.009.
[131] T.B. Matias, V. Roche, R.P. Nogueira, G.H. Asato, C.S. Kiminami, C. Bolfarini, W. J. Botta, A.M. Jorge, Mg-Zn-Ca amorphous alloys for application as temporary implant: Effect of Zn content on the mechanical and corrosion properties, Mater. Des. 110 (2016) 188–195, https://doi.org/10.1016/j.matdes.2016.07.148.
[132] D.M. Miskovic, K. Pohl, N. Birbilis, K.J. Laws, M. Ferry, Examining the elemental contribution towards the biodegradation of Mg–Zn–Ca ternary metallic glasses, J. Mater. Chem. B 4 (2016) 2679–2690, https://doi.org/10.1039/C6TB00342G.
[133] F. Qin, G. Xie, Z. Dan, S. Zhu, I. Seki, Corrosion behavior and mechanical properties of Mg–Zn–Ca amorphous alloys, Intermetallics 42 (2013) 9–13, https://doi.org/10.1016/j.intermet.2013.04.021.
[134] J.D. Cao, P. Martens, K.J. Laws, P. Boughton, M. Ferry, Quantitative *in vitro* assessment of $Mg_{65}Zn_{30}Ca_{5}$ degradation and its effect on cell viability, J. Biomed. Mater. Res. 101B (2013) 43–49, https://doi.org/10.1002/jbm.b.32811.
[135] J. Chen, J. Dong, H. Fu, H. Zhang, L. Tan, D. Zhao, K. Yang, In vitro and in vivo studies on the biodegradable behavior and bone response of Mg69Zn27Ca4 metal glass for treatment of bone defect, J. Mater. Sci. Technol. 35 (2019) 2254–2262, https://doi.org/10.1016/j.jmst.2019.04.031.
[136] H. Li, S. Pang, Y. Liu, P.K. Liaw, T. Zhang, In vitro investigation of Mg-Zn-Ca-Ag bulk metallic glasses for biomedical applications, J. Non Cryst. Solids 427 (2015) 134–138, https://doi.org/10.1016/j.jnoncrysol.2015.07.043.
[137] S.F. Guo, K.C. Chan, X.Q. Jiang, H.J. Zhang, D.F. Zhang, J.F. Wang, B. Jiang, F. S. Pan, Atmospheric RE-free Mg-based bulk metallic glass with high bio-corrosion resistance, J. Non Cryst. Solids 379 (2013) 107–111, https://doi.org/10.1016/j.jnoncrysol.2013.07.036.
[138] M. Chlewicka, G. Cieślak, A. Dobkowska, J. Mizera, The impact of different volume fractions of crystalline structures on the electrochemical behaviour of $Mg_{67}Zn_{29}Ca_{4}$ alloys for biomedical applications, Corros. Eng. Sci. Technol. 54 (2019) 659–665, https://doi.org/10.1080/1478422X.2019.1655199.
[139] K. Zhao, J.F. Li, D.Q. Zhao, M.X. Pan, W.H. Wang, Degradable Sr-based bulk metallic glasses, Scr. Mater. 61 (2009) 1091–1094, https://doi.org/10.1016/j.scriptamat.2009.08.042.
[140] W. Jiao, K. Zhao, X.K. Xi, D.Q. Zhao, M.X. Pan, W.H. Wang, Zinc-based bulk metallic glasses, J. Non Cryst. Solids 356 (2010) 1867–1870, https://doi.org/10.1016/j.jnoncrysol.2010.07.017.
[141] Y.B. Wang, X.H. Xie, H.F. Li, X.L. Wang, M.Z. Zhao, E.W. Zhang, Y.J. Bai, Y. F. Zheng, L. Qin, Biodegradable CaMgZn bulk metallic glass for potential skeletal application, Acta Biomater. 7 (2011) 3196–3208, https://doi.org/10.1016/j.actbio.2011.04.027.
[142] W. Jiao, H.F. Li, K. Zhao, H.Y. Bai, Y.B. Wang, Y.F. Zheng, W.H. Wang, Development of CaZn based glassy alloys as potential biodegradable bone graft substitute, J. Non Cryst. Solids 357 (2011) 3830–3840, https://doi.org/10.1016/j.jnoncrysol.2011.08.003.
[143] J.D. Cao, N.T. Kirkland, K.J. Laws, N. Birbilis, M. Ferry, Ca-Mg-Zn bulk metallic glasses as bioresorbable metals, Acta Biomater. 8 (2012) 2375–2383, https://doi.org/10.1016/j.actbio.2012.03.009.
[144] H.F. Li, K. Zhao, Y.B. Wang, Y.F. Zheng, W.H. Wang, Study on bio-corrosion and cytotoxicity of a Sr-based bulk metallic glass as potential biodegradable metal, Journal of Biomedical Materials Research - Part B Applied Biomaterials 100 B (2012) 368–377, https://doi.org/10.1002/jbm.b.31958.
[145] H.F. Li, X.H. Xie, K. Zhao, Y.B. Wang, Y.F. Zheng, W.H. Wang, L. Qin, In vitro and in vivo studies on biodegradable CaMgZnSrYb high-entropy bulk metallic glass, Acta Biomater. 9 (2013) 8561–8573, https://doi.org/10.1016/j.actbio.2013.01.029.
[146] H. Li, W. He, S. Pang, P.K. Liaw, T. Zhang, In vitro responses of bone-forming MC3T3-E1 pre-osteoblasts to biodegradable Mg-based bulk metallic glasses, Mater. Sci. Eng. C 68 (2016) 632–641, https://doi.org/10.1016/j.msec.2016.06.022.
[147] J. Wang, Y. Ma, S. Guo, W. Jiang, Q. Liu, Effect of Sr on the microstructure and biodegradable behavior of Mg–Zn–Ca-Mn alloys for implant application, Mater. Des. 153 (2018) 308–316, https://doi.org/10.1016/j.matdes.2018.04.062.
[148] J. Li, F.S. Gittleson, Y. Liu, J. Liu, A.M. Loye, L. McMillon-Brown, T.R. Kyriakides, J. Schroers, A.D. Taylor, Exploring a wider range of Mg-Ca-Zn metallic glass as biocompatible alloys using combinatorial sputtering, Chem. Commun. 53 (2017) 8288–8291, https://doi.org/10.1039/c7cc02733h.
[149] C.C. Wong, P.C. Wong, P.H. Tsai, J.S.C. Jang, C.K. Cheng, H.H. Chen, C.H. Chen, Biocompatibility and osteogenic capacity of Mg-Zn-Ca Bulk metallic glass for rabbit tendon-bone interference fixation, International Journal of Molecular Sciences 20 (2019), https://doi.org/10.3390/ijms20092191.
[150] S. Paul, P. Ramasamy, M. Das, D. Mandal, O. Renk, M. Calin, J. Eckert, S. Bera, New Mg-Ca-Zn amorphous alloys: Biocompatibility, wettability and mechanical properties, Materialia 12 (2020), https://doi.org/10.1016/j.mtla.2020.100799.
[151] G. Poologasundarampillai, A. Nommeots-Nomm, Materials for 3D printing in medicine: Metals, polymers, ceramics, hydrogels, in: D.M. Kalaskar (Ed.), 3D Printing in Medicine, Elsevier Ltd, 2017: pp. 43–71. doi: 10.1016/B978-0-08-100717-4.00002-8.
[152] Ringer's solution, Cold Spring Harbor Protocols 2007 (2007) pdb.rec11071. doi: 10.1101/pdb.rec11071.
[153] H. Li, S. Pang, Y. Liu, L. Sun, P.K. Liaw, T. Zhang, Biodegradable Mg-Zn-Ca-Sr bulk metallic glasses with enhanced corrosion performance for biomedical applications, Mater. Des. 67 (2015) 9–19, https://doi.org/10.1016/j.matdes.2014.10.085.
[154] X. Gu, Y. Zheng, S. Zhong, T. Xi, J. Wang, W. Wang, Corrosion of, and cellular responses to Mg-Zn-Ca bulk metallic glasses, Biomaterials 31 (2010) 1093–1103, https://doi.org/10.1016/j.biomaterials.2009.11.015.
[155] M.L. Morrison, R.A. Buchanan, O.N. Senkov, D.B. Miracle, P.K. Liaw, Electrochemical behavior of Ca-based bulk metallic glasses, Metall. Mater. Trans. A 37 (2006) 1239–1245, https://doi.org/10.1007/s11661-006-1075-x.
[156] K. Cesarz-Andraczke, R. Nowosielski, Surface structure and corrosion behavior of $Mg68-xZn28+xCa4(x = 0.4)$ bulk metallic glasses after immersion in Ringer's solution, J. Mater. Eng. Perform. 28 (2019) 2365–2377, https://doi.org/10.1007/s11665-019-04001-6.
[157] O.N. Senkov, J.M. Scott, Glass forming ability and thermal stability of ternary Ca-Mg-Zn bulk metallic glasses, J. Non Cryst. Solids 351 (2005) 3087–3094, https://doi.org/10.1016/j.jnoncrysol.2005.07.022.
[158] M. Ramya, S.G. Sarwat, V. Udhayabanu, B. Raj, K.R. Ravi, Exploring Mg-Zn-Ca-based bulk metallic glasses for biomedical applications based on thermodynamic approach, Metall. Mater. Trans. A 46 (2015) 5962–5971, https://doi.org/10.1007/s11661-015-3124-9.
[159] S.J.B. Bin, K.S. Fong, B.W. Chua, M. Gupta, Mg-based bulk metallic glasses: A review of recent developments, J. Magnesium Alloys (2021), https://doi.org/10.1016/j.jma.2021.10.010.
[160] F. Kiani, C. Wen, Y. Li, Prospects and strategies for magnesium alloys as biodegradable implants from crystalline to bulk metallic glasses and composites—A review, Acta Biomater. 103 (2020) 1–23, https://doi.org/10.1016/j.actbio.2019.12.023.
[161] M.P. Staiger, A.M. Pietak, J. Huadmai, G. Dias, Magnesium and its alloys as orthopedic biomaterials: A review, Biomaterials 27 (2006) 1728–1734, https://doi.org/10.1016/j.biomaterials.2005.10.003.
[162] F. Witte, N. Hort, C. Vogt, S. Cohen, K.U. Kainer, R. Willumeit, F. Feyerabend, Degradable biomaterials based on magnesium corrosion, Curr. Opin. Solid State Mater. Sci. 12 (2008) 63–72, https://doi.org/10.1016/j.cossms.2009.04.001.
[163] M.H. Emily Walker, Magnesium, Iron and Zinc Alloys, the Trifecta of Bioresorbable Orthopaedic and Vascular Implantation - A Review, J Biotechnol Biomater 05 (2015), https://doi.org/10.4172/2155-952X.1000178.
[164] M. Erinc, W.H. Sillekens, R. Mannens, R.J. Werkhoven, Applicability of existing magnesium alloys as biomedical implant materials, in: Magnesium Technology, Wiley TMS, 2009, pp. 209–214.
[165] H.H. Bayraktar, E.F. Morgan, G.L. Niebur, G.E. Morris, E.K. Wong, T.M. Keaveny, Comparison of the elastic and yield properties of human femoral trabecular and cortical bone tissue, J. Biomech. 37 (2004) 27–35, https://doi.org/10.1016/S0021-9290(03)00257-4.
[166] Y. Chen, Z. Xu, C. Smith, J. Sankar, Recent advances on the development of magnesium alloys for biodegradable implants, Acta Biomater. 10 (2014) 4561–4573, https://doi.org/10.1016/j.actbio.2014.07.005.
[167] Y.F. Zheng, X.N. Gu, F. Witte, Biodegradable metals, Mater. Sci. Eng. R. Rep. 77 (2014) 1–34, https://doi.org/10.1016/j.mser.2014.01.001.
[168] D. Vojtěch, J. Kubásek, J. Čapek, Comparative mechanical and corrosion studies on magnesium, zinc and iron alloys as biodegradable metals, Mater. Tehnol. 49 (2015) 877–882, https://doi.org/10.17222/mit.2014.129.

[169] K. Schwibbert, A.M. Richter, J. Krüger, J. Bonse, Laser-Textured Surfaces: A Way to Control Biofilm Formation? Laser Photonics Rev. 18 (2024) 2300753, https://doi.org/10.1002/lpor.202300753.

[170] D. Campoccia, L. Montanaro, C.R. Arciola, The significance of infection related to orthopedic devices and issues of antibiotic resistance, Biomaterials 27 (2006) 2331–2339, https://doi.org/10.1016/j.biomaterials.2005.11.044.

[171] D. Campoccia, L. Montanaro, C.R. Arciola, A review of the biomaterials technologies for infection-resistant surfaces, Biomaterials 34 (2013) 8533–8554, https://doi.org/10.1016/j.biomaterials.2013.07.089.

[172] X. Li, B. Wu, H. Chen, K. Nan, Y. Jin, L. Sun, B. Wang, Recent developments in smart antibacterial surfaces to inhibit biofilm formation and bacterial infections, J. Mater. Chem. B 6 (2018) 4274–4292, https://doi.org/10.1039/C8TB01245H.

[173] S. Ferraris, A. Cochis, M. Cazzola, M. Tortello, A. Scalia, S. Spriano, L. Rimondini, Cytocompatible and Anti-bacterial Adhesion Nanotextured Titanium Oxide Layer on Titanium Surfaces for Dental and Orthopedic Implants, Front. Bioeng. Biotechnol. 7 (2019) 103, https://doi.org/10.3389/fbioe.2019.00103.

[174] H. Huang, P. Zhang, Z. Yu, X. Zhang, L. Shen, H. Shi, H. Yan, L. Wang, Y. Tian, Effects of periodic surface structures induced by femtosecond laser irradiation on the antibacterial properties of Zr-based amorphous material, Optik 268 (2022) 169760, https://doi.org/10.1016/j.ijleo.2022.169760.

[175] D.P. Linklater, V.A. Baulin, S. Juodkazis, R.J. Crawford, P. Stoodley, E.P. Ivanova, Mechano-bactericidal actions of nanostructured surfaces, Nat. Rev. Microbiol. 19 (2021) 8–22, https://doi.org/10.1038/s41579-020-0414-z.

[176] K.A. Whitehead, J. Colligon, J. Verran, Retention of microbial cells in substratum surface features of micrometer and sub-micrometer dimensions, Colloids Surf. B: Biointerfaces 41 (2005) 129–138, https://doi.org/10.1016/j.colsurfb.2004.11.010.

[177] J. Hasan, Y. Xu, T. Yarlagadda, M. Schuetz, K. Spann, P.K.D.V. Yarlagadda, Antiviral and antibacterial nanostructured surfaces with excellent mechanical properties for hospital applications, ACS Biomaterials Science and Engineering 6 (2020) 3608–3618, https://doi.org/10.1021/acsbiomaterials.0c00348.

[178] S. Papa, M. Maalouf, P. Claudel, X. Sedao, Y. Di Maio, H. Hamzeh-Cognasse, M. Thomas, A. Guignandon, V. Dumas, Key topographic parameters driving surface adhesion of Porphyromonas gingivalis, Sci Rep 13 (2023) 15893, https://doi.org/10.1038/s41598-023-42387-5.

[179] B.R. Chrcanovic, A.R. Pedrosa, M.D. Martins, Chemical and topographic analysis of treated surfaces of five different commercial dental titanium implants, Mater. Res. 15 (2012) 372–382, https://doi.org/10.1590/S1516-14392012005000035.

[180] F. Xue, J. Liu, L. Guo, L. Zhang, Q. Li, Theoretical study on the bactericidal nature of nanopatterned surfaces, J. Theor. Biol. 385 (2015) 1–7, https://doi.org/10.1016/j.jtbi.2015.08.011.

[181] E. Medilanski, K. Kaufmann, L.Y. Wick, O. Wanner, H. Harms, Influence of the surface topography of stainless steel on bacterial adhesion, Biofouling 18 (2002) 193–203, https://doi.org/10.1080/08927010290011370.

[182] X. Li, Bactericidal mechanism of nanopatterned surfaces, Phys. Chem. Chem. Phys. 18 (2016) 1311–1316, https://doi.org/10.1039/C5CP05646B.

[183] J.M. Rice, J.A. Hunt, J.A. Gallagher, P. Hanarp, D.S. Sutherland, J. Gold, Quantitative assessment of the response of primary derived human osteoblasts and macrophages to a range of nanotopography surfaces in a single culture model in vitro, Biomaterials 24 (2003) 4799–4818, https://doi.org/10.1016/S0142-9612(03)00381-8.

[184] R.A. Gittens, T. McLachlan, R. Olivares-Navarrete, Y. Cai, S. Berner, R. Tannenbaum, Z. Schwartz, K.H. Sandhage, B.D. Boyan, The effects of combined micron-/submicron-scale surface roughness and nanoscale features on cell proliferation and differentiation, Biomaterials 32 (2011) 3395–3403, https://doi.org/10.1016/j.biomaterials.2011.01.029.

[185] C.H. Choi, S.H. Hagvall, B.M. Wu, J.C.Y. Dunn, R.E. Beygui, C.J.C.J. Kim, Cell interaction with three-dimensional sharp-tip nanotopography, Biomaterials 28 (2007) 1672–1679, https://doi.org/10.1016/j.biomaterials.2006.11.031.

[186] M.J. Dalby, M.O. Riehle, D.S. Sutherland, H. Agheli, A.S.G. Curtis, Morphological and microarray analysis of human fibroblasts cultured on nanocolumns produced by colloidal lithography, Eur. Cell. Mater. 9 (2005) 1–8, https://doi.org/10.22203/eCM.v009a01.

[187] A. Wilkinson, R.N. Hewitt, L.E. McNamara, D. McCloy, R.M. Dominic Meek, M. J. Dalby, Biomimetic microtopography to enhance osteogenesis in vitro, Acta Biomaterialia 7 (2011) 2919–2925, https://doi.org/10.1016/j.actbio.2011.03.026.

[188] N. Gui, W. Xu, A.N. Abraham, R. Shukla, M. Qian, Osteoblast responses to titanium-coated subcellular scaled microgrooves, ACS Applied Bio Materials 2 (2019) 2405–2413, https://doi.org/10.1021/acsabm.9b00094.

[189] A.I. Teixeira, G.A. McKie, J.D. Foley, P.J. Bertics, P.F. Nealey, C.J. Murphy, The effect of environmental factors on the response of human corneal epithelial cells to nanoscale substrate topography, Biomaterials 27 (2006) 3945–3954, https://doi.org/10.1016/j.biomaterials.2006.01.044.

[190] N. Gui, W. Xu, D.E. Myers, R. Shukla, H.P. Tang, M. Qian, The effect of ordered and partially ordered surface topography on bone cell responses: A review, Biomater. Sci. 6 (2018) 250–264, https://doi.org/10.1039/c7bm01016h.

[191] V. Hasirci, N. Hasirci, Nano- and microarchitecture of biomaterial surfaces, in: Fundamentals of Biomaterials, Springer, 2018: pp. 303–329. doi: 10.1007/978-1-4939-8856-3.

[192] C.J. Bettinger, R. Langer, J.T. Borenstein, Engineering substrate topography at the micro- and nanoscale to control cell function, Angewandte Chemie - International Edition 48 (2009) 5406–5415, https://doi.org/10.1002/anie.200805179.

[193] V. Hasirci, B.J. Pepe-Mooney, Understanding the cell behavior on nano-/micro-patterned surfaces, Nanomedicine 7 (2012) 1375–1389, https://doi.org/10.2217/nnm.12.7.

[194] M. Ermis, E. Antmen, V. Hasirci, Micro and Nanofabrication methods to control cell-substrate interactions and cell behavior: A review from the tissue engineering perspective, Bioact. Mater. 3 (2018) 355–369, https://doi.org/10.1016/j.bioactmat.2018.05.005.

[195] P.K. Mattila, P. Lappalainen, Filopodia: molecular architecture and cellular functions, Nat. Rev. Mol. Cell Biol. 9 (2008) 446–454, https://doi.org/10.1038/nrm2406.

[196] C. Matschegewski, S. Staehlke, R. Loeffler, R. Lange, F. Chai, D.P. Kern, U. Beck, B.J. Nebe, Cell architecture-cell function dependencies on titanium arrays with regular geometry, Biomaterials 31 (2010) 5729–5740, https://doi.org/10.1016/j.biomaterials.2010.03.073.

[197] E. Skoulas, A. Manousaki, C. Fotakis, E. Stratakis, Biomimetic surface structuring using cylindrical vector femtosecond laser beams, Sci Rep 7 (2017) 45114, https://doi.org/10.1038/srep45114.

[198] J.G. Lunney, R. Jordan, Pulsed laser ablation of metals, Appl. Surf. Sci. 127–129 (1998) 941–946, https://doi.org/10.1016/S0169-4332(97)00770-8.

[199] A. Semerok, B. Sallé, J.F. Wagner, G. Petite, Femtosecond, picosecond, and nanosecond laser microablation: Laser plasma and crater investigation, Laser and Particle Beams 20 (2002) 67–72, https://doi.org/10.1017/S0263034602201093.

[200] L. Hribar, P. Gregorčič, M. Senegačnik, M. Jezešek, The influence of the processing parameters on the laser-ablation of stainless steel and brass during the engraving by nanosecond fiber laser, Nanomaterials 12 (2022), https://doi.org/10.3390/nano12020232.

[201] G.D. Tsibidis, The influence of dynamical change of optical properties on the thermomechanical response and damage threshold of noble metals under femtosecond laser irradiation, J. Appl. Phys. 123 (2018), https://doi.org/10.1063/1.5011738.

[202] C. Dowding, Laser ablation, in: Advances in Laser Materials Processing: Technology, Research and Application, 2010: pp. 575–628. doi: 10.1533/9781845699819.7.575.

[203] B.N. Chichkov, C. Momma, S. Nolte, F. Von Alvensleben, A. Tünnermann, Femtosecond, picosecond and nanosecond laser ablation of solids, Appl. Phys. A Mater. Sci. Process. 63 (1996) 109–115, https://doi.org/10.1007/BF01567637.

[204] A.Y. Vorobyev, C. Guo, Direct femtosecond laser surface nano/microstructuring and its applications: Direct femtosecond laser surface nano/microstructuring and its applications, Laser Photonics Rev. 7 (2013) 385–407, https://doi.org/10.1002/lpor.201200017.

[205] E.M. Sebastian, S.K. Jain, R. Purohit, S.K. Dhakad, R.S. Rana, Nanolithography and its current advancements, Materials Today: Proceedings 26 (2019) 2351–2356. doi: 10.1016/j.matpr.2020.02.505.

[206] P. Bhagoria, E.M. Sebastian, S.K. Jain, J. Purohit, R. Purohit, Nanolithography and its alternate techniques, Materials Today: Proceedings 26 (2019) 3048–3053. doi: 10.1016/j.matpr.2020.02.633.

[207] M. Ganjian, K. Modaresifar, H. Zhang, P.L. Hagedoorn, L.E. Fratila-Apachitei, A. A. Zadpoor, Reactive ion etching for fabrication of biofunctional titanium nanostructures, Sci. Rep. 9 (2019) 1–20, https://doi.org/10.1038/s41598-019-55093-y.

[208] Z. Lin, M. Hong, Femtosecond laser precision engineering: From micron, submicron, to nanoscale, Ultrafast Science (2021), https://doi.org/10.34133/2021/9783514.

[209] G. Nemickas, G. Kontenis, A. Žemaitis, V. Purlys, L. Jonušauskas, Industrial-grade processing of metal surfaces via femtosecond laser, Jphys Photonics 2 (2020), https://doi.org/10.1088/2515-7647/ab7b11.

[210] C. Florian, S.V. Kirner, J. Krüger, J. Bonse, Surface functionalization by laser-induced periodic surface structures, J. Laser Appl. 32 (2020) 022063, https://doi.org/10.2351/7.0000103.

[211] E.M. Garcell, S.C. Singh, H. Li, B. Wang, S.A. Jalil, C. Guo, Comparative study of femtosecond laser-induced structural colorization in water and air, Nanoscale Advances 2 (2020) 2958–2967, https://doi.org/10.1039/c9na00804g.

[212] A. Dostovalov, K. Bronnikov, V. Korolkov, S. Babin, E. Mitsai, A. Mironenko, M. Tutov, D. Zhang, K. Sugioka, J. Maksimovic, T. Katkus, S. Juodkazis, A. Zhizhchenko, A. Kuchmizhak, Hierarchical anti-reflective laser-induced periodic surface structures (LIPSSs) on amorphous Si films for sensing applications, Nanoscale 12 (2020) 13431–13441, https://doi.org/10.1039/d0nr02182b.

[213] M.J. Wood, P. Servio, A.M. Kietzig, The tuning of lipss wettability during laser machining and through post-processing, Nanomaterials 11 (2021), https://doi.org/10.3390/nano11040973.

[214] A. Cunha, A.M. Elie, L. Plawinski, A.P. Serro, A.M. Botelho Do Rego, A. Almeida, M.C. Urdaci, M.C. Durrieu, R. Vilar, Femtosecond laser surface texturing of titanium as a method to reduce the adhesion of Staphylococcus aureus and biofilm formation, Appl. Surf. Sci. 360 (2016) 485–493, https://doi.org/10.1016/j.apsusc.2015.10.102.

[215] A.H.A. Lutey, L. Gemini, L. Romoli, G. Lazzini, F. Fuso, M. Faucon, R. Kling, Towards laser-textured antibacterial surfaces, Sci. Rep. 8 (2018) 1–11, https://doi.org/10.1038/s41598-018-28454-2.

[216] F. Fraggelakis, G. Mincuzzi, J. Lopez, I. Manek-Hönninger, R. Kling, Controlling 2D laser nano structuring over large area with double femtosecond pulses, Appl. Surf. Sci. 470 (2019) 677–686, https://doi.org/10.1016/j.apsusc.2018.11.106.

[217] M. Birnbaum, Semiconductor surface damage produced by ruby lasers, J. Appl. Phys. 36 (1965) 3688–3689, https://doi.org/10.1063/1.1703071.

[218] J. Bonse, S. Höhm, S.V. Kirner, A. Rosenfold, J. Krüger, Laser-induced periodic surface structures - A scientific evergreen, IEEE J. Sel. Top. Quantum Electron. 23 (2017), https://doi.org/10.1109/JSTQE.2016.2614183.

[219] J. Bonse, J. Kru, Femtosecond laser-induced periodic surface structures, J. Laser Appl. 24 (2012) 1–7, https://doi.org/10.2351/1.4712658.

[220] J.E. Sipe, J.E. Young, J.S. Preston, H.M. Van Driel, Laser-induced periodic surface structure. I. Theory, Phys. Rev. B 27 (1983) 1141–1154, https://doi.org/10.1016/0169-4332(95)00495-5.
[221] A. Rudenko, A. Abou-Saleh, F. Pigeon, C. Mauclair, F. Garrelie, R. Stoian, J. P. Colombier, High-frequency periodic patterns driven by non-radiative fields coupled with Marangoni convection instabilities on laser-excited metal surfaces, Acta Mater. 194 (2020) 93–105, https://doi.org/10.1016/j.actamat.2020.04.058.
[222] A. Nakhoul, A. Rudenko, C. Maurice, S. Reynaud, F. Garrelie, F. Pigeon, J. Colombier, Boosted spontaneous formation of high-aspect ratio nanopeaks on ultrafast laser-irradiated ni surface, Advanced Science 9 (2022) 2200761, https://doi.org/10.1002/advs.202200761.
[223] A. Nakhoul, J. Colombier, Beyond the microscale: advances in surface nanopatterning by laser-driven self-organization, Laser Photonics Rev. (2024) 2300991, https://doi.org/10.1002/lpor.202300991.
[224] D. Iabbaden, J. Amodeo, C. Fusco, F. Garrelie, J.-P. Colombier, Molecular dynamics simulation of structural evolution in crystalline and amorphous CuZr alloys upon ultrafast laser irradiation, Phys. Rev. Materials 6 (2022) 126001, https://doi.org/10.1103/PhysRevMaterials.6.126001.
[225] D. Iabbaden, J. Amodeo, C. Fusco, F. Garrelie, J.-P. Colombier, Dynamics of Cu–Zr metallic glass devitrification under ultrafast laser excitation revealed by atomistic modeling, Acta Materialia 263 (2024) 119487, https://doi.org/10.1016/j.actamat.2023.119487.
[226] J. Antonowicz, P. Zalden, K. Sokolowski-Tinten, K. Georgarakis, R. Minikayev, A. Pietnoczka, F. Bertram, M. Chaika, M. Chojnacki, P. Dłużewski, K. Fronc, A. L. Greer, C. Jastrzębski, D. Klinger, Ch. Lemke, O.M. Magnussen, B. Murphy, K. Perumal, U. Ruett, J. Warias, R. Sobierajski, Devitrification of thin film Cu–Zr metallic glass via ultrashort pulsed laser annealing, J. Alloy. Compd. 887 (2021) 161437, https://doi.org/10.1016/j.jallcom.2021.161437.
[227] S. Comby-Dassonneville, L. Roiban, A. Borroto, A. Malchère, S. Cardinal, T. Douillard, C. Langlois, J.-F. Pierson, J.M. Pelletier, P. Steyer, Better understand the crystallization dynamics of ZrCu TFMGs: benefits of combining global and local in situ approaches, J. Alloy. Compd. (2024) 174233, https://doi.org/10.1016/j.jallcom.2024.174233.
[228] P. Dominic, D. Iabbaden, F. Bourquard, S. Reynaud, A. Nakhoul, A. Weck, J.-P. Colombier, F. Garrelie, Unveiling nature and consequences of tungsten oxidation upon ultrafast laser irradiation, Appl. Surf. Sci. 655 (2024) 159580, https://doi.org/10.1016/j.apsusc.2024.159580.
[229] H. Huang, P. Zhang, M. Tang, L. Shen, Z. Yu, H. Shi, Y. Tian, Biocompatibility of micro/nano structures on the surface of Ti6Al4V and Ti-based bulk metallic glasses induced by femtosecond laser, Biomaterials Advances 139 (2022) 212998, https://doi.org/10.1016/j.bioadv.2022.212998.
[230] C. Zwahr, A. Welle, T. Weingärtner, C. Heinemann, B. Kruppke, N. Gulow, M. G. Holthaus, A. Fabián Lasagni, Ultrashort pulsed laser surface patterning of titanium to improve osseointegration of dental implants, Adv Eng Mater 21 (2019) 1900639, https://doi.org/10.1002/adem.201900639.
[231] J. Zheng, B. Yang, H. Wang, L. Zhou, Z. Zhang, Z. Zhou, Temperature-responsive, femtosecond laser-ablated ceramic surfaces with switchable wettability for on-demand droplet transfer, ACS Appl. Mater. Interfaces 15 (2023) 13740–13752, https://doi.org/10.1021/acsami.2c22335.
[232] K. Müller, F. Mirabella, X. Knigge, M. Mezera, M. Weise, M. Sahre, K. Wasmuth, H. Voss, A. Hertwig, J. Krüger, J. Radnik, V.-D. Hodoroaba, J. Bonse, Chemical and Topographical Changes upon Sub-100-nm Laser-Induced Periodic Surface Structure Formation on Titanium Alloy: The Influence of Laser Pulse Repetition Rate and Number of Over-Scans, Physica Status Solidi (a) (2023) 2300719. doi: 10.1002/pssa.202300719.
[233] G. Giannuzzi, C. Gaudiuso, R. Di Mundo, L. Mirenghi, F. Fraggelakis, R. Kling, P. M. Lugarà, A. Ancona, Short and long term surface chemistry and wetting behaviour of stainless steel with 1D and 2D periodic structures induced by bursts of femtosecond laser pulses, Appl. Surf. Sci. 494 (2019) 1055–1065, https://doi.org/10.1016/j.apsusc.2019.07.126.
[234] C. Florian, R. Wonneberger, A. Undisz, S.V. Kirner, K. Wasmuth, D. Spaltmann, J. Krüger, J. Bonse, Chemical effects during the formation of various types of femtosecond laser-generated surface structures on titanium alloy, Appl. Phys. A 126 (2020) 266, https://doi.org/10.1007/s00339-020-3434-7.
[235] B.E.J. Lee, H. Exir, A. Weck, K. Grandfield, Characterization and evaluation of femtosecond laser-induced sub-micron periodic structures generated on titanium to improve osseointegration of implants, Appl. Surf. Sci. 441 (2018) 1034–1042, https://doi.org/10.1016/j.apsusc.2018.02.119.
[236] M. Wolff, R. Wonneberger, K.E. Freiberg, A. Hertwig, J. Bonse, L. Giebeler, A. Koitzsch, C. Kunz, H. Weber, J.K. Hufenbach, F.A. Müller, S. Gräf, Formation of laser-induced periodic surface structures on Zr-based bulk metallic glasses with different chemical composition, Surf. Interfaces 42 (2023) 103305, https://doi.org/10.1016/j.surfin.2023.103305.
[237] M. Prudent, D. Iabbaden, F. Bourquard, S. Reynaud, Y. Lefkir, A. Borroto, J.-F. Pierson, F. Garrelie, J.-P. Colombier, High-Density Nanowells Formation in Ultrafast Laser-Irradiated Thin Film Metallic Glass, Nano-Micro Lett. 14 (2022) 103, https://doi.org/10.1007/s40820-022-00850-4.
[238] S. Marinier, L.J. Lewis, Femtosecond laser ablation of CuxZr1-x bulk metallic glasses: A molecular dynamics study, Physical Review B - Condensed Matter and Materials Physics 92 (2015), https://doi.org/10.1103/PhysRevB.92.184108.
[239] Y. Zhu, J. Fu, C. Zheng, Z. Ji, Effect of nanosecond pulse laser ablation on the surface morphology of Zr-based metallic glass, Opt. Laser Technol. 83 (2016) 21–27, https://doi.org/10.1016/j.optlastec.2016.03.021.
[240] H. Huang, J. Yan, Surface patterning of Zr-based metallic glass by laser irradiation induced selective thermoplastic extrusion in nitrogen gas, J. Micromech. Microeng. 27 (2017), https://doi.org/10.1088/1361-6439/aa71d5.
[241] Y. Jiao, E. Brousseau, Q. Han, H. Zhu, S. Bigot, Investigations in nanosecond laser micromachining on the Zr52.8Cu17.6Ni14.8Al9.9Ti4.9 bulk metallic glass: experimental and theoretical study, Journal of Materials Processing Technology 273 (2019) 116232, https://doi.org/10.1016/j.jmatprotec.2019.05.013.
[242] Y. Jiao, E. Brousseau, X. Shen, X. Wang, Q. Han, H. Zhu, S. Bigot, W. He, Investigations in the fabrication of surface patterns for wettability modification on a Zr-based bulk metallic glass by nanosecond laser surface texturing, J. Mater. Process. Technol. 283 (2020) 116714, https://doi.org/10.1016/j.jmatprotec.2020.116714.
[243] Y. Qian, H. Huang, C. Wang, P. Yu, J. Xu, Z. Zhang, Formation of leaf-shaped microstructure on Zr-based metallic glass via nanosecond pulsed laser irradiation, J. Manuf. Process. 72 (2021) 61–70, https://doi.org/10.1016/j.jmapro.2021.10.016.
[244] Y. Qian, M. Jiang, Z. Zhang, H. Huang, J. Yan, Surface functionalization of Zr-based metallic glass by direct nanosecond laser texturing, Vacuum 194 (2021) 110635, https://doi.org/10.1016/j.vacuum.2021.110635.
[245] T. Shinonaga, M. Tsukamoto, Femtosecond and nanosecond laser irradiation for microstructure formation on bulk metallic glass, Trans. JWRI 38 (2009) 81–84.
[246] W. Zhang, G. Cheng, X.D. Hui, Q. Feng, Abnormal ripple patterns with enhanced regularity and continuity in a bulk metallic glass induced by femtosecond laser irradiation, Appl. Phys. A Mater. Sci. Process. 115 (2014) 1451–1455, https://doi.org/10.1007/s00339-013-8062-z.
[247] C. Li, H. Zhang, G. Cheng, N. Faure, D. Jamon, J.P. Colombier, R. Stoian, Initial cumulative effects in femtosecond pulsed laser-induced periodic surface structures on bulk metallic glasses, Journal of Laser Micro Nanoengineering 11 (2016) 357–365, https://doi.org/10.2961/jlmn.2016.03.0014.
[248] Y. Lei, J. Yang, C. Cong, C. Guo, Fabrication of homogenous subwavelength grating structures on metallic glass using double-pulsed femtosecond lasers, Opt. Lasers Eng. 134 (2020), https://doi.org/10.1016/j.optlaseng.2020.106273.
[249] M. Prudent, F. Bourquard, A. Borroto, J.F. Pierson, F. Garrelie, J.P. Colombier, Initial morphology and feedback effects on laser-induced periodic nanostructuring of thin-film metallic glasses, Nanomaterials 11 (2021), https://doi.org/10.3390/nano11051076.
[250] J. Wang, P. Zhang, L. Shen, Z. Yu, H. Shi, Y. Tian, The femtosecond laser induced Zr64.13Cu15.75Ni10.12Al10 amorphous periodic surface structure, J. Manuf. Process. 69 (2021) 613–620, https://doi.org/10.1016/j.jmapro.2021.08.020.
[251] Y. Qian, H. Huang, M. Jiang, J. Yan, Nanosecond pulsed laser-induced formation of nanopattern on Fe-based metallic glass surface, Appl. Surf. Sci. 577 (2022) 151976, https://doi.org/10.1016/j.apsusc.2021.151976.
[252] J.J.J. Nivas, S. Amoruso, Generation of supra-wavelength grooves in femtosecond laser surface structuring of silicon, Nanomaterials 11 (2021) 1–20, https://doi.org/10.3390/nano11010174.
[253] A. Papadopoulos, E. Skoulas, G.D. Tsibidis, E. Stratakis, Formation of periodic surface structures on dielectrics after irradiation with laser beams of spatially variant polarisation: a comparative study, Appl. Phys. A Mater. Sci. Process. 124 (2018) 1–12, https://doi.org/10.1007/s00339-018-1573-x.
[254] K.M. Tanvir Ahmmed, C. Grambow, A.M. Kietzig, Fabrication of micro/nano structures on metals by femtosecond laser micromachining, Micromachines 5 (2014) 1219–1253, https://doi.org/10.3390/mi5041219.
[255] J. Chen, J.P. Ulerich, E. Abelev, A. Fasasi, C.B. Arnold, W.O. Soboyejo, An investigation of the initial attachment and orientation of osteoblast-like cells on laser grooved Ti-6Al-4V surfaces, Mater. Sci. Eng. C 29 (2009) 1442–1452, https://doi.org/10.1016/j.msec.2008.11.014.
[256] R. Kumari, T. Scharnweber, W. Pfleging, H. Besser, J.D. Majumdar, Laser surface textured titanium alloy (Ti-6Al-4V) - Part II - Studies on bio-compatibility, Appl. Surf. Sci. 357 (2015) 750–758, https://doi.org/10.1016/j.apsusc.2015.08.255.
[257] S. Mukherjee, S. Dhara, P. Saha, Enhancing the biocompatibility of Ti6Al4V implants by laser surface microtexturing: An in vitro study, Int. J. Adv. Manuf. Technol. 76 (2015) 5–15, https://doi.org/10.1007/s00170-013-5277-2.
[258] Z. Yu, G. Yang, W. Zhang, J. Hu, Investigating the effect of picosecond laser texturing on microstructure and biofunctionalization of titanium alloy, J. Mater. Process. Technol. 255 (2018) 129–136, https://doi.org/10.1016/j.jmatprotec.2017.12.009.
[259] O. Raimbault, S. Benayoun, K. Anselme, C. Mauclair, T. Bourgade, A.M. Kietzig, P. L. Girard-Lauriault, S. Valette, C. Donnet, The effects of femtosecond laser-textured Ti-6Al-4V on wettability and cell response, Mater. Sci. Eng. C 69 (2016) 311–320, https://doi.org/10.1016/j.msec.2016.06.072.
[260] N. Epperlein, F. Menzel, K. Schwibbert, R. Koter, J. Bonse, J. Sameith, J. Krüger, J. Toepel, Influence of femtosecond laser produced nanostructures on biofilm growth on steel, Appl. Surf. Sci. 418 (2017) 420–424, https://doi.org/10.1016/j.apsusc.2017.02.174.
[261] A. Carvalho, L. Cangueiro, V. Oliveira, R. Vilar, M.H. Fernandes, F.J. Monteiro, Femtosecond laser microstructured Alumina toughened Zirconia: A new strategy to improve osteogenic differentiation of hMSCs, Appl. Surf. Sci. 435 (2018) 1237–1245, https://doi.org/10.1016/j.apsusc.2017.11.206.
[262] X. Luo, S. Yao, H. Zhang, M. Cai, W. Liu, R. Pan, C. Chen, X. Wang, L. Wang, M. Zhong, Biocompatible nano-ripples structured surfaces induced by femtosecond laser to rebel bacterial colonization and biofilm formation, Opt. Laser Technol. 124 (2020) 105973, https://doi.org/10.1016/j.optlastec.2019.105973.
[263] X. Wu, H. Ao, Z. He, Q. Wang, Z. Peng, Surface modification of titanium by femtosecond laser in reducing bacterial colonization, Coatings 12 (2022) 414, https://doi.org/10.3390/coatings12030414.
[264] S. Papa, A. Abou Khalil, H. Hamzeh-Cognasse, M. Thomas, M. Maalouf, Y. Di Maio, X. Sedao, A. Guignandon, V. Dumas, Dual-functionalized titanium by ultrafast laser texturing to enhance human gingival fibroblasts adhesion and

minimize Porphyromonas gingivalis colonization, Applied Surface Science 606 (2022) 154784, https://doi.org/10.1016/j.apsusc.2022.154784.
[265] M. Maalouf, A. Abou Khalil, Y. Di Maio, S. Papa, X. Sedao, E. Dalix, S. Peyroche, A. Guignandon, V. Dumas, Polarization of femtosecond laser for titanium alloy nanopatterning influences osteoblastic differentiation, Nanomaterials 12 (2022) 1619, https://doi.org/10.3390/nano12101619.
[266] T.T.D. Huynh, A. Petit, N. Semmar, Picosecond laser induced periodic surface structure on copper thin films, Applied Surface Science 302 (2014) 109–113, https://doi.org/10.1016/j.apsusc.2013.10.172.
[267] A.Y. Vorobyev, C. Guo, Femtosecond laser structuring of titanium implants, Appl. Surf. Sci. 253 (2007) 7272–7280, https://doi.org/10.1016/j.apsusc.2007.03.006.
[268] A. Cunha, O.F. Zouani, L. Plawinski, A.M. Botelho do Rego, A. Almeida, R. Vilar, M.-C. Durrieu, Human mesenchymal stem cell behavior on femtosecond laser-textured Ti-6Al-4V surfaces, Nanomedicine 10 (2015) 725–739, https://doi.org/10.2217/nnm.15.19.
[269] V.M. Villapún, B. Qu, P.A. Lund, W. Wei, L.G. Dover, J.R. Thompson, J. O. Adesina, C. Hoerdemann, S. Cox, S. González, Optimizing the antimicrobial performance of metallic glass composites through surface texturing, Mater. Today Commun. 23 (2020), https://doi.org/10.1016/j.mtcomm.2020.101074.
[270] Y. Jiao, E. Brousseau, W. Nishio Ayre, E. Gait-Carr, X. Shen, X. Wang, S. Bigot, H. Zhu, W. He, In vitro cytocompatibility of a Zr-based metallic glass modified by laser surface texturing for potential implant applications, Appl. Surf. Sci. 547 (2021), https://doi.org/10.1016/j.apsusc.2021.149194.
[271] H. Huang, P. Zhang, Z. Yu, L. Shen, H. Shi, Y. Tian, Femtosecond laser-induced transformation mechanism from 1D groove structure to 2D microholes structure on the surface of Zr-based metallic glasses, Opt. Laser Technol. 146 (2022) 107555, https://doi.org/10.1016/j.optlastec.2021.107555.
[272] C. Du, C. Wang, T. Zhang, X. Yi, J. Liang, H. Wang, Reduced bacterial adhesion on zirconium-based bulk metallic glasses by femtosecond laser nanostructuring, Proc. Inst. Mech. Eng. [h] 234 (2020) 387–397, https://doi.org/10.1177/0954411919898011.
[273] C. Du, H. Yuan, X. Zhu, T. Zhang, Z. Liu, C. Wang, Fabrication of antibacterial Zr-BMG biomimetic surfaces by femtosecond laser, Surf. Interfaces 37 (2023) 102740, https://doi.org/10.1016/j.surfin.2023.102740.
[274] C.A. Baumann, B.D. Crist, Nickel allergy to orthopaedic implants: A review and case series, Journal of Clinical Orthopaedics and Trauma 11 (2020) S596–S603, https://doi.org/10.1016/j.jcot.2020.02.008.